Politecnico di Milano

SCHOOL OF INDUSTRIAL AND INFORMATION ENGINEERING
Master of Science – Nuclear Engineering

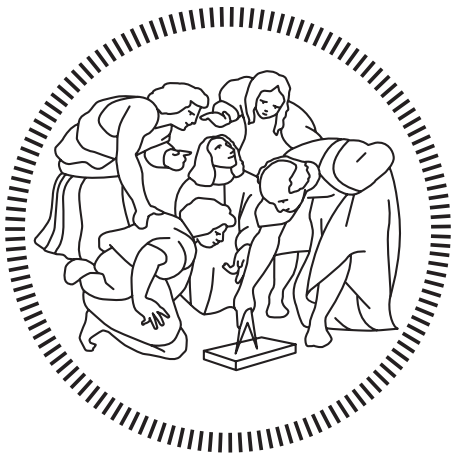

Preliminary Power Plant Simulator for Modelling of Hybrid Systems Scenarios

Supervisor
Chiar.mo Prof. Marco E. Ricotti

Co-Supervisors
Chiar.mo Prof. Antonio Cammi
Chiar.mo Prof. Stefano Lorenzi

Candidate
RICCARDO CHEBAC – 916781

Academic Year 2019 – 2020

Acknowledgements

Without any doubt the most difficult part of this entire thesis work is that of showing, in just few words, how grateful I am to the people who stood by my side during all these years of hard work and dedication.

I would like to express my very great appreciation to the professors of the department of Nuclear Energy in particular to prof. Ricotti and prof. Cammi for the trust, patience and support given me throughout all the work. I am also particularly grateful for the indispensable assistance and availability of prof. Lorenzi. Moreover I would like to thanks prof. Sokolova and prof. Fedorovich that proposed the intial outlines of this work. I wish to acknowledge the help provided by Seyed Hadi Ghazaie and Khashayar Sadeghi for their important contribution to this thesis.

Moreover I wish to thank my fellow colleagues and friends Piergiorgio, Pierfranceco, Mario, Letizia, Jacopo, Arianna, Francesco, Irene and Lorenzo which always were present and made me face every problem with a smile. I would like to offer my special thanks to my longtime friends Camilla, Valerio, Lucilla, Mattia, Gabriele, Giuliano and to Federico and his family which has welcomed me as their own son.

From my Russian experience I wish to acknowledge the help provided by my tutor Maria and by my friends Camilla and Karim for their thoughtfulness and sincerity that distinguishes them.

A heartfelt thanks goes to my family in particular to my grandparents. Thank you for following me in this path with your love and kindness which not only helped my during the difficult times but also made me a better person. I have to be especially grateful to my grandmother Gabriella, too unfortunate that for so little she will not see me graduate.

Finally my greatest thanks of all have to go to my Mom Stefania, my Dad Dan and my brother Marco of which I'm really proud of. Every accomplishments, all the experiences I lived and all I've learnt, started from you. The person that I am, is thanks to you. So trust me if I say that being grateful to you is a gross underestimation.

THANK YOU

Abstract

In the near future a substantial share of the world energy production will be given by renewable energy sources. Given their intrinsic intermittency, a study of future power generation and distribution needs to be assessed. Therefore a change in how grids are developed and built is necessary to ensure high reliability and frequency stability. For this purpose Generation-IV reactors should be developed to operate in a flexible manner. In the present work, a model of the Advanced Lead Fast Reactor European Design (ALFRED) will be created and put inside a simulated fully meshed grid environment. A suitable controller for said reactor will be developed to cope with grid frequency stabilization and steam extraction for cogenertion options. Given the large thermal inertia of this technology, a novel control strategy compared to the widely adopted one for light water reactors will be used by keeping constant the thermal power while the mechanical power at the alternator is adjusted via the turbine admission valve. Verification tests show the feasibility of this strategy taking into account the physical constraints of the system. Various studies found that the *Load following by cogeneration* is an economically more viable option compared to the well known thermal power variation. Therefore an effort has been made to develop models of different desalination technologies such as reverse osmosis (RO), multi-effect distillation (MED) and multi-stage flashing (MSF) to be studied in conjunction with the reactor. Preliminary simulations show that RO and MED are more suitable to be coupled with energy production systems. To further add completeness to the model, wind and photovoltaic power generation as well as battery storage systems have been implemented. The 13^{th} of July 2020 for both meteorological and energy demand data was simulated. Various scenarios pertaining: preprogrammed cogeneration, excess electricity redirection to the RO plant, preprogrammed time dependant charge/discharge battery control strategy and RO with battery coupling were simulated. The load follow by cogeneration was simulated for a reactor otherwise working in base load. All the other simulations were carried out both for a base load and a load following reactor configuration. The results show a higher degree in load following by using battery and RO technology for base load configuration and RO only for load following configuration. The latter happens to be the best option overall in terms of grid stability and meeting the electrical demand requirements. Given the modularity of this simulator, further systems can be added in future as new reactors, hydrogen and bio-fuel production etc. The outcomes of every simulation could then be used as an input to a further techno-economical study.

Sommario

Nel prossimo futuro una quota sostanziale della produzione mondiale di energia sarà data da sorgenti rinnovabili. Data la loro intrinseca intermittenza, è necessario valutre futuri scenari di generazione e distribuzione di energia. Pertanto è necessario un cambiamento nel modo in cui le reti vengono sviluppate e costruite per garantire un'elevata affidabilità e stabilità di frequenza. A tal fine, i reattori di quarta generazione dovrebbero essere sviluppati per funzionare in modo flessibile. Nel presente lavoro, un modello del progetto europeo avanzato del reattore veloce al piombo (ALFRED) verrà creato e inserito all'interno di un modello di rete fortemente magliata. Un controllore adatto per detto reattore sarà sviluppato per far fronte alla stabilizzazione della frequenza di rete e all'estrazione del vapore per opportune opzioni di cogenerazione. Data la grande inerzia termica di questa tecnologia, verrà utilizzata una nuova strategia di controllo rispetto a quella ampiamente adottata per i reattori ad acqua leggera mantenendo costante la potenza termica mentre la potenza meccanica all'alternatore viene regolata tramite la valvola d'ammissione in turbina. I test di verifica mostrano la fattibilità di questa strategia tenendo conto dei vincoli fisici del sistema. Vari studi hanno evidenziato che una strategia di *Load following by cogeneration* è un'opzione economicamente più praticabile rispetto alla ben nota variazione di potenza termica. Pertanto è stato fatto uno sforzo per sviluppare modelli di diverse tecnologie di desalinizzazione come l'osmosi inversa (RO), la distillazione multieffetto (MED) e il flashing multistadio (MSF) per essere studiato in combinazione con il reattore. Le simulazioni preliminari mostrano che RO e MED sono più adatti per essere accoppiati a sistemi di produzione energetica. Per aggiungere ulteriore completezza al modello, sono stati implementati sistemi di generazione di energia eolica e fotovoltaica, nonché sistemi di accumulo delle batterie. È stato simulato il 13 di luglio 2020 avendo i dati meteorologici ed energetici a disposizione. Sono stati simulati vari scenari. Il primo relativo alla cogenerazione preprogrammata durante le ore notturne. Gli altri scenari sono stati analizzati con due configurazioni del reattore: una in carico base ed una per l'inseguimento del carico. Su queste configurazioni sono state simulate: la possibilità di reindirizzamento dell'elettricità prodotta in eccesso all'impianto RO, la strategia di controllo per il pacco batterie e l'accoppiamento fra queste due. I risultati mostrano un migliore inseguimento del carico nel caso di utilizzo congiunto di batterie con RO per la configurazione carico base. La configurazione per l'inseguimento del carico trova invece la soluzione migliore nell'utilizzare solamente l'impianto RO. Quest'ultima è stata trovata essere, fra tutte, la soluzione migliore per avvicinare domanda e produzione elettrica. Data la modularità di questo sistema, in futuro potranno essere aggiunti ulteriori sistemi come nuovi reattori, produzione di idrogeno e biocarburanti, ecc. I risultati delle simulazioni potranno poi essere utilizzati come input per un possibile studio tecnico-economico.

Estratto

Affinché si riesca a raggiungere gli obiettivi prefissati dagli accordi di Parigi, ovvero di mantenere l'incremento medio di temperatura della Terra sotto i $2\,°C$, nel futuro prossimo bisognerà spostare la produzione d'energia da fonti fossili ad alternative senza emissioni di CO_2. A tal scopo è previsto un incremento dell'utilizzo di fonti rinnovabili quali solare e eolico che passerà dall'attuale 26.6% a 45%. Una così forte penetrazione di queste tecnologie nella rete elettrica mondiale porterà a dover rimodellare e cambiare le reti stesse in cui esse risiedono. Questo è dovuto principalmente ai limiti fisici delle rinnovabili quali intermittenza, incertezza di produzione e variazione di efficacia in base all'area geografica in cui sono installate. Se si vuole dunque incrementare lo share delle rinnovabili, un drastico cambiamento nella rete e in come produciamo l'energia dovrà essere apportato. Questo sarà possibile con l'utilizzo di sistemi di accumulo e con la creazione di impianti che possano facilmente ed economicamente lavorare ai carichi parziali. Una delle tecnologie che dovrà essere rielaborata sulle basi di quanto appena detto è il nucleare. Storicamente questi impianti sono stati creati per assolvere al compito di copertura del carico base, non variabile. Nazioni come Francia e Germania sono riuscite a seguire con successo il carico. Questo è stato possibile tramite appropriati sistemi di controllo sulla potenza del reattore. Tipicamente gli unici problemi riscontrati sono stati l'usura accelerata delle componenti del reattore e la riduzione del guadagno avendo dovuto far lavorare l'impianto a condizioni inferiori a quelle nominali. Un'alternativa proposta che può migliorare l'economia dell'inseguimento del carico per un reattore e quella del *load following by cogeneration*. In questa tecnica il livello di potenza del reattore rimane invariato e si reindirizza il surplus energetico su impianti secondari quali desalatori, produzione d'idrogeno e molti altri. In quest'ottica, una flotta di SMR è molto interessante in quanto permetterebbe di far lavorare tutti i reattori a carico nominale e di scollegare dalla rete una parte di essi durante le ore a bassa richiesta energetica. Se si parla di cogenerazione è di fondamentale importanza capire che processi industriali si vogliono accoppiare, in modo tale da definire le temperature d'esercizio e di conseguenza la tipologia di reattore più adeguata.

Il seguente studio verterà sullo sviluppo di un simulatore di un reattore di IV generazione raffreddato al piombo, ALFRED il quale verrà immesso a lavorare in una rete fortemente penetrata da rinnovabili, in particolare eolico e solare, verrà accoppiato a diverse tecnologie di desalazione, osmosi inversa e distillazione multi-effetto, e ad un sistema di accumulo basato sulla tecnologia delle batterie agli ioni di litio.

Il simulatore dell'intero impianto nucleare è stato sviluppato all'interno del software *Dymola* basato sul linguaggio di *Open Modelica*. Il vantaggio di questo sistema rispetto

ad altri è la possibilità di sfruttare un approccio di tipo acausale cioè non vi sono input ed output definiti. Questo permette una migliore descrizione dei sistemi fisici che hanno relazioni fortemente non lineari. Inoltre è altamente modulare e ogni componente rappresenta una zona o componente fisico dell'impianto.

Il nocciolo, mostrato in figura 1, è stato riprodotto sfruttando la cinetica puntuale del reattore, un modello 1-dimensionale per lo scambio termico e un modello dei precursori basato su 8 gruppi. Il nocciolo a sua volta è diviso in tre componenti: *Kinetics* che descrive l'evoluzione temporale dei neutroni e dei precursori, *Fuel Rods* il quale descrive l'andamento termico delle barre di combustibile tramite l'equazione di Fourier tempo dipendente, *Lead Tube* descrivente il flusso del piombo fuso in tubi cilindrici.

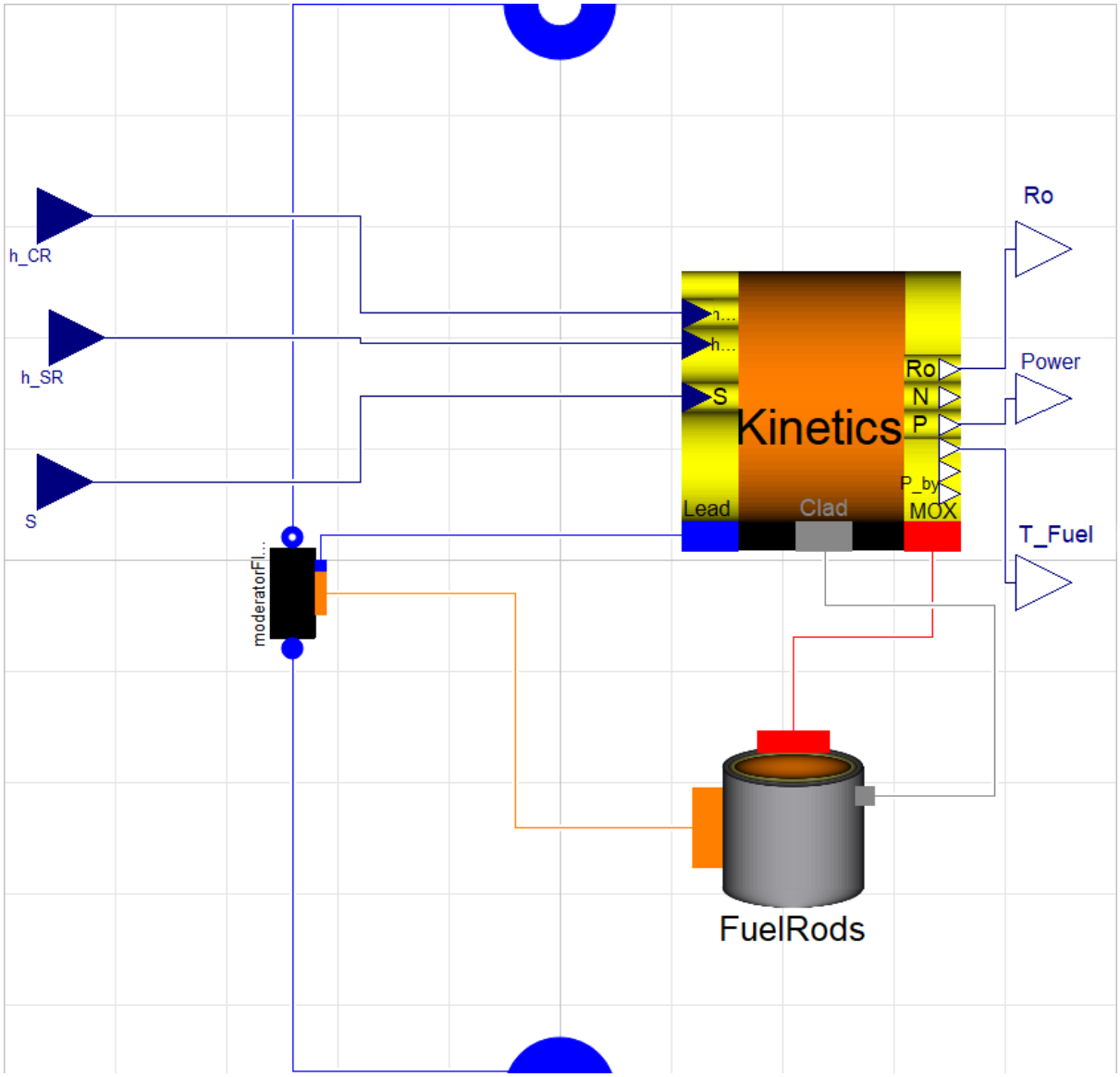

Figure 1: Modello nocciolo in Dymola

Per il circuito primario due piscine e due tubi sono stati utilizzati per modellare la gamba calda e fredda con relative inerzie termiche. Un modello 1-dimensionale per il generatore di vapore a baionetta in contro corrente è stato implementato. Il blocco creato utilizza come modello di scambio termico lato acqua la correlazione di Dittus-Boelter per condizioni monofase e Chen per il bifase. Lato piombo la correlazione di Ibragimov-Subbotin-Uhakov è stata ritenuta adatta da essere implementata. Da notare che nel progetto del reattore i generatori di vapori usati sono otto mentre qui è stato modellizzato un solo generatore avente le prestazioni totali. Il blocco turbina (figura 2) è stato creato utilizzando due stadi, alta e bassa pressione con efficienze meccaniche ed isoentropiche mediate sugli stadi reali. Fra i due stadi sono state interposte due valvole, *Bleed* e *Bleed*1 che permettono l'estrazione di vapore alla pressione desiderata. La valvola d'ammissione in turbina verrà utilizzata per la regolazione della frequenza primaria mentre la valvola di bypass come controllo sulla pressione del secondario.

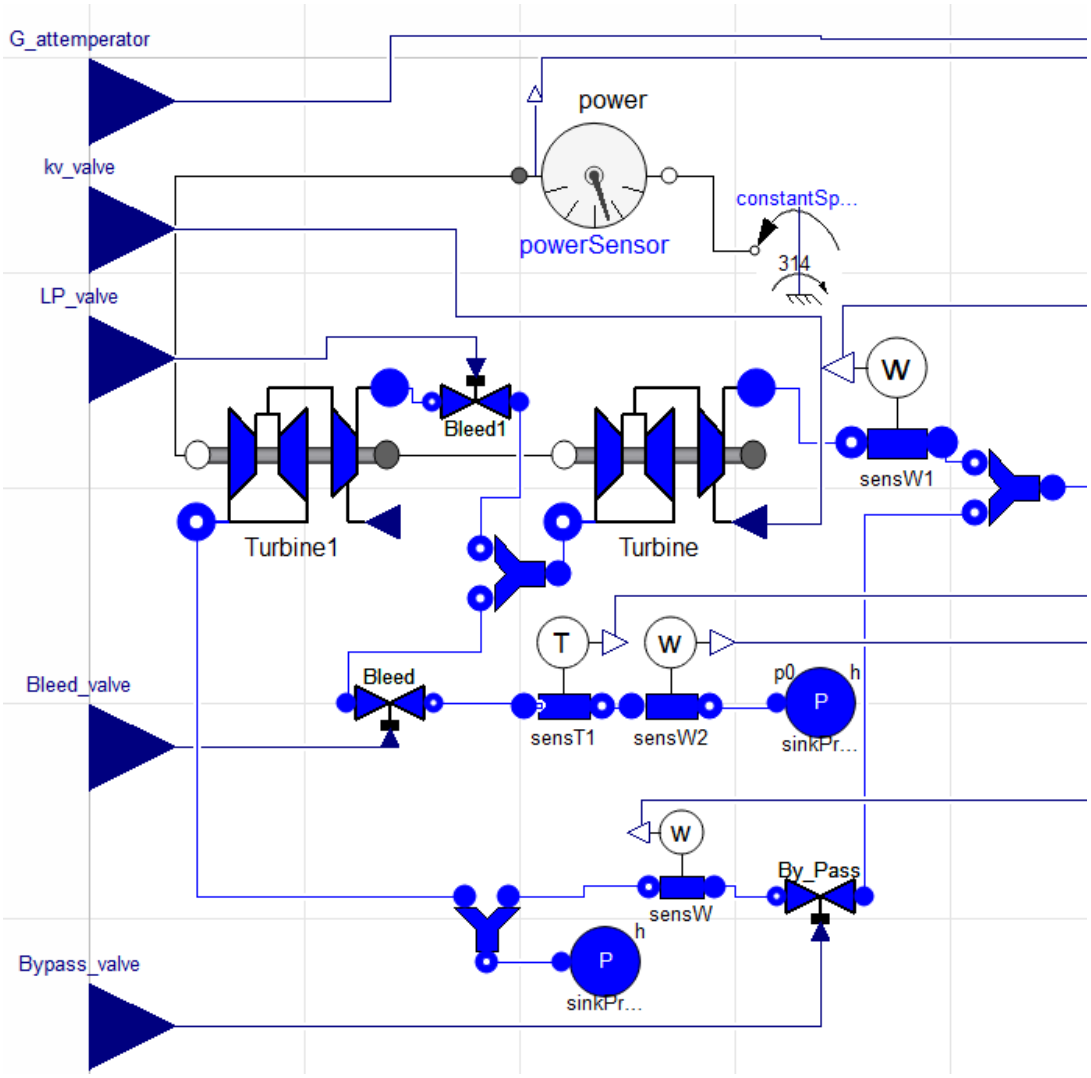

Figure 2: Modello di turbina con valvole per l'estrazione di vapore

Costruito il modello si è andata a testare la dinamica libera dell'intero impianto. Sono

stati eseguiti test mediante variazione dell'altezza delle barre di controllo, incremento della portata di acqua nel secondario e verifica della capacità di estrazione delle valvole *Bleed* e *Bleed*1. I risultati mostrano una buona vicinanza tra i valori di progetto e quelli di simulazione nonché tempi caratteristici congruenti al comportamento dinamico atteso. Verificato che il modello simulasse correttamente l'impianto, l'intero blocco è stato esportato in Simulink dove si è aggiunto un controllore. Le variabili controllate sono:

- Potenza termica
- Pressione secondario
- Temperatura gamba fredda
- Calore per cogenerazione
- Potenza meccanica

Considerando la velocità e inerzia termica del piombo, un inseguimento del carico basato sul cambio di potenza termica, come nei reattori ad acqua leggera, è impensabile date le veloci costanti di tempo richieste dalla rete. Tenendo ciò in considerazione, si è deciso di lavorare esclusivamente sul secondario espellendo il vapore non necessario alla produzione elettrica e indirizzandolo direttamente al condensatore. Inoltre una strategia denominata *Constant Pressure* è stata adoperata sempre sul secondario per far lavorare il generatore di vapore in condizioni nominali. Per il controllo della frequenza di rete, il controllore è stato sviluppato in modo tale da avere un valore desiderato di *droop* intorno al $4 - 5.7\%$ tipico dei reattori nucleari. Per testare la bontà del controllore, l'impianto così creato è stato collegato ad una semplice rete sincrona trifase con carico statico a 130 MWe (figura 3). Qui si è verificato la capacità del controllore di mantenere la facility ai valori nominali durante un incremento di potenza termica. Inoltre è stato testato il controllo per cogenerazione in un caso semplice di inseguimento del carico. In entrambi i casi il controllore è riuscito nel suo intento con le dinamiche e tempistiche richieste.

Successivamente sono stati svilupati i modelli degli impianti di desalazione, in particolare:

- RO
- MED
- MSF

Gli ultimi due impianti sono di tipo termico e richiedono calore per il corretto funzionamento. I risultati mostrano una netta superiorità dell'osmosi inversa sulle altre due tecnologie in quanto produce molta più acqua a parità d'energia in ingresso. Inoltre l'utilizzo di quest'ultima permetta una semplificazione dell'impianto in quanto non richiedente modifiche alla turbina per l'estrazione di vapore. Bisogna però notare che

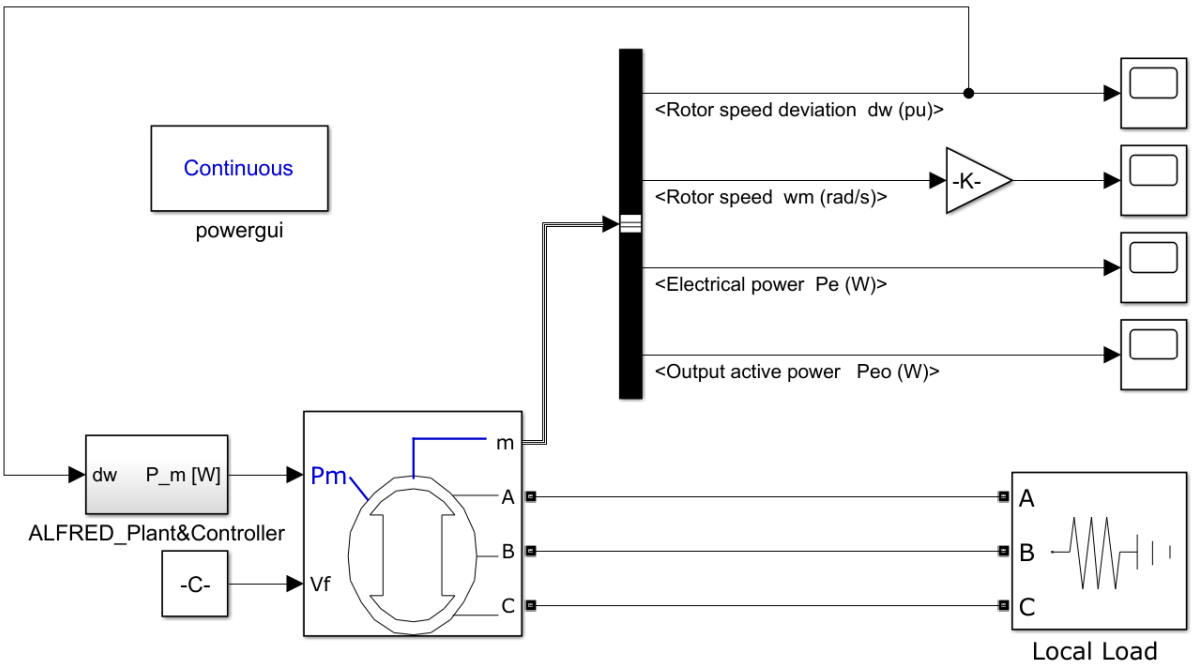

Figure 3: Impianto ALFRED connesso ad una rete trifase statica

l'RO non è economicamente vantaggioso per gli alti costi di O&M associati alle acque ad alto contenuto salino. In questi casi bisogna scegliere una fra le due tecnologie rimanenti. Qui i risultati mostrano un netto vantaggio del MED sul MSF. Per il primo sia la richiesta termica che elettrica è inferiore. Inoltre bisogna paragonare le temperature alle quali questi due sistemi lavorano. Il MED infatti lavora intorno ai $70 - 80\,°C$ mentre l'MSF sui $120\,°C$. Questo implica che, oltre alla maggiore efficienza energetica, il MED ha anche un minore impatto sulle performance dell'impianto permettendo al vapore di espandere maggiormente in turbina. Dunque si è ritenuto che i due sistemi da dover simulare fossero l'osmosi inversa e la distillazione multi-effetto. La tabella 1 evidenzia la superiorità del MED sul MSF sfruttando i risultati dei modelli sviluppati.

Desalination Plant	Required electrical energy (MWE)	Capacity (m^3/day)
MED	6.78	4160
MSF	12.69	3910

Table 1: Capacità e calore richiesto per impianti MSF e MED a fronte di un input termico a 10 MWth

Per i simulatori di impianto eolico, fotovoltaico e d'accumulo è stata utilizzata la libreria di Mathworks *Microgrid system development and analysis* previa la modifica dei singoli blocchi per poter funzionare in una rete a 50 Hz invece che a 60 Hz. La scelta è stata fatta data la semplicità di questi modelli che direttamente possono essere collegati ad una rete trifase senza il bisogno di aggiungere alternatori e altri componenti. Sia l'impianto solare che eolico sono stati dimensionati per una potenza massima di 10

MWe. La potenza del pacco batterie è stata fissata a 5 MWe. L'impianto solare richiede come input l'irradianza in W/m^2, l'eolico la velocità del vento in m/s. Avendo ora tutti i blocchi testati e verificati si è passato alla costruzione del modello di rete elettrica. E' stata simulata una rete fortemente magliata alla quale sono stati collegati il pacco batterie, i due impianti rinnovabili, gli impianti di desalazione ed il reattore. E' stato inoltre aggiunto un blocco *Variable Load* che permette di creare una curva di carico reale all'interno del nostro simulatore (figure 4 e 5). Sono stati utilizzati come input i dati meteorologici e riguardanti la richiesta energetica del 13 Luglio 2020 relativi alla zona di Milano.

Varie simulazioni sono state eseguite dove si verificavano diversi metodi per seguire la curva di carico per due configurazioni diverse del reattore nucleare: una in carico base ed una che permette di seguire il carico variando la potenza meccanica del reattore tramite l'apertura della valvola d'ammissione in turbina. Per entrambe le configurazioni sono stati simulati i seguenti scenari:

- Inseguimento del carico tramite carica/scarica programmata del pacco batterie
- Reindirizzamento dell'energia elettrica in eccesso all'impianto di desalazione RO
- Inseguimento del carico mediante carica/scarica prgogrammata del pacco batterie con reindirizzamento dell'energia elettrica in eccesso all'impianto di desalazione RO

Inoltre per la configurazione in carico base è stata aggiunta la possibilità di inseguire il carico tramite cogenerazione di 15 MWth programmata per l'impianto MED. I risultati mostrano che l'utilizzo di anche un semplice sistema di controllo di tipo carica/scarica (figura 7) programmato permette di ridurre sensibilmente la differenza fra la curva di carico e l'energia prodotta rispetto al caso sprovvisto di un sistema di accumulo (figura 6) per la configurazione carico base. Tecniche di controllo più sofisticate permetterebbero di ridurre la capacità del pacco batteria e avere una differenza fra le due curve minore. Risulta invece svantaggioso l'utilizzo del pacco batterie nel caso in cui venga fatta variare la potenza del reattore per inseguire il carico come si può notare nel paragonare figura 9 e 10 . Ovviamente se si utilizzano gli impianti di desalazione la curva di carico riesce ad essere seguita bene solo quando vi è un eccesso di produzione elettrica. Nel caso opposto la distanza fra le due curve rimane invariata. L'impianto MED (figura 8) necessita di un controllo più sofisticato dove si va a correlare l'energia elettrica a quella termica per ottimizzare l'inseguimento del carico. L'impianto RO ha una produzione di acqua fresca sensibilmente più alta rispetto alla controparte termica e permette una semplificazione d'impianto notevole. L'utilizzo congiunto di batterie e desalatore permette un miglior inseguimento del carico a scapito di una minor produzione d'acqua fresca per la configurazione carico base mentre non si può dire o stesso sulla configurazione per l'inseguimento del carico. In quest'ultimo scenario l'utilizzo del reattore solamente per seguire la richiesta permette di avere un eccesso di energia praticamente costante durante la giornata permettendo così di usare l'impianto di desalazione al massimo delle sue potenzialità e al contempo avere l'inseguimento del carico migliore.

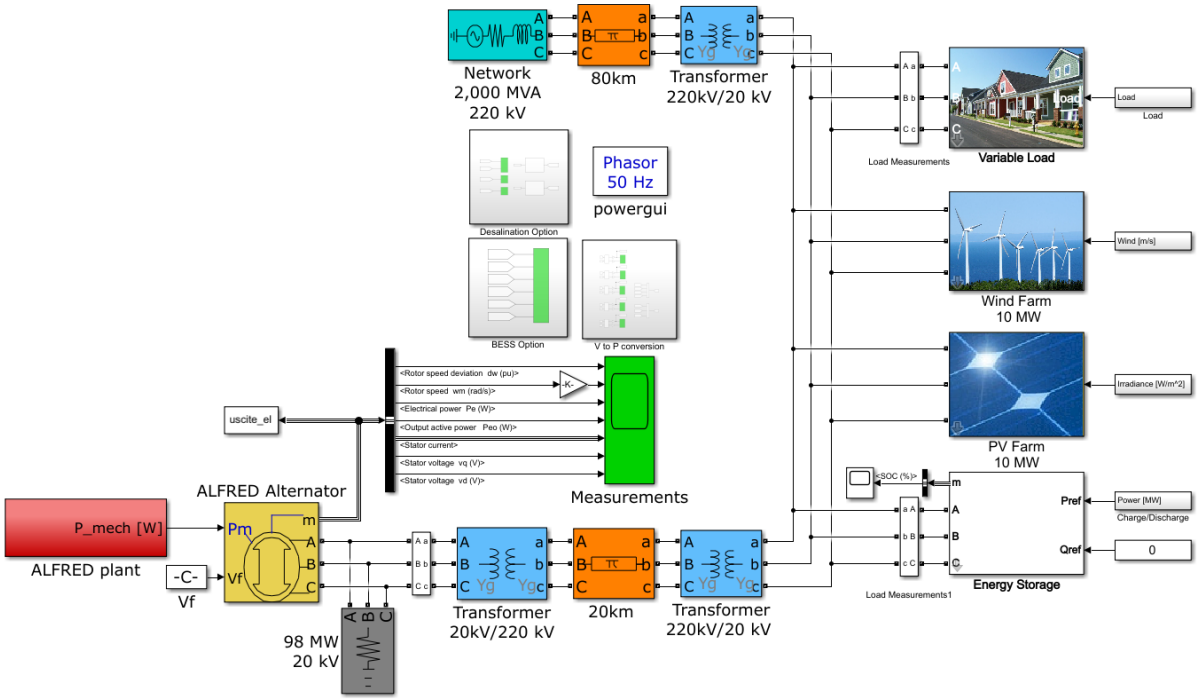

Figure 4: Modello elettrico di rete con sistemi puramente elettrici

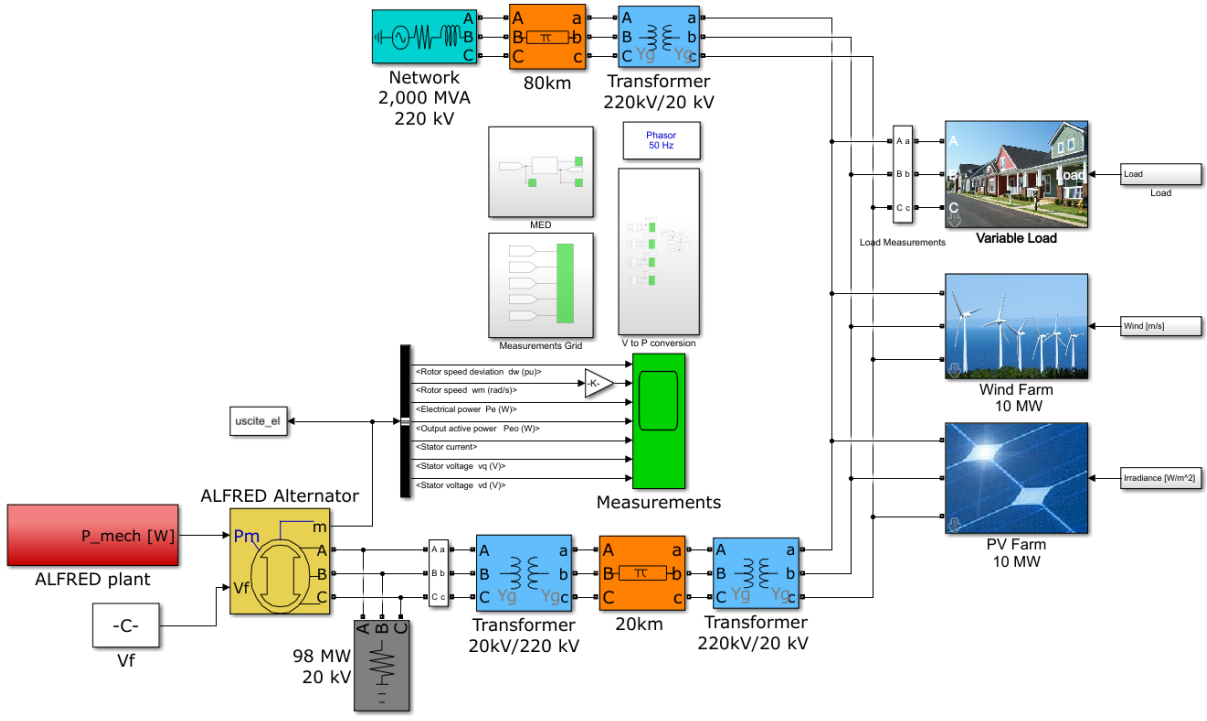

Figure 5: Modello elettrico di rete con sistemi cogenerativi

I risultati di produzione di acqua fresca nei vari scenari è riportata in tabella 2

Scenario	Produzione d'acqua (m^3)
RO con batterie	$4.1 \cdot 10^3$
RO senza batterie	$1.2 \cdot 10^4$
RO inseguimento carico con batterie	$5.73 \cdot 10^3$
RO inseguimento carico senza batterie	$1.49 \cdot 10^4$
MED	$7.9 \cdot 10^2$

Table 2: Produzione totale di acqua fresca giornaliera nei vari scenari

Da notare che per quanto gli impianti di desalazione possono lavorare a carichi parziali, è comunque consigliato tenerli ai valori nominali per un fattore puramente di tipo economico. Di conseguenza un inseguimento di carico programmato anche per l'osmosi inversa permetterebbe di scegliere il valore ottimale di capacità dell'impianto con però un ampliamento della differenza fra curva di carico ed elettricità prodotta. Questo problema non sussiste nel caso in cui si usi il reattore che insegue il carico accoppiato all'osmosi inversa dove la produzione è circa costante.

Si è dunque riusciti a creare un simulatore altamente modulare per lo studio della sinergia tra nucleare, rinnovabili, sistemi di accumulo e cogenerazione. E' possibile in futuro ampliare questa libreria aggiungendo altri impianti nucleari, impianti fossili, sistemi di accumulo termico e diversi processi industriali quali la produzione di idrogeno e bioetanolo etc. I risultati di queste simulazioni potranno poi essere usati come input per un'analisi tecnico-economica per permettere di comprendere la bontà degli scenari sopracitati e determinare quale sia la scelta migliore caso per caso.

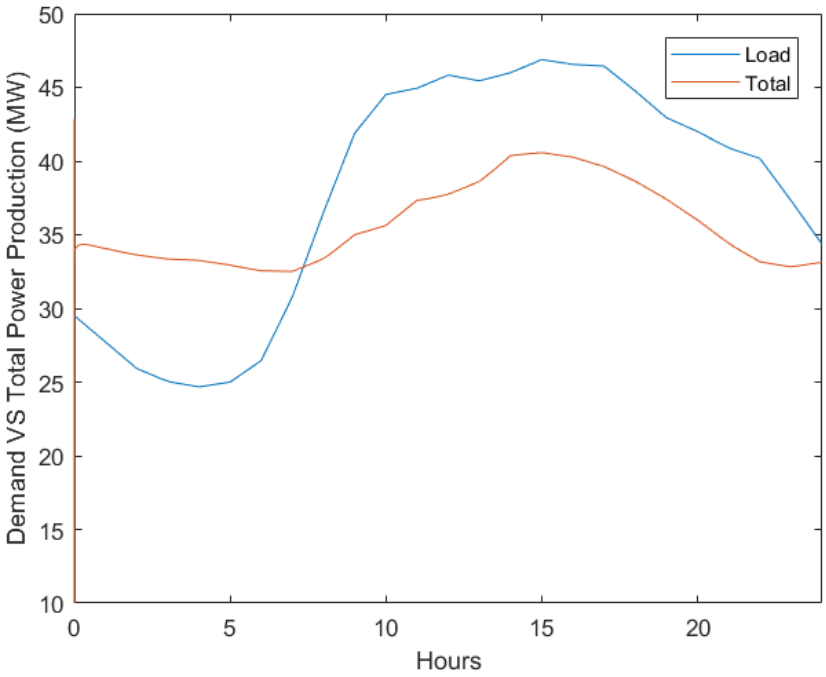

Figure 6: Richiesta VS produzione energetica senza sistemi di accumulo

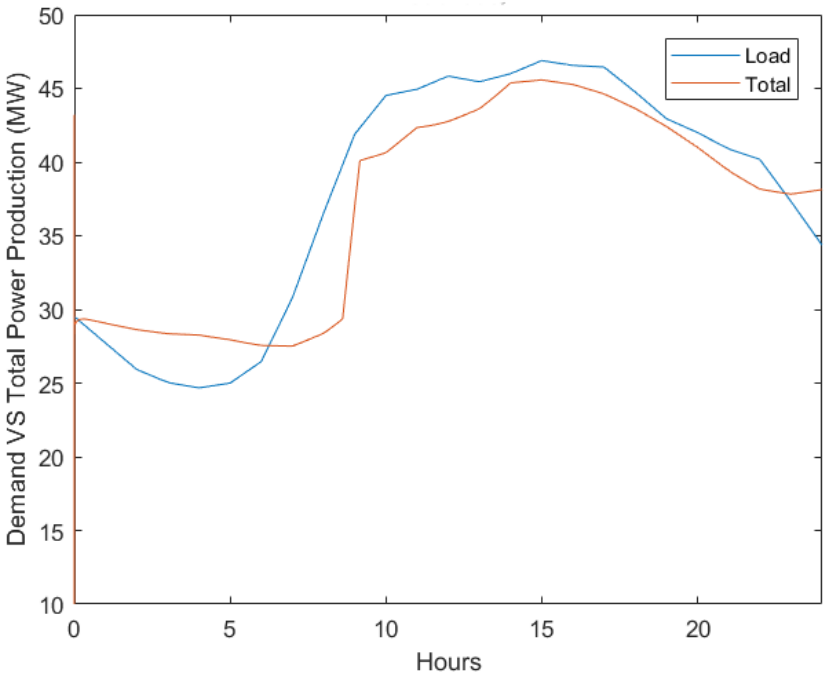

Figure 7: Richiesta VS produzione energetica con sistemi di accumulo

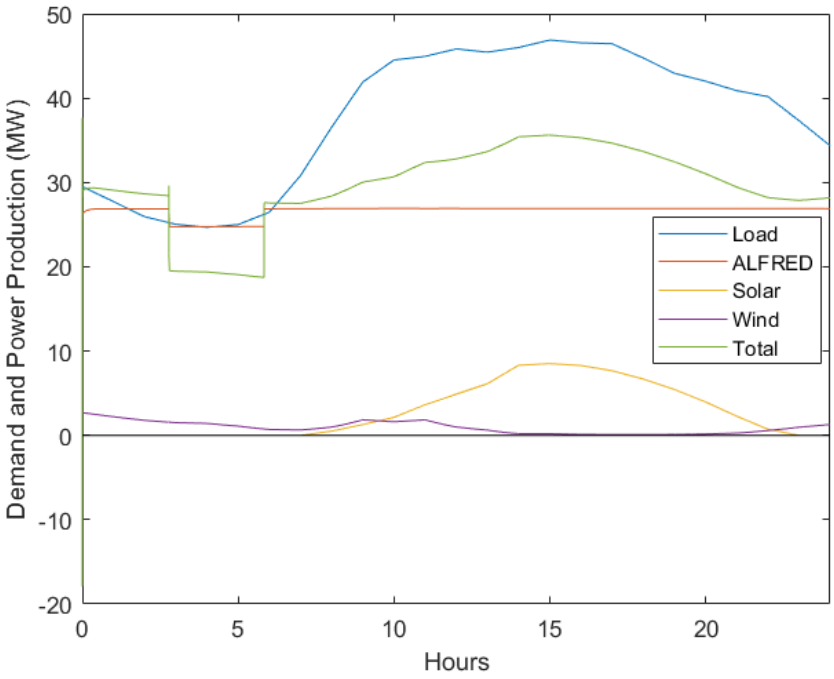

Figure 8: Richiesta e produzione di energia elettrica dalle varie fonti nel caso di cogenerazione con MED

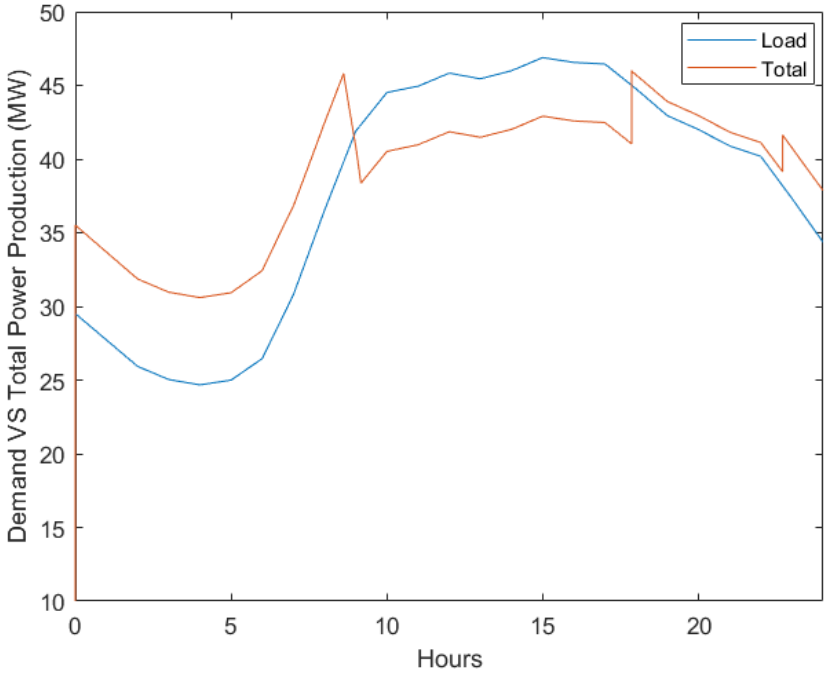

Figure 9: Richiesta VS produzione energetica in configurazione inseguimento carico con sistemi di accumulo

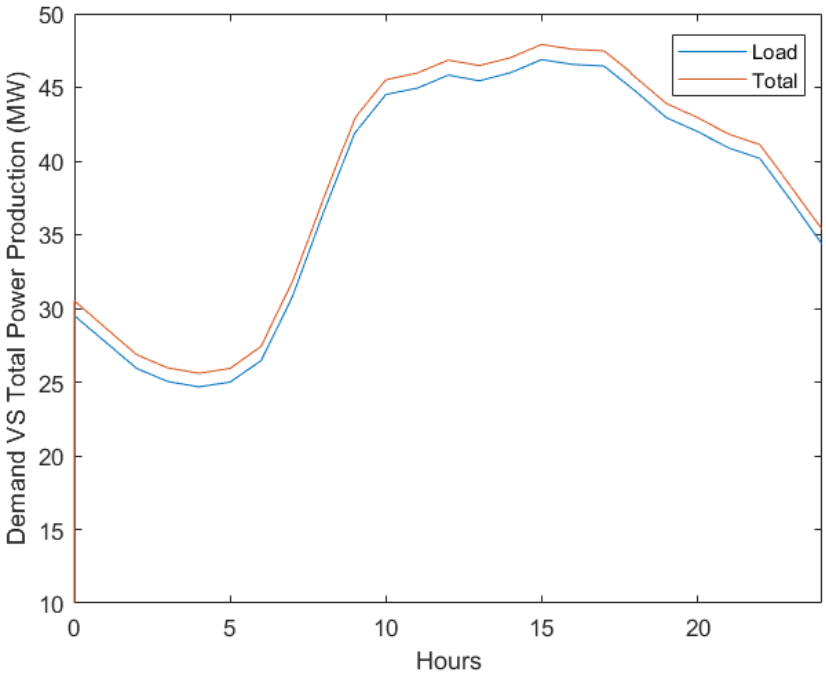

Figure 10: Richiesta VS produzione energetica in configurazione inseguimento carico

Contents

Acknowledgements iii

Abstract v

Sommario vii

Estratto ix

Contents xxii

List of Figures xxv

List of Tables xxvii

List of Symbols xxix

List of Acronyms xxxiii

1 Introduction 1

2 State of the Art 7
2.1 SMR Historical Overview . . . 7
2.2 ALFRED . . . 7
2.3 Renewable Energy Systems . . . 9
2.3.1 PV Technology Overview . . . 9
2.3.2 Wind Turbine Technology Overview . . . 15
2.4 Desalination . . . 20
2.4.1 Reverse Osmosis . . . 21
2.4.2 Multistage Flash Distillation . . . 22
2.4.3 Multieffect Distillation . . . 23
2.5 Energy Storage . . . 24
2.5.1 Battery Storage Systems . . . 26
2.6 Grid Frequency . . . 28

3 Dymola NPP Simulator 31
3.1 Dymola Software . . . 31
3.2 ALFRED Nuclear Power Plant . . . 31
3.2.1 Core . . . 32

3.2.2 Thermal Inertia and Transport Phenomena Modeling 36
3.2.3 Steam Generator 36
3.2.4 Turbine 37
3.3 Model Testing 38
3.3.1 Control Rod Step Insertion and Extraction 38
3.3.2 Water Mass Flow Rate Ramp Increase 43
3.3.3 Turbine Steam Extraction 46
3.4 Considerations 48

4 Simulink Library Development **51**
4.1 Plant Controller 51
4.2 Controller Testing 54
4.2.1 Reactor Thermal Power Increase 55
4.2.2 Cogeneration Control 60
4.3 Desalination Plant Models 65
4.4 Battery Energy Storage System, Solar and Wind Farm Models 67
4.5 Considerations 68

5 Complete Grid Model **71**
5.1 Final Model Assembly 71
5.2 Grid with Battery Storage System 73
5.3 Grid with Reverse Osmosis Plant 75
5.4 Grid with MED Plant 77
5.5 Reactor Load Follow 79
5.5.1 With Battery Energy Storage System 79
5.5.2 Without Battery Energy Storage System 84
5.6 Considerations 85

6 Conclusions **87**

List of Figures

1 Modello nocciolo in Dymola x
2 Modello di turbina con valvole per l'estrazione di vapore xi
3 Impianto ALFRED connesso ad una rete trifase statica xiii
4 Modello elettrico di rete con sistemi puramente elettrici xv
5 Modello elettrico di rete con sistemi cogenerativi xv
6 Richiesta VS produzione energetica senza sistemi di accumulo xvii
7 Richiesta VS produzione energetica con sistemi di accumulo xvii
8 Richiesta e produzione di energia elettrica dalle varie fonti nel caso di cogenerazione con MED xviii
9 Richiesta VS produzione energetica in configurazione inseguimento carico con sistemi di accumulo xviii
10 Richiesta VS produzione energetica in configurazione inseguimento carico xix

1.1 Forecast of the world electricity generation by source 2
1.2 Temperature ranges of heat application processes and types of nuclear power plant 3
1.3 Scheme of grid with hybrid systems implemented 4
1.4 Thesis work flowchart 6

2.1 ALFRED 3-D sketch and reactor block vertical sections 8
2.2 Bayonet SG configuration 9
2.3 Schematic of a PV cell 10
2.4 PV cell equivalent circuit 10
2.5 I-V and P-V characteristic curves 11
2.6 I-V characteristic at different Temperatures 12
2.7 Average irradiance annual sum in Italy 13
2.8 Average irradiance annual sum in Europe 14
2.9 Power and C_p behavior as a function of the wind speed 15
2.10 C_p behavior at constant speed with different pitch angle configurations . 16
2.11 Wind turbine area increase over the years 16
2.12 Wind speed variation in different geographical areas at different heights . 17
2.13 Wind speed distribution in Italy 18
2.14 Wind speed distribution in Europe 19
2.15 Desalination technologies overview 20
2.16 RO plant schematic 22
2.17 MSF plant schematic 23
2.18 MED process configuration: Forward feed 24

2.19 Grapical interpretation of a "$top - down$" model 25
2.20 Grapical interpretation of a "$top - down$" model with renewables 26
2.21 Energy density versus peak power 27
2.22 Peak shaving using battery technology 27
2.23 Primary, secondary and tertiary grid frequency definition 29

3.1 Dymola core model 34
3.2 Dymola *Hot Leg* and *Hot Pool* model 36
3.3 Dymola model of the Bayonet SG 37
3.4 Dymola model turbine group with extraction valve 39
3.5 Reactivity transient by control rod height variation 40
3.6 Reactivity transient close up by control rod height variation 40
3.7 Thermal power transient by control rod height variation 41
3.8 Mechanical power transient by control rod height variation 42
3.9 Temperature transient by control rod height variation 42
3.10 Water mass flow rate increase transient 43
3.11 Thermal power variation to a ramp increase in water mass flow rate . . . 44
3.12 Mechanical power variation to a ramp increase in water mass flow rate . 44
3.13 Temperature variation to a ramp increase in water mass flow rate 45
3.14 Pressure variation to a ramp increase in water mass flow rate 45
3.15 Turbine inlet mass flow rate 47
3.16 Mechanical power variation given by steam extraction 47
3.17 Thermal power not being affected by the steam extraction 48
3.18 Temperatures not being affected by the steam extraction 49
3.19 Efficiency variation given by steam extraction 49
3.20 Utilization factor increase given by the Q_{ut} 50
3.21 Mass flow rate of the extracted steam 50

4.1 ALFRED power plant controller 52
4.2 ALFRED power plant and controller 54
4.3 ALFRED power plant connected to a static grid 54
4.4 ALFRED power plant increase in thermal power 56
4.5 Mechanical power control 56
4.6 Turbine admission valve 57
4.7 Grid primary frequency 57
4.8 Pressure of the secondary loop during the transient 58
4.9 Turbine inlet mass flow rate 58
4.10 Temperature of the primary and secondary loop during the transient . . 59
4.11 Bypass valve during the transient 59
4.12 Thermal power for cogeneration 60
4.13 Steam extraction flow rate for cogeneration 61
4.14 Turbine admission valve 62
4.15 Grid frequency 62
4.16 Turbine inlet mass flow rate 63
4.17 Mechanical power production 63
4.18 Secondary loop pressure 64
4.19 Core thermal power 64

4.20 Temperatures of the primary and secondary loop 65

5.1 Entire grid model for electrical systems only 72
5.2 Entire grid model for thermal cogeneration systems 72
5.3 Electrical demand and separate contributions of every energy device . . . 74
5.4 Electrical demand VS. Total energy produced without battery storage system 74
5.5 Electrical demand VS. Total energy produced with battery storage system 75
5.6 Capacity of the RO plant during the day 76
5.7 Capacity of the RO plant during the day with batteries 76
5.8 Eergy demand and total energy production 77
5.9 MED electrical energy requirement related to a 15MWth input 78
5.10 MED heat input 78
5.11 MED capacity 79
5.12 Reactor load components 80
5.13 Reactor load following with battery pack 81
5.14 Grid frequency during the reactor load follow with battery pack 81
5.15 Grid frequency close up at 17 p.m 82
5.16 Plant pressure 82
5.17 Plant pressure close up 83
5.18 Reverse osmosis capacity with reactor following the load and battery pack 83
5.19 Reactor load following with no battery pack 84
5.20 Reverse osmosis capacity with reactor following the load and no battery pack 85

6.1 Electrical energy taken from the grid to compensate the demand 89
6.2 Libraries developed within the thesis work 90

List of Tables

1 Capacità e calore richiesto per impianti MSF e MED a fronte di un input termico a 10 MWth xiii
2 Produzione totale di acqua fresca giornaliera nei vari scenari xvi

2.1 Operational and performance parameters of most common desalination technologies 21

3.1 ALFRED main core parameters 32
3.2 Single bayonet SG parameters 37

4.1 Pairings between input and output variables for the control strategy . . . 52
4.2 Capacity and required heat of MSF and MED plant for a 10 MWth input 66
4.3 Solar farm 67
4.4 Wind farm 68
4.5 Battery storage system 68

5.1 Total fresh water produced in the various scenarios 86

List of Symbols

α	Heat Transfer Coefficient $\left(\frac{W}{m^2 k}\right)$
β	Effective delayed neutron precursor yield of group i $(-)$
Γ	Mass Flow Rate $\left(\frac{kg}{s}\right)$
Λ	Mean Generation Time (s)
λ	Precursors Decay Constant $\left(\frac{1}{s}\right)$
ω	Tube Perimeter (m)
Φ	Heat flux $\left(\frac{W}{m^2}\right)$
ρ	Density $\left(\frac{kg}{m^3}\right)$
ρ_c	Cladding Density $\left(\frac{kg}{m^3}\right)$
ρ_f	Fuel Density $\left(\frac{kg}{m^3}\right)$
ρ_g	Gap Density $\left(\frac{kg}{m^3}\right)$
ρ_{reac}	Reactivity (pcm)
σ	Droop $(-)$
τ	Integral Time (s)
c_c	Cladding Specific Heat$\left(\frac{kJ}{kgK}\right)$
C_f	Fanning friction factor$(-)$
c_f	Fuel Specific Heat$\left(\frac{kJ}{kgK}\right)$
c_g	Gap Specific Heat$\left(\frac{kJ}{kgK}\right)$
c_i	Precursor density of the i-th group $\left(\frac{1}{cm^3}\right)$
c_p	Specific Heat at Constant Pressure$\left(\frac{kJ}{kgK}\right)$

I_0	Saturation Current (A)
I_{Di}	Current through the diode (A)
I_{pv}	Photo-current (A)
k_c	Cladding conductivity $\left(\frac{W}{mK}\right)$
K_D	Doppler Constant (pcm)
k_f	Fuel conductivity $\left(\frac{W}{mK}\right)$
k_g	Gap conductivity $\left(\frac{W}{mK}\right)$
k_v	Admission valve coefficient $(-)$
n_{series}	Number of Series connected Cells $(-)$
q'''	Specific Heat $\left(\frac{W}{m^3}\right)$
R_s	Series resistor (Ω)
R_s	Shunt resistor (Ω)
T_{be}	Average boiling point elevation $(°C)$
T_{ih}	Temperature of heated water after the brine heater $(°C)$
T_{im}	Intermediate loop condenser return temperature $(°C)$
T_{ls}	Temperature of last effect in desalination system $(°C)$
T_{ov}	Overall water plant working temperature $(°C)$
V_T	Thermal voltage (V)
A	Area (m^2)
a	Ideality Factor of the Diode $(-)$
ATD	Average temperature drop between stages of MED plant$(°C)$
cvm	average specific heat of the brine $\left(\frac{kJ}{kgK}\right)$
f	Grid frequency (Hz)
h	Specific Hentalpy $\left(\frac{kJ}{kg}\right)$
I	Output Current (A)
IFR	Water flow through the intermediate heat exchanger$\left(\frac{m^3}{day}\right)$
IP	Intermediate loop pressure (bar)

IPE	Intermediate heat exchanger pump efficiency$(-)$
MBT	Maximum Brine Temperature $(°C)$
n	Neutron Density $\left(\frac{1}{cm^3}\right)$
P	Power (MW)
p	Pressure (Pa)
Q	Heat (MW)
r	Radius (cm)
S	Neutron source $\left(\frac{1}{cm^3 s}\right)$
T	Temperature $(°C)$
V	Output voltage (V)
v	Velocity $\left(\frac{m}{s}\right)$
W	Desalination capacity $\left(\frac{m^3}{day}\right)$
x	Steam quality $(-)$

List of Acronyms

ALFRED Advanced Lead Fast Reactor European Demonstrator. v, vii, ix, xxvii, 4, 5, 7, 8, 32, 36, 41, 46, 48, 51, 87, 88

AP Advanced Passive. 7

APWR Advanced Pressurized Water Reactor. 7

BWR Boiling Water Reactor. 2

DBP Driving Booster Pump. 66

DHR Decay Heat Removal. 8

EPR European Pressurized Reactor. 7

FA Fuel Assemblies. 8, 32

GIF Generation IV International Forum. 7

GOR Gain Output Ratio. 21, 65

HPP High-Pressure Pump. 66

IAEA International Atomic Energy Agency. 7

IC Isolation Condenser. 8

LFR Lead-cooled Fast Reactor. 4, 7, 51

LWR Light-Water Reactor. 3, 51

MED Multi-effect Distillation. v, vii, xii–xiv, xxv, xxvii, 21, 23, 24, 38, 46, 53, 60, 65, 66, 68, 71, 77–79, 85, 86, 88, 89

MOX Mixed Oxide (plutonium/uranium nuclear fuel). 7, 8, 32

MPa Mega Pascal. 8

MSF Multistage Flash Distillation. v, vii, xii, xiii, xxiii, xxvii, 21–24, 38, 60, 65, 66, 77, 88

MWe Megawatt Electric. xii, xiv, 5, 7, 53–55, 61, 66, 67, 77, 88

MWth Megawatt Thermal. xiii, xiv, xxv, xxvii, 8, 36, 60, 66, 77, 78, 88

NPP Nuclear Power Plant. 2, 3, 7, 53, 69, 86, 87

OE Other Expenses. 66

PID Proportional Integral Derivative. 53, 87

PV Photo-Voltaic. xxiii, 5, 9–11, 67

PWR Pressurized Water Reactor. 2

RO Reverse Osmosis. v, vii, xii–xiv, xxiii, xxv, 5, 21–23, 65–67, 71, 73, 75–77, 80, 85–88

SEC Specific Electricity Consumption. 66

SG Steam Generator. xxiii, xxiv, xxvii, 8, 9, 31, 36, 37, 43, 51

SMR Small Modular Reactor. ix, 2, 7

SP Seawater Pump. 66

STC Standard Test Condition. 11

Introduction

Throughout mostly the past two decades, the penetration of renewable energy power plants into the electrical grid has steadily increased. Considering both the public acceptability of this technology and the goals of the *Paris Agreement* [1] of keeping the Earth's average temperature below the $2\,°C$ increase from the pre-industrial level, it is foreseeable that in the near future the share of renewable energies in the global energy market will surely increase. It is expected that by 2040 their share will pass from nowadays 26.6% to approximately 45%(fig.1.1). The main advantages of this technology is the possibility of electricity production without emissions of greenhouse gasses, on-site power generation, reduction in fossil fuel dependence and a practically inexhaustible source of energy.

The fundamental electrical grid structure is slowly changing. Once there was a clear distinction between the producer, basically a large power plant, and the consumer. Nowadays renewable energy sources are leading the transition from a centralized power production unit to several small distributed plants. Therefore, to reach the goals envisioned, a radical revision of the current power grid infrastructure has to be undertaken. This is given by the intrinsic physical limitations of these technologies. Even though we are talking about different systems each with its own mean of power production such as solar and wind, all have in common some problems that ought to be solved or mitigated. The main issues are the variability due to meteorological and temporal availability of the source and the uncertainty given by unexpected changes in boundary conditions such as clouds, which reduce the overall irradiance reaching the solar panels, or gusts of wind that may cause the $cut\ off$ of the turbine with sudden interruption of power generation. Moreover geographical characteristics of each nation will make renewables more or less effective depending where they're built making them $location\ specific$.

Given these technical difficulties, a transition to high shares of renewables need a drastic change in grid design, a rethinking on how power plants are envisioned. Having a high share or intermittent energy brings the need for all the programmable power plants such as fossil fuel and nuclear to contribute heavily in the load following strategy. In such a context, supply and demand will be matched in a much more flexible and diverse manner. Moreover a strong penetration of renewable energy sources will bring to primary grid frequency destabilization which is of utmost importance to keep under certain maximum variations.

With all these considerations taken into account, a re-thinking on how nuclear power

plants deliver electricity to the grid must be undertaken. Historically NPP have been deployed for the production of base load electricity. Some countries such as France and Germany have successfully used their reactors also in load follow mode [2] by varying the power generation by means of control rod height adjustment in PWRs and by changing the coolant flow rate in BWRs.

The control strategies before mentioned aim at varying the reactivity of the fission reaction thus the nominal power output, therefore introducing thermomechanical stresses in the fuel which in modern reactors have to be kept minimal. This requires the reactor to operate under determined stability ramps, defined by the authorities therefore limiting the load following capabilities of these systems. A second major problem when instead we're dealing with primary frequency stabilization is the consistent loss of revenues given by the need to operate the reactor at a power level $2 - 3\%$ lower than nominal thus increasing the incidence of the capital cost per unit power output [3].

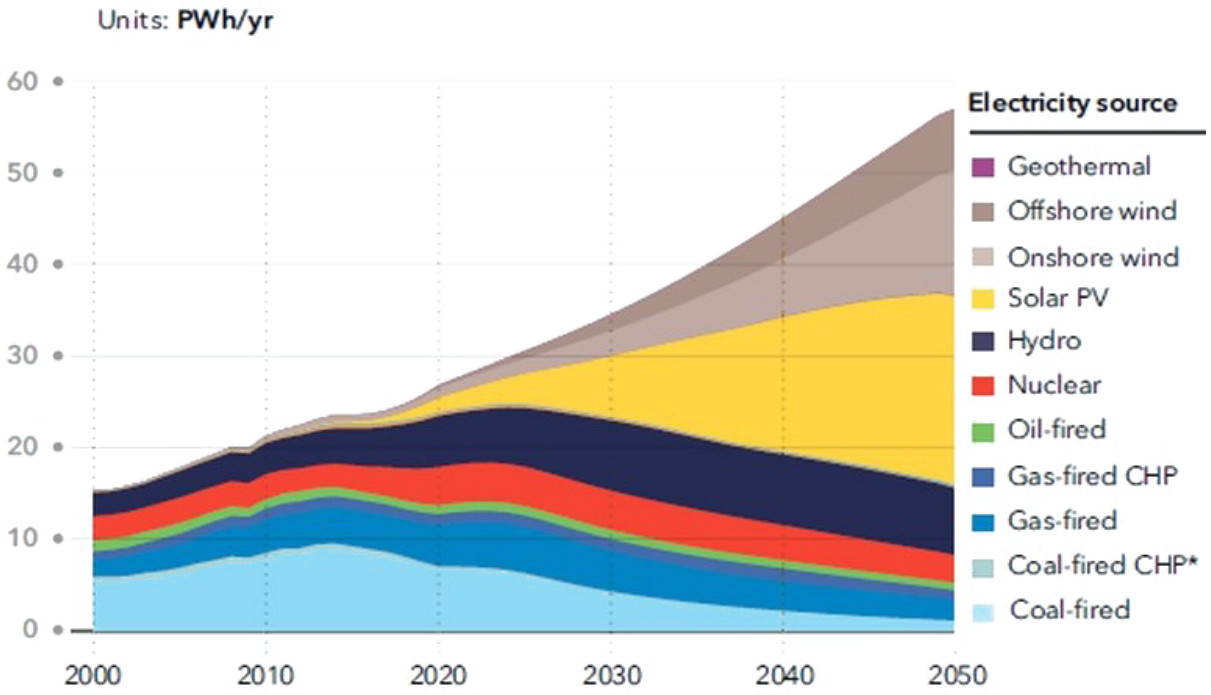

Figure 1.1: Forecast of the world electricity generation by source

An alternative solution can be *Load following by cogeneration* [3] where the nominal thermal power remains untouched and during the high load/high price hours of the day, all the heat is converted to electricity while during low demand/low price moments the excess power will be redirected to external, high energy requiring systems such as desalination plants, fuel or hydrogen production facilities and district heating.

For this purpose, a fleet of SMRs could be particularly advantageous over a conventional large reactor since the intrinsic modularity of the system opens the possibility of keeping all the reactors at 100% power and diverting, when needed, part or all of the heat produced by some of the reactors while keeping the others untouched.

While dealing with cogeneration it is of upmost importance to define the system we're considering. Different processes require different amounts of heat with temperatures ranging from $65 - 150°C$ [4]. Thus different reactor types will be more suitable for different types of cogeneration. Fig.1.2 gives a resume of the reactors usable in defined heat application processes. As it can be seen, LWR are not the best suitable reactor for load following by cogeneration. GEN IV reactors on the other hand have the possibility to be much more versatile and competitive in many diverse industries.

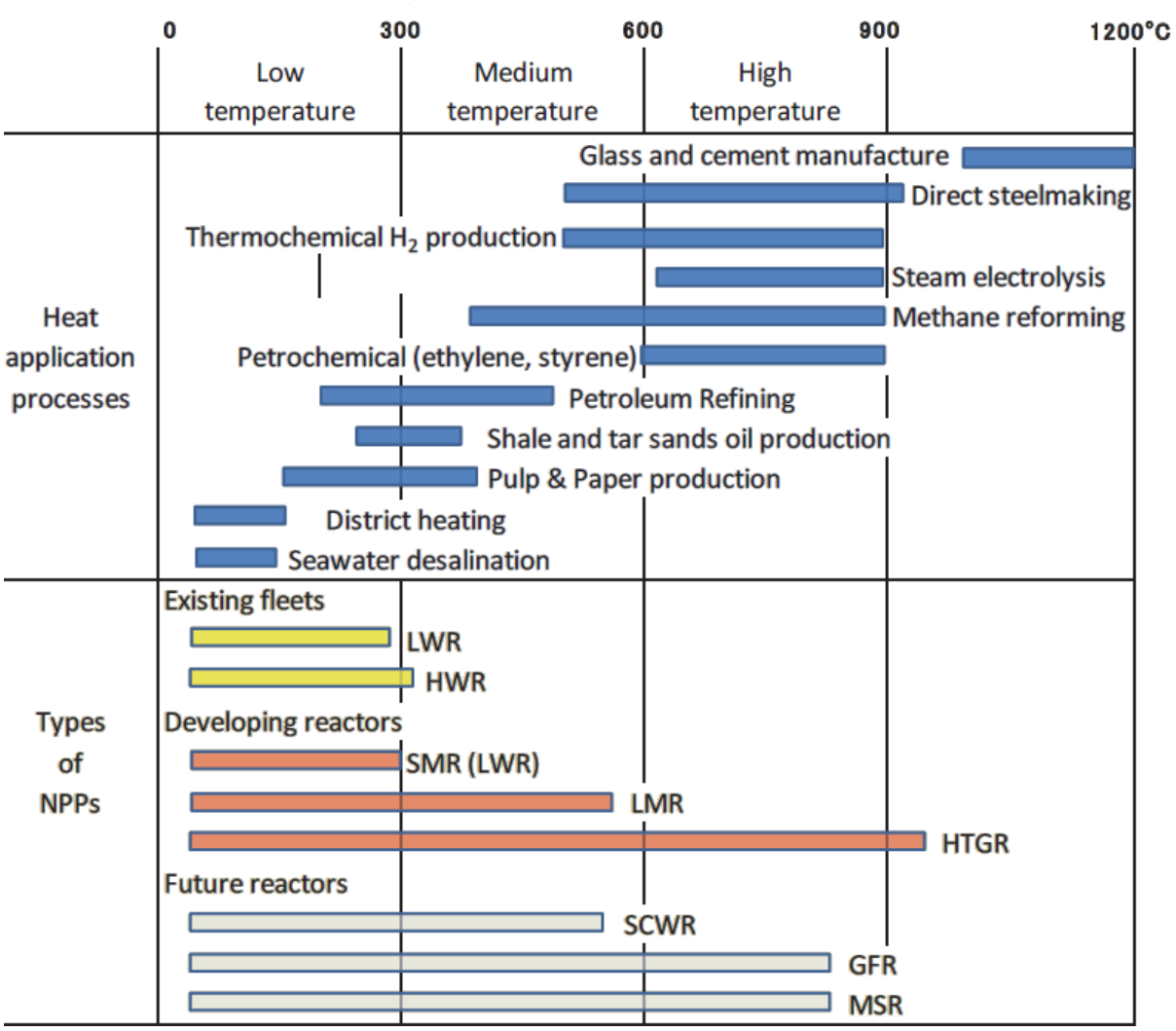

Figure 1.2: Temperature ranges of heat application processes and types of nuclear power plant

Because of all the different reactor technologies and industrial processes it is interesting to see which couplings are optimal and how the synergy between the two could be beneficial inside a grid with an important share of renewable sources. Furthermore it is important to understand what repercussions would have choosing a determined grid stabilization method like the one done by an NPP compared to a battery pack from a technical point of view. The International Atomic Energy Agency (IAEA) already carried out studies regarding the economic potential of hybrid systems in different scenarios [5] showing a higher profitability when nuclear is coupled with low capital costs industrial processes since are more likely

to utilize their flexibility to switch between electricity and the industrial product more often than their higher capital cost configurations increasing the profitability of the system.

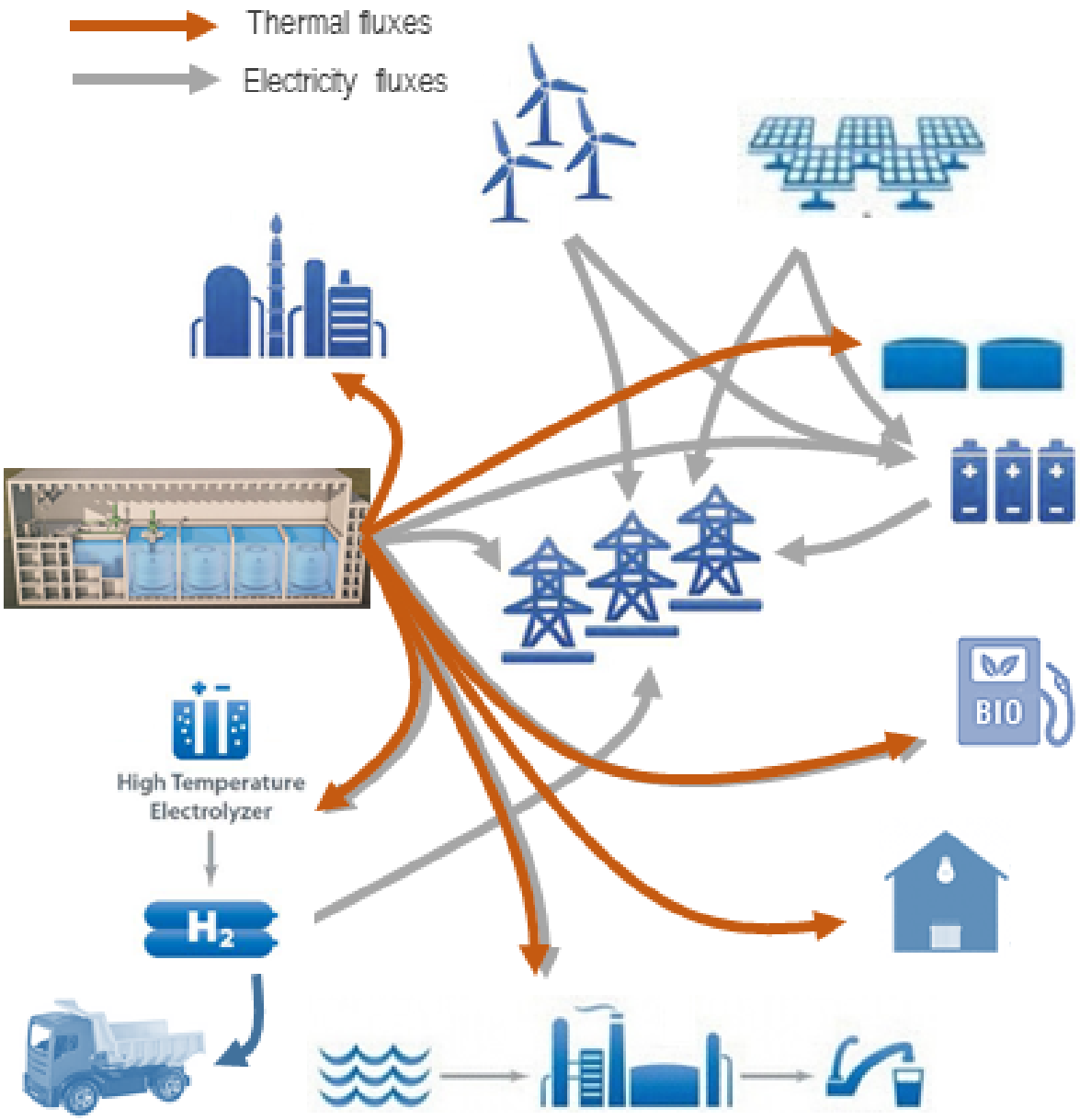

Figure 1.3: Scheme of grid with hybrid systems implemented

For these reasons in this thesis work a modular simulator capable of analyzing different scenarios and evaluate the the technical feasibility of each hybrid system will be created. The object oriented nature and the modularity of the built simulator will make this process extremely easy to accomplish by simply dragging and dropping the different sub-models created. Herein after a study will be held where a simulation of the LFR ALFRED, suitably modified to enable steam extraction from the turbine unit for heat application processes, will show the possibilities of this reactor to follow the load via cogeneration

in a grid deeply penetrated with renewables (10 MWe PV and a MWe wind farm) and compare this choice with the adoption of a classical load follow configuration and a base load configuration with, in both cases, the addition of different electrical systems such as battery storage system and RO technology.

In particular in Section 2 a state of the art review of the SMR technologies, thermal and electrical desalination plants and energy storage systems will be given. In Section 3 a detailed analysis of the Dymola simulator of ALFRED plant will be shown with different test cases (pertaining free dynamics conditions) to prove the validity of the model. A suitable controller will then be developed in Simulink in Section 4 as well as the models for desalination, battery energy storage systems, photo-voltaic and wind farms will be described and tested. Finally in Section 5 two complete grid models considering one only electrical systems and one thermal cogeneration will be simulated and the results will be discussed. The results aim to identify which configuration will induce less stress to the outer grid by better managing the load follow.

It has to be noted that this simulator will be used to give technical results on the physical feasibility of the system and could be used as an input to an economical analysis which is of fundamental importance for the overall understanding of the competitiveness of the system but outside of the scope of this work.

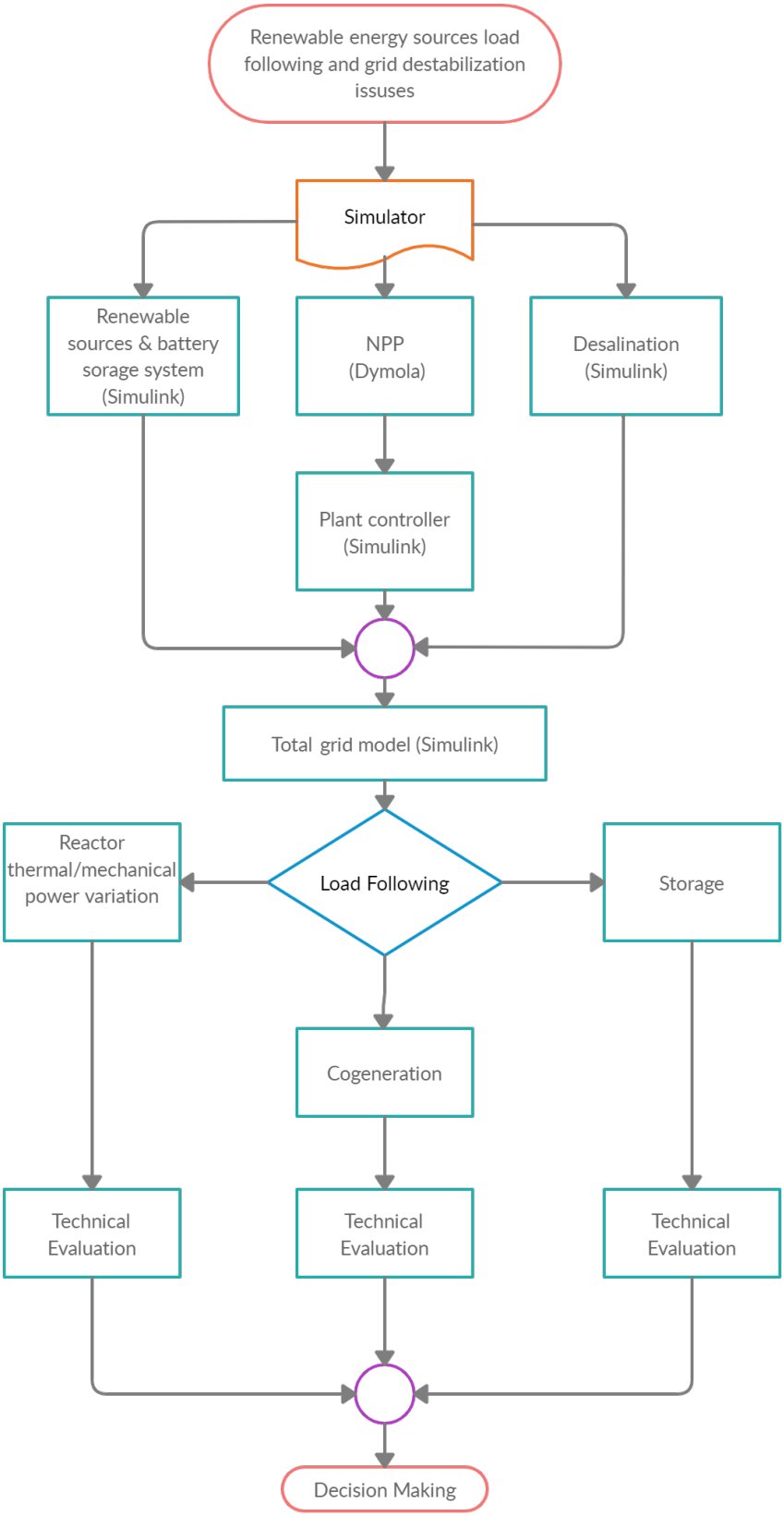

Figure 1.4: Thesis work flowchart

State of the Art

2.1 SMR Historical Overview

The NPP development in the last decades throughout different programs had a common trend where increasing the reactor size seemed the best way to make this technology competitive on the market. Economy of scale was ultimately what led to the evolution from the Westinghouse AP600 to the AP1000. Other generation III reactors showed the same behavior such as the APWR-Mistubushi and the EPR-AREVA with a nominal electrical power of 1700MWe the former and 1600MWe the latter. Unfortunately, as stated by Locatelli [6], the continuous delays and non-respect of the budget constraints during the plants construction makes the economies of scale fail and as such we now have mega-projects to deal with. Considering also the constantly increasing prices of oil, the now widespread attention to environmental related issues such as greenhouse gasses emissions and a more stringent regulatory system concerning safety of NPPs, renewed attention has been given to the SMR technology. Defined by the IAEA as reactors with nominal power equal or less to 300MWe, the SMR have enhanced safety features, easy portability, possibility to be manufactured in factories and lower financial risk.

2.2 ALFRED

Identified by the GIF as one of the six most promising GEN IV systems [7], the LFR technology is based on a fast neutron energy spectrum and a closed fuel cycle capable of efficiently managing minor actinides and convert fertile ${}^{238}_{92}U$ into fissionable ${}^{239}_{94}Pu$.

Lead as a coolant has interesting performances such as being inert, thus permitting important design simplifications, high boiling point which will lead to lower operational pressures and higher temperature therefore increasing the plant efficiency. Moreover it can use technologies already developed for the light-water counterparts such as passive heat removal systems, thereby enhancing the overall safety of the system. As an added bonus the use of MOX fuel make this technology an extremely unattractive route for theft of weapon-grade materials.

ALFRED is designed to have a nominal power of 125MWe. It will contain all the primary coolant in the reactor vessel in what is defined as a pool-type configuration as

shown in figure 2.1. The position of the core with respect to the riser, the SG and the downcomer enables natural circulation to occur.

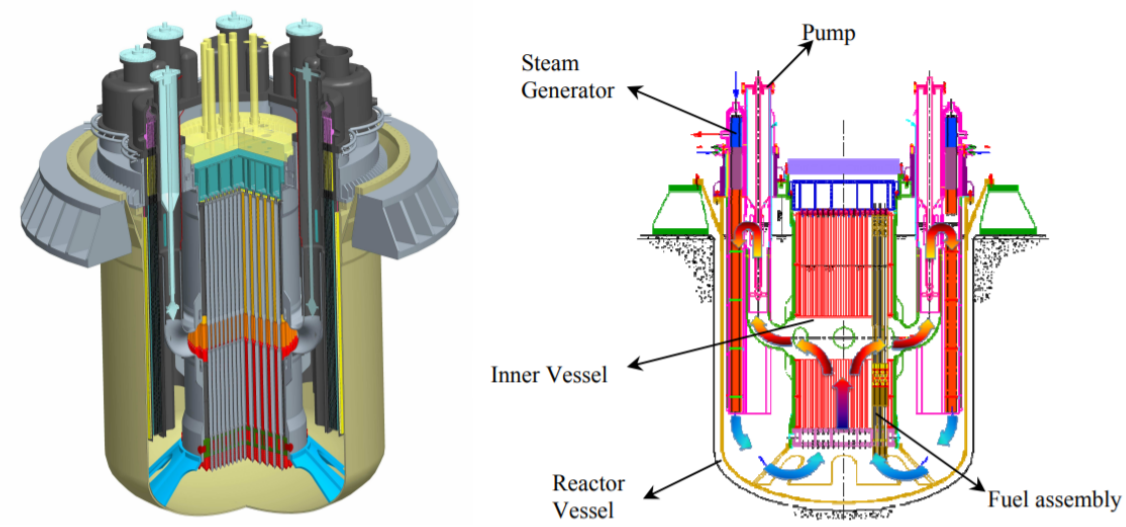

Figure 2.1: ALFRED 3-D sketch and reactor block vertical sections

An innovative solution has been used for the SG where a bayonet-type (fig.2.2) configuration ensures the production of super-heated steam at pressures of 180 MPa and temperatures of 450 $°C$. Thus enabling an estimated plant net efficiency of about 41%.

From a safety standpoint ALFRED uses two passive, independent Decay Heat Removal (DHR) system each having four ICs designed on a single failure criteria (i.e. if one IC fails the DHR still works).

As previously mentioned the core uses MOX fuel. The nuclear fuel is inside wrapped hexagonal FA and produces a nominal thermal power of 300 MWth.

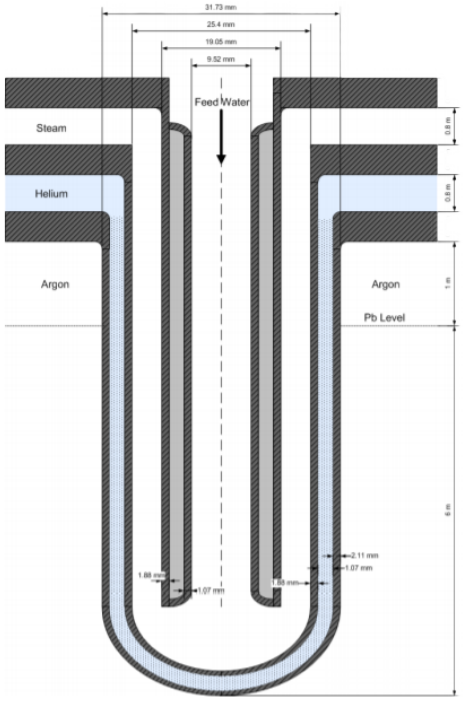

Figure 2.2: Bayonet SG configuration

2.3 Renewable Energy Systems

By definition the term "renewable" is used for all those energy sources that are non-depletable or naturally replenishable. They're considered as the fastest growing energy source and is envisioned that by 2024 the renewable source make up on the global electricity production will increase from 26% to 30% moreover they will expand by 50% in the next fifty years. Unfortunately these technologies have important drawbacks such as intermittency, the need for storage and geographical limitations. Among all the different technological solution herein it will be analyzed the impact of two of the most common and well known systems: wind turbines and solar PV.

2.3.1 PV Technology Overview

Working Principals

The PV effect is the direct conversion of light to electricity via the photo-electric phenomenon. A solar cell is basically a p-n junction diode. The absorption of light creates a number of electron-hole pairs by breaking the thermodynamic equilibrium condition of the junction (fig. 2.3). The diffusion of the holes to the p-junction and of the electrons to the n-junctions creats a voltage in between which can be used when a load is connected to it.

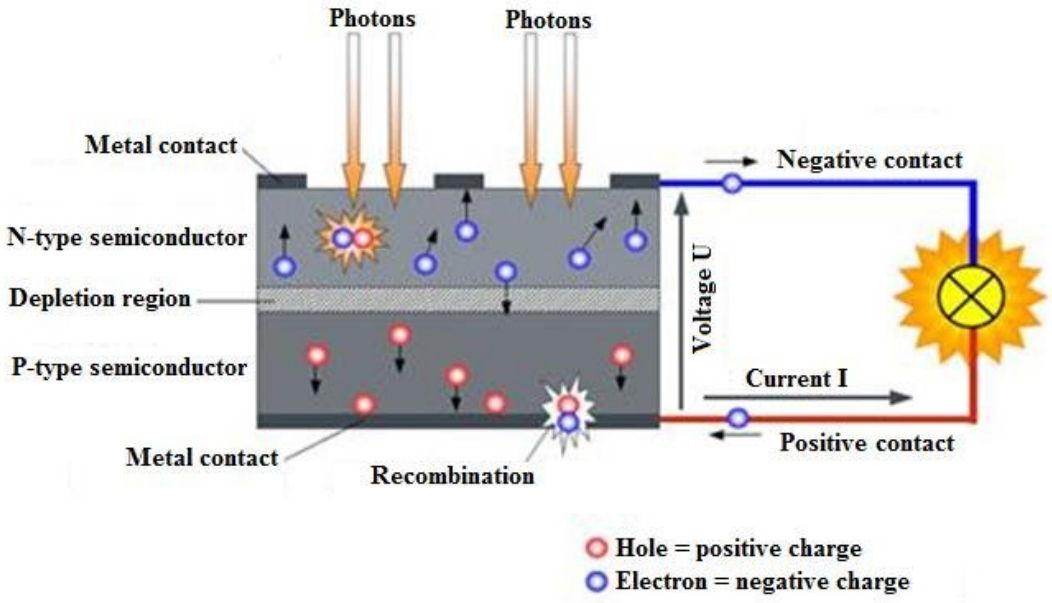

Figure 2.3: Schematic of a PV cell

Nowadays solar cell are usually modeled using equivalent circuits [8] like in fig.2.4. The behavior of such circuit is defined by the implicit eq.2.1

$$I = I_{pv} - I_{Di} + \frac{(V + IR_s)}{R_{sh}} = I_{pv} - I_0 \left[e^{(\frac{(V+IR_s)}{n_{series} a V_T})} - 1 \right] - \frac{(V + IR_s)}{R_{sh}} \tag{2.1}$$

From which the characteristic I-V nd P-V curve can be derived as in fig.2.5.

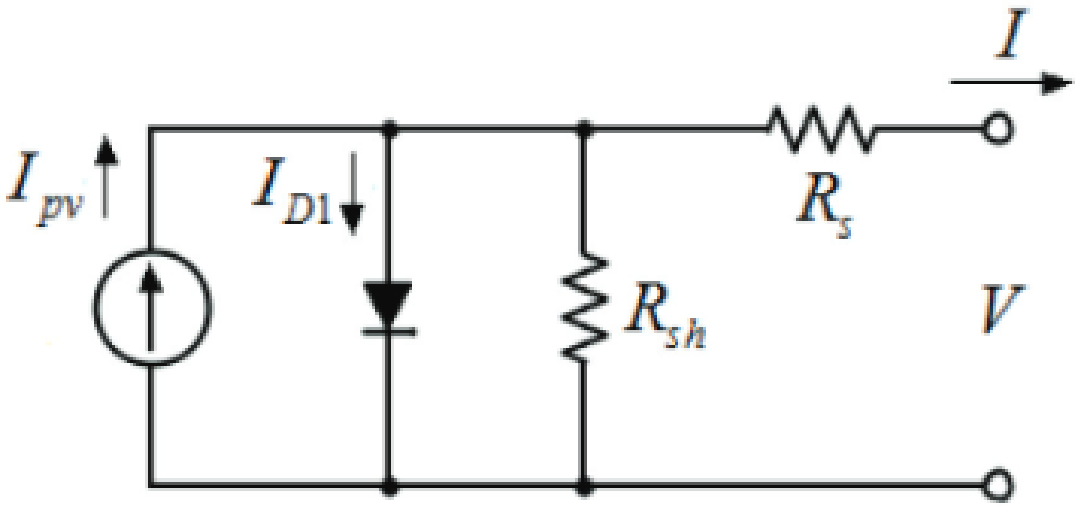

Figure 2.4: PV cell equivalent circuit

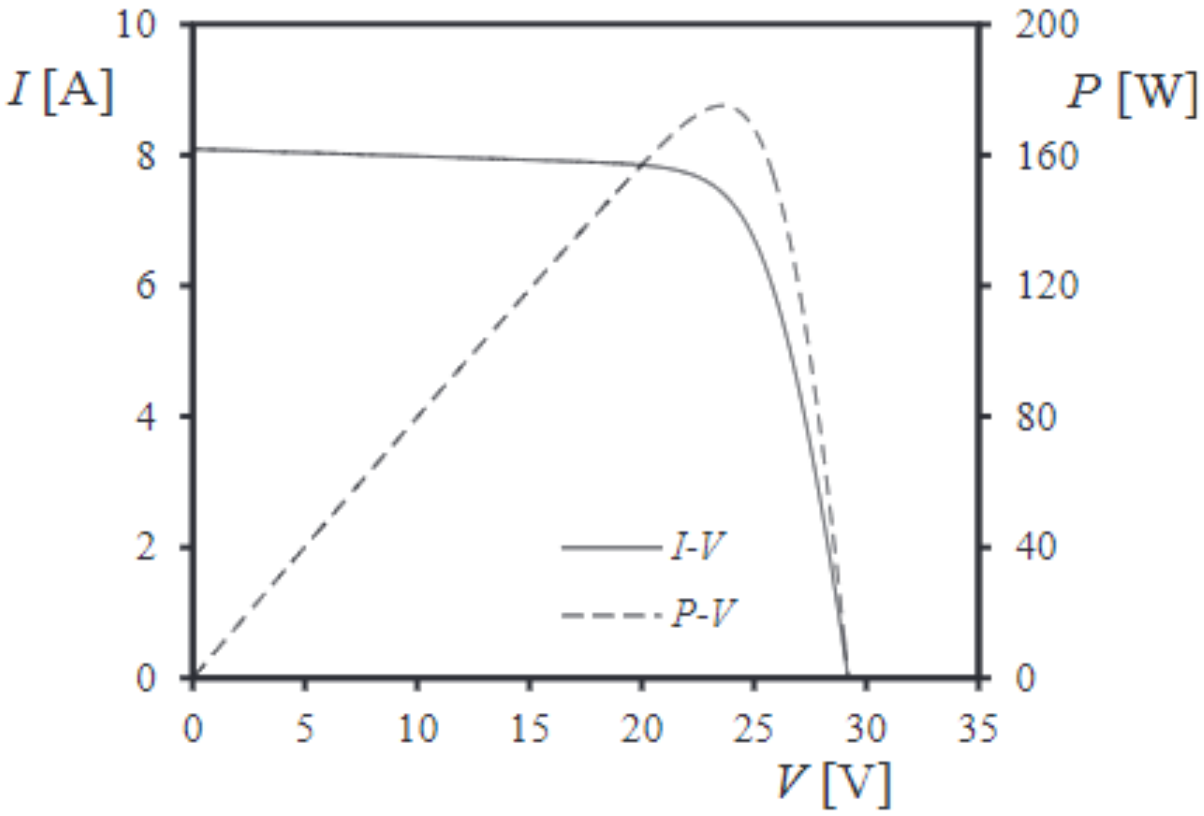

Figure 2.5: I-V and P-V characteristic curves

Currently over 90% of the PV modules around the global market are based on a variation of the silicon technology (either polycrystalline, monocrystalline or amorphous).

The efficiency of this technology is highly susceptible to boundary conditions such as temperature (fig. 2.6) of the panel, inclination with respect to the incident light and manufacturing process. If we consider STC the rated efficiency is around about $15 - 18\%$.

Being semiconductor devices, solar panels are greatly affected by temperature. The increase in temperature automatically decreases the band gap therefore lower energy is needed to create a hole-electron pair. The parameter mostly influenced by it is the open-circuit voltage. As shown in fig.2.6 for lower voltages we have the same output current but considering eq.2.2 this is translated in a decrease in maximum power obtainable by the cell for the same incident amount of sunlight.

$$P = V \cdot I \tag{2.2}$$

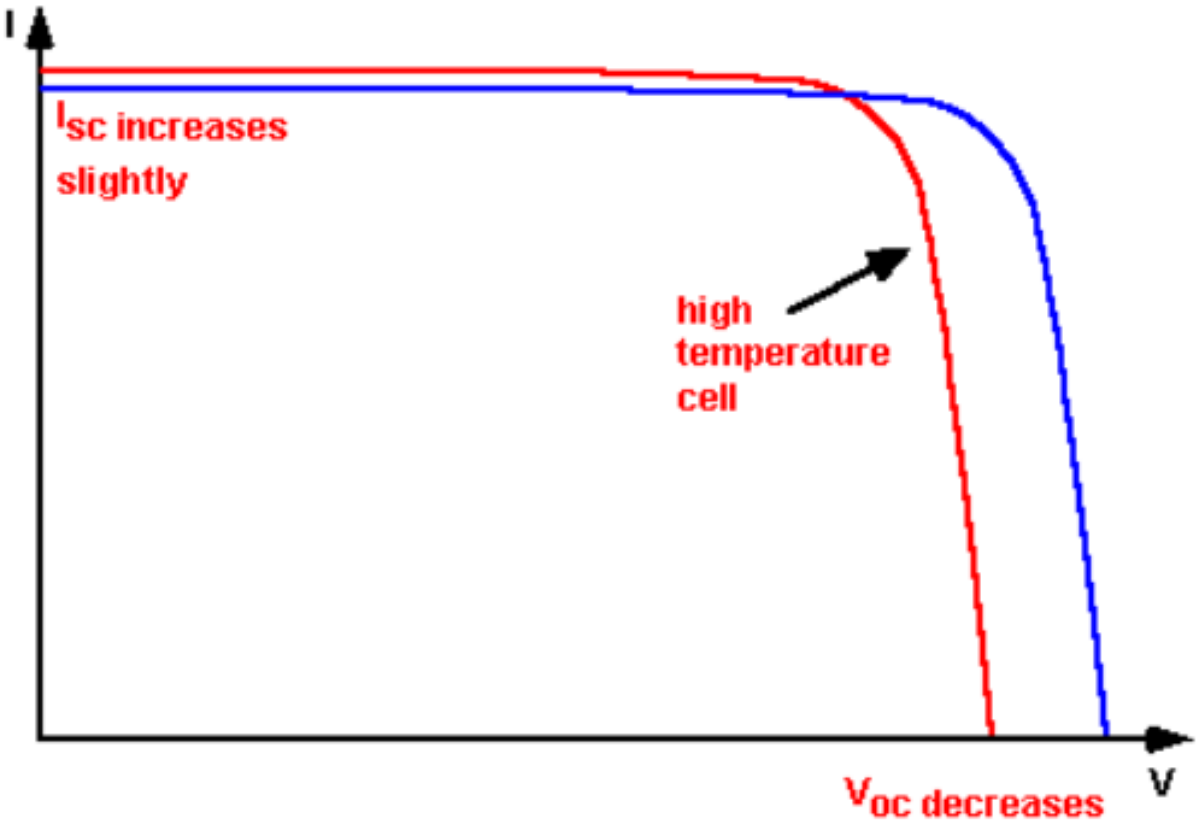

Figure 2.6: I-V characteristic at different Temperatures

Solar Irradiation Mapping

To have a coherent estimation, from our simulator, of the possible electricity production, hence its cost, a mapping both on the European and Italian scale of the solar irradiance is undertaken. As it can be seen by fig.2.7 substantially different situations can be found between the north and south with the latter able to deliver nearly double the energy production of the former. Nevertheless particular attention has to be given to the average temperatures in the various regions. Zones with high irradiance are usually associated with higher temperature thus limiting the maximum nominal power of each module. Similar considerations can be done to the analysis of all the European continent as seen in fig.2.8.

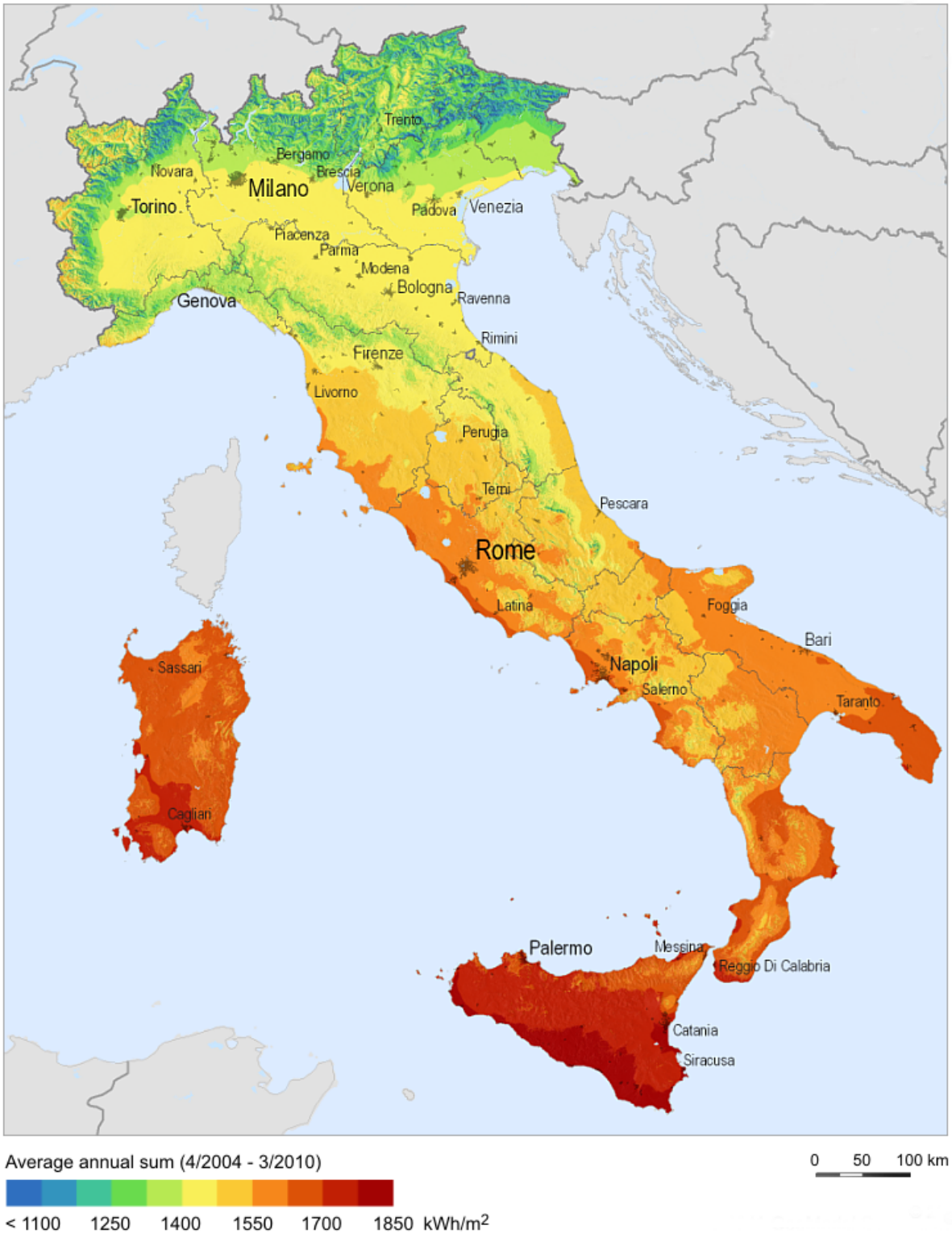

Figure 2.7: Average irradiance annual sum in Italy

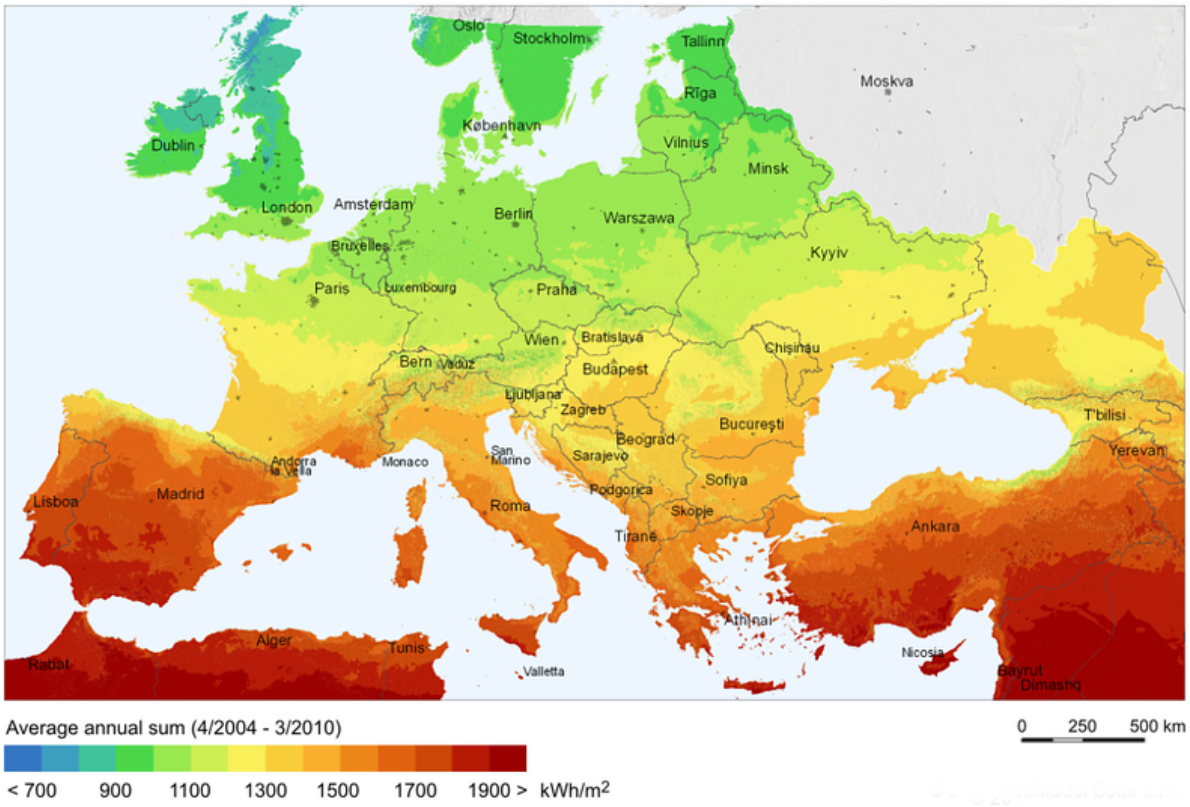

Figure 2.8: Average irradiance annual sum in Europe

2.3.2 Wind Turbine Technology Overview

Working Principles

Wind turbines work by converting the kinetic energy in the wind first into rotational kinetic energy in the turbine and then, via a generator, to electrical energy. The maximum power that can be extracted by a wind turbine is governed by eq.2.3.

$$P_{WT} = \frac{1}{2} C_P \rho_{air} A_{rotor} v^3 \tag{2.3}$$

Where C_P is the power coefficient (usually measuring between $0.3 \div 0.4$). The maximum theoretical value obtainable by this coefficient is $C_{P-max} = 0.59$ and is better known as Betz Limit [9]. Unfortunately this parameter is not constant but is a function of the wind speed. This brings us to notice that there is a maximum power that is producible by a wind generator as shown in figure 2.9.

The efficiency of this technology can be sensibly improved, out of nominal conditions, by implementing a pitch control mechanism. Hence,if we keep all the other parameters constant, by changing the rotor blade pitch angle along the rotor axis more power is extractable as shown in fig.2.10.

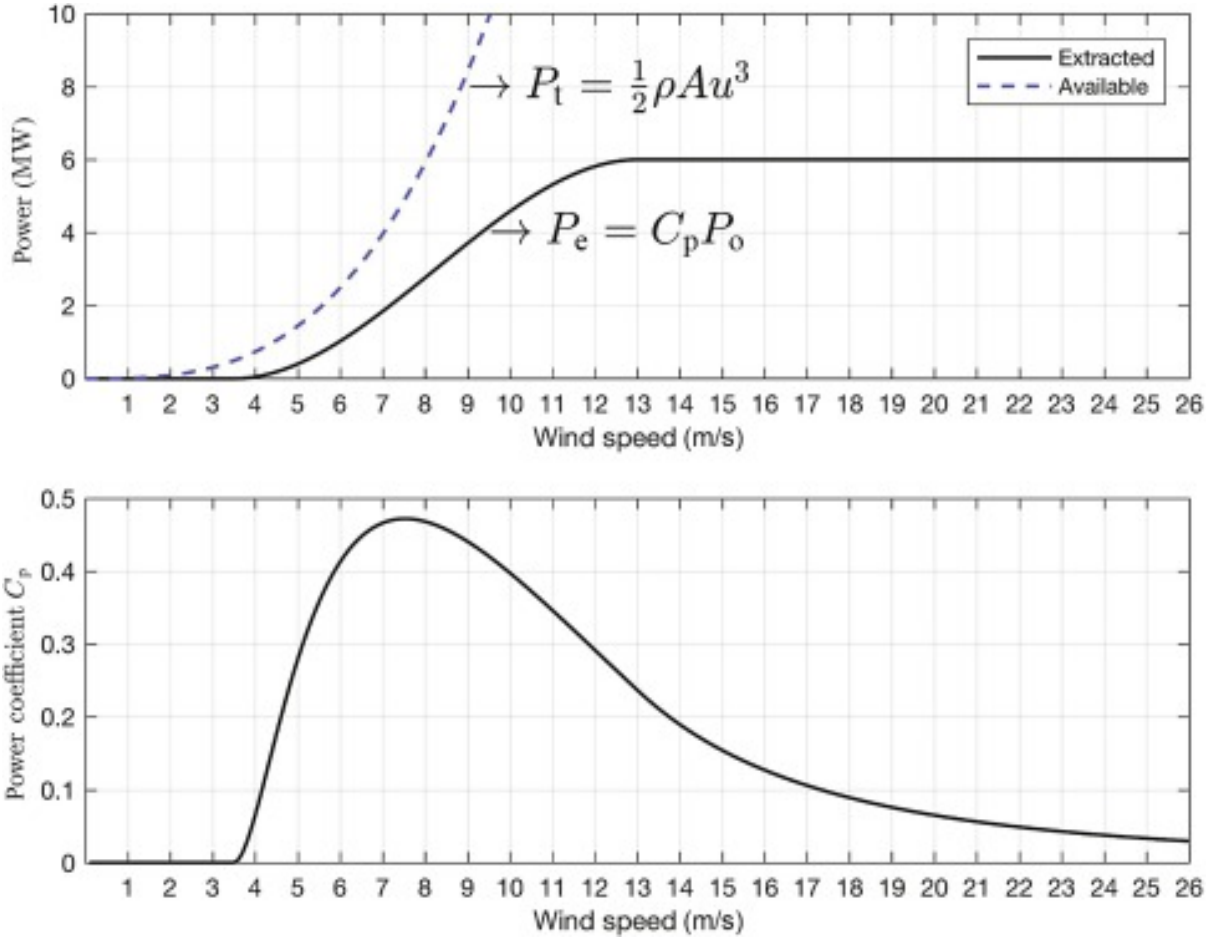

Figure 2.9: Power and C_p behavior as a function of the wind speed

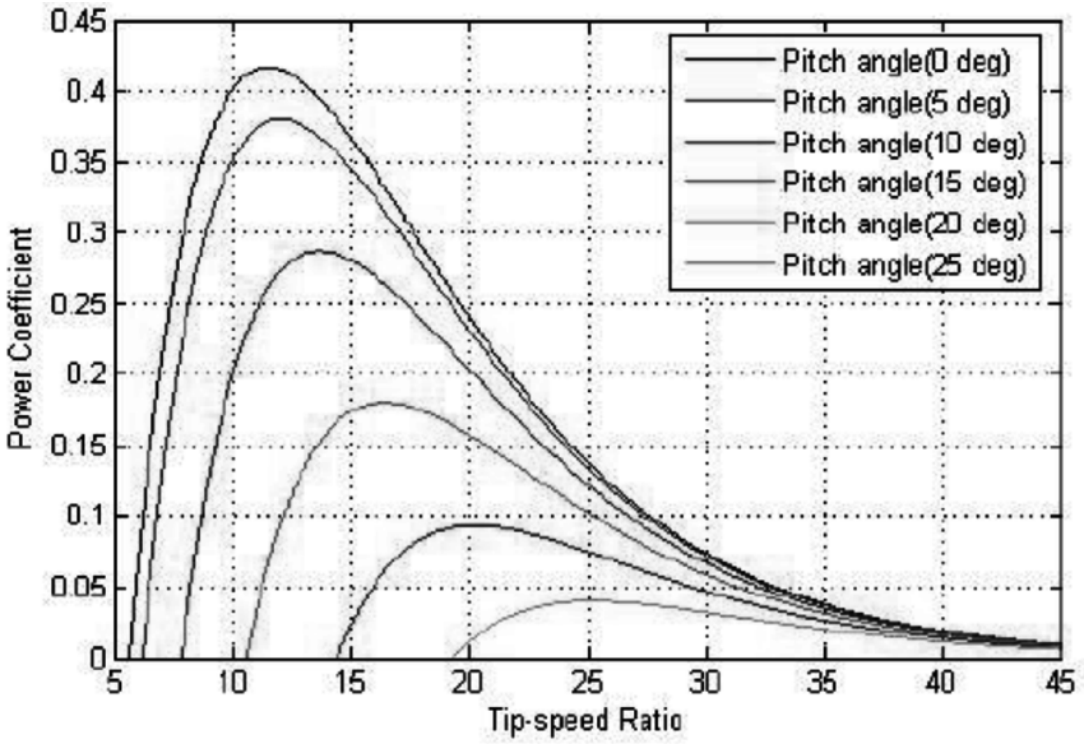

Figure 2.10: C_p behavior at constant speed with different pitch angle configurations

Latest trend in wind turbine technology has been that of increasing the rotor size (fig.2.11). This leads, of course, also to an increase in the overall height of the wind turbine itself which is an added benefit since wind speed also increases as shown in fig.2.12

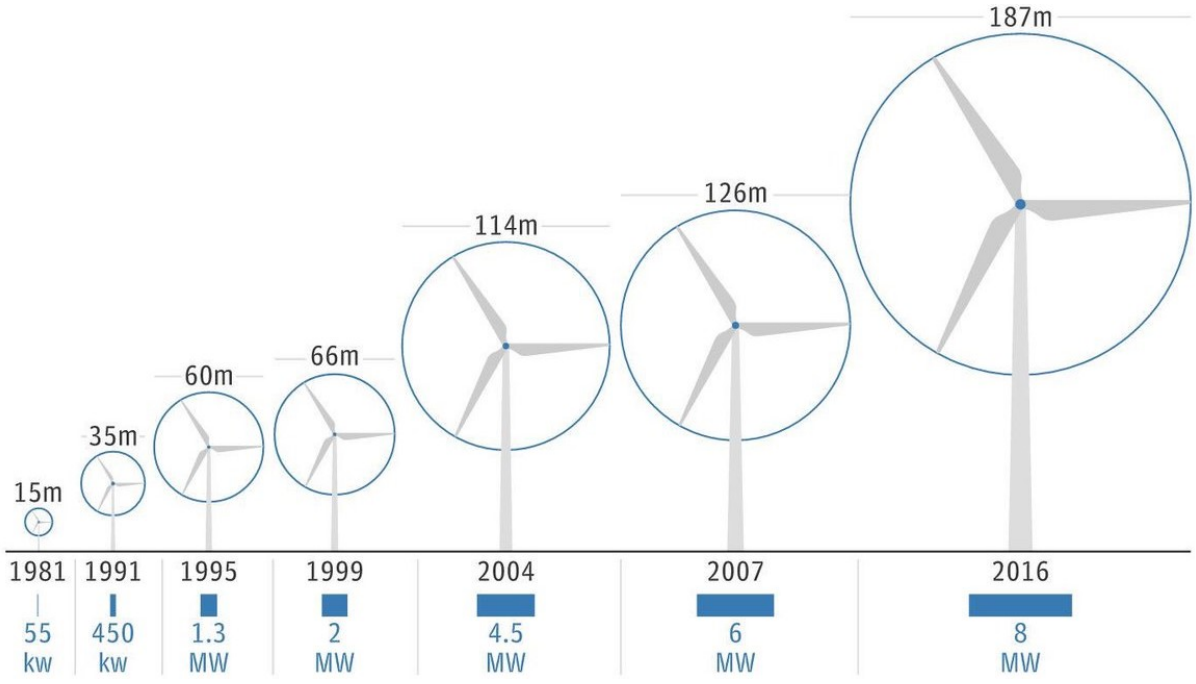

Figure 2.11: Wind turbine area increase over the years

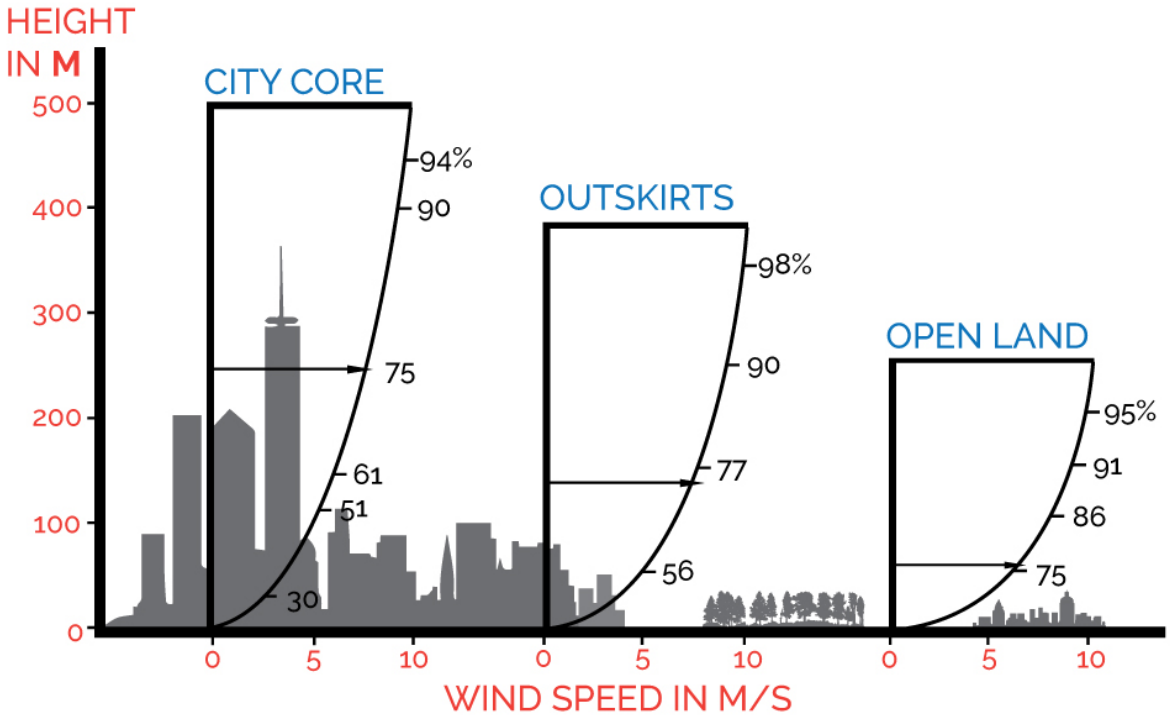

Figure 2.12: Wind speed variation in different geographical areas at different heights

Wind Mapping

Same considerations as in subsection 2.3.1 will be undertaken. From fig.2.13 we can appreciate an relatively heterogeneous situation. The Southern part has wind speed up to three times higher than in the Northern region especially if we look at the islands. Different is the situation in Europe. As shown in fig.2.14 the most favorable areas where to exploit wind are in the northern regions. Particularly attractive is an off-shore option.

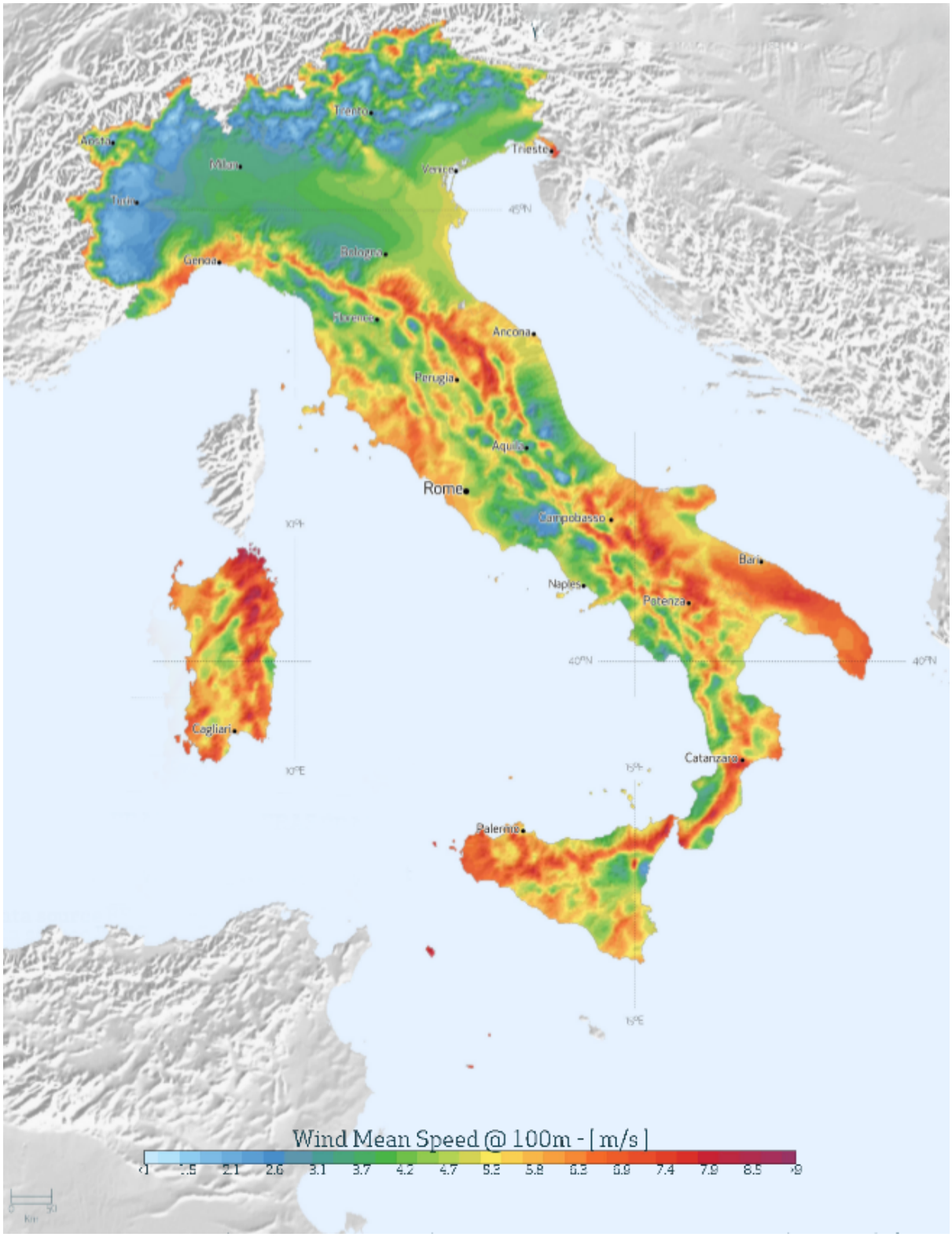

Figure 2.13: Wind speed distribution in Italy

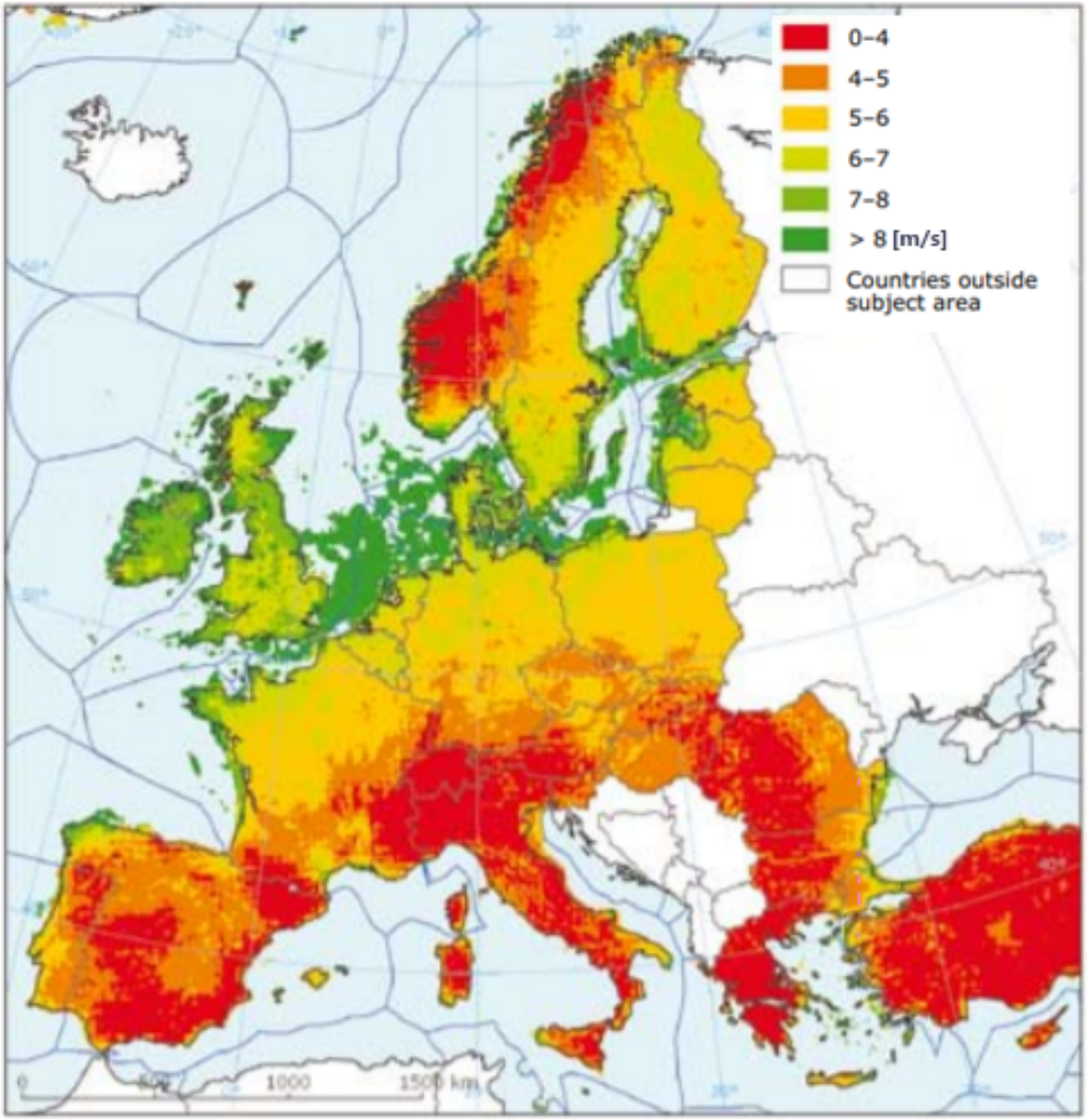

Figure 2.14: Wind speed distribution in Europe

2.4 Desalination

Facing the problems of an exponentially growing population and climate change that is increasing the frequency of droughts all around the world, desalination is becoming an attractive technology that could help mitigate if not partially solve these issues. Moreover, the high capacity and extreme flexibility of these plants makes them suitable for emergency situations where an urgent spike in water demand is required.

Desalination for fresh water production, at present moment, can be subdivided into two macro-groups (fig.2.15): membrane and thermal processes. Given the rapid development and higher efficiencies, the former overtook the latter in this industry in 2005. Since then the global desalination effort is encompassed for 65% by membrane technology and only for 35% by thermal. New technologies such as microbial desalination are now in their early infancy therefore will not be taken into account in this study.

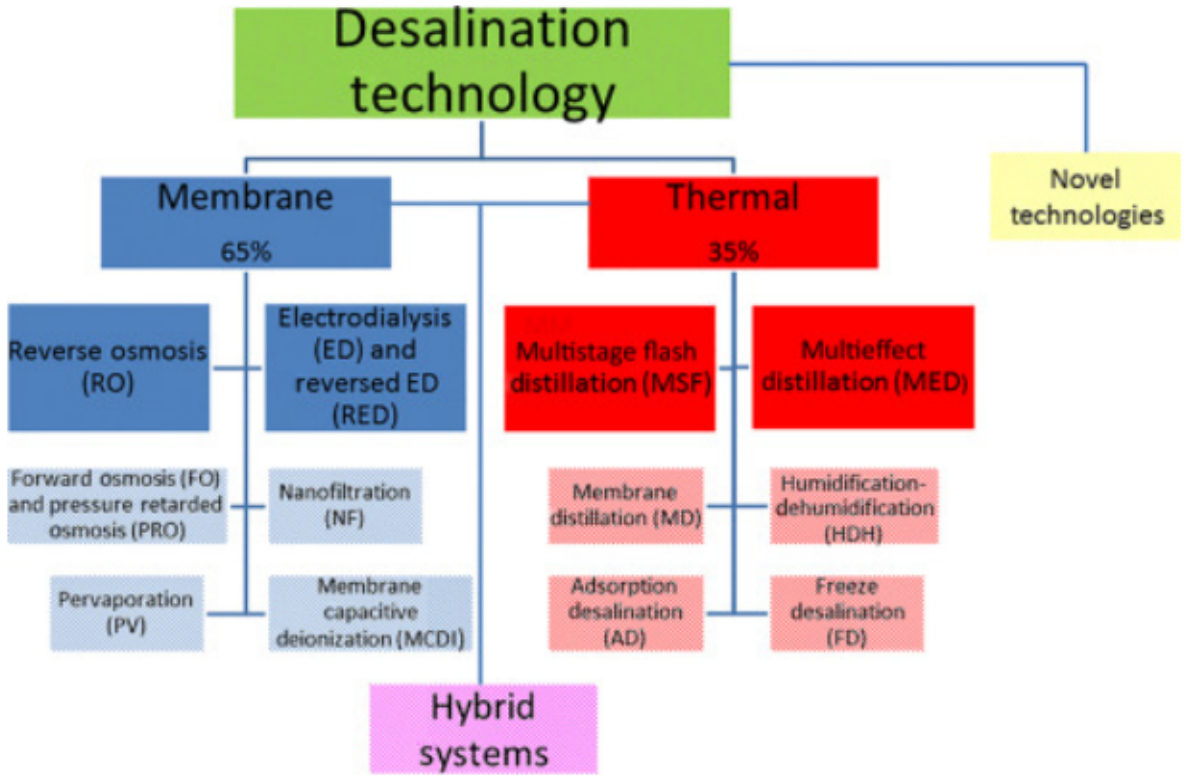

Figure 2.15: Desalination technologies overview

The fundamental of any desalination plant is based on five main parts; two inputs (feed water and energy), two outputs (produced freshwater and rejected water) and the central system of the desalination plant. This system, which can be known as the core of the desalination plant, is designed based on the water desalination technologies. Broadly, the large-scale desalination plant technologies are classified into two main groups; evaporation/condensation (also is called thermal method) and membrane.

The major sub-methods of thermal desalination systems are Multi-Stage Flash Distillation (MSF) and Multi-Effect Distillation (MED). Both these technologies need thermal and electrical forms of energy to operate. The membrane method also can be sub-divided into several technologies, based on the fundamental of their process. Reverse osmosis (RO) is the leading pressure-driven membrane processes, which has come to dominate the large-scale desalination plants. Unlike thermal methods, this technology needs only electrical energy.

Presently, the share of RO units in overall produced freshwater worldwide is almost 60 percent. During recent decades, numerous researchers have conducted several studies on analyzing the specifications of various seawater desalination technologies [10]. Advances in the large-scale desalination plants have been made in the area of total cost reduction of produced water and increasing the total efficiency of the co-generation plant. Regarding these parameters, the hybrid desalination methods based on the coupling of two or even three different technologies, including MSF+RO, MED+RO, and MSF+MED+RO have been developed by researchers. Table 2.1 summaries the operational and performance parameters of various desalination schemes [11].

Parameter	MED	MSF	RO
Operating temperatures ($^{\circ}C$)	$65-70$	$90-110$	Ambient
Thermal energy $\left(\frac{kWh_{th}}{m^3}\right)$	$40-65$	$53-70$	NA
Electrical energy $\left(\frac{kWh_e}{m^3}\right)$	$2-2.5$	$2.5-5$	$4-6$
CO_2 emissions $\left(\frac{kg}{m^3_{H_O}}\right)$	$7-17.6$	$15.6-25$	$1.7-2.8$
GOR	$8-10$	$8-16$	NA

Table 2.1: Operational and performance parameters of most common desalination technologies

Where the gain output ratio (GOR) is a measure of how much thermal energy is consumed in a desalination process, typically defined as eq.2.4.

$$GOR = \frac{kg_{H_2O}}{kg_{steam}} \tag{2.4}$$

2.4.1 Reverse Osmosis

RO is the most widely used membrane process. It is able to eliminate nearly all colloidals from the solution. The treatment of salt-rich water is divided into four main steps (fig.2.16): pretreatment, pressurization, separation and stabilization.

Pretreatment is the adjustment of water parameters such as pH, removal of suspended solids etc. to make it compatible with the membrane. Since RO needs a high differential pressure, pressurization via pumps is mandatory for the whole system to work. Now applying the feedwater to the membranes permits the separation to occur. finally a stabilization of pH and degasification is required to enable the distribution as potable water.

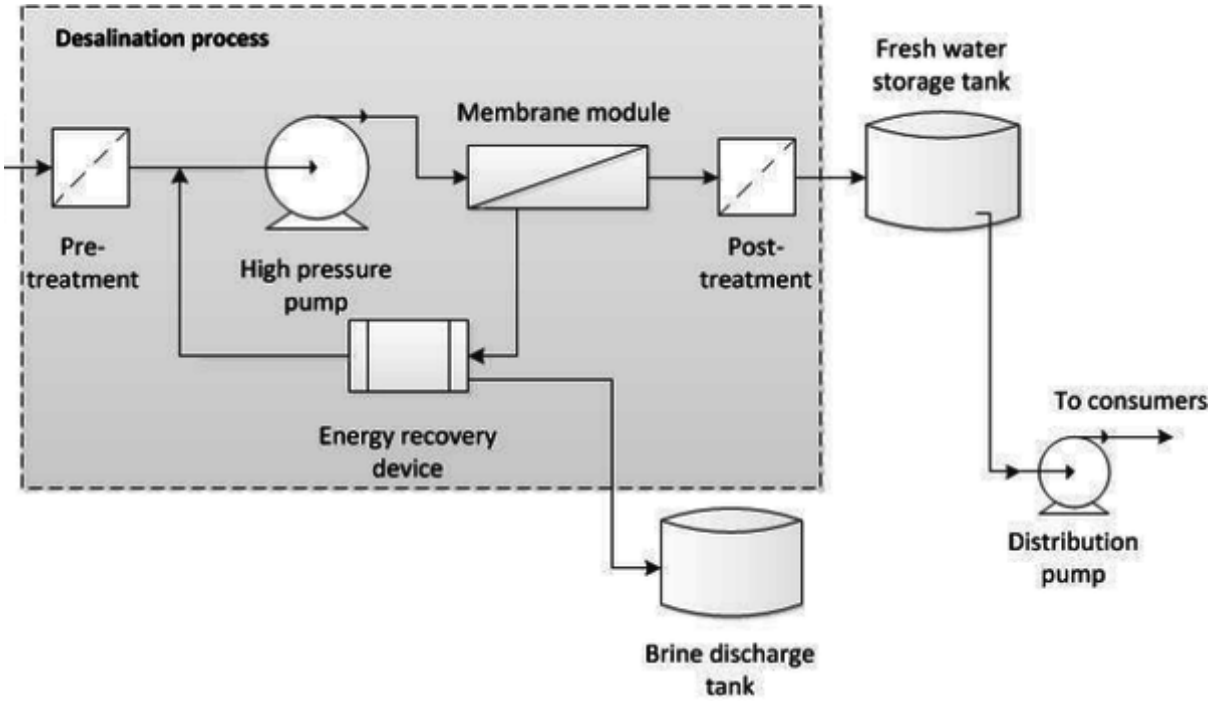

Figure 2.16: RO plant schematic

This technology is most suitable in regions where brackish groundwater or seawater are easily available. It has several advantages such as simplicity of the plant with low needed maintenance, high space/capacity ratio ($25000 - 60000 \frac{l}{day \cdot m^2}$), possibility to use seawater, low environmental impact related only to brine disposal and minimal chemical use.

2.4.2 Multistage Flash Distillation

The MSF process is based on the distillation of water via a rapid pressure drop (flashing). The plant id divided in stages each having both a heat exchanger and a condensate collector (fig.2.17).

Heated brine is introduced to a chamber (stage) where the pressure is below the saturated vapour pressure of the brine at that temperature. Immediate conversion to the vapour phase (flashing) takes place and the resulting vapour passes to the next stage. After passing through a demister, a proportion of this vapour is then condensed on the tubes of the second stage, giving up its latent heat of vaporisation to the feed stream. The feedstream is heated progressively in each stage before passing through the brine heater used to feed the first stage. The condensate collected in each stage forms the product, and

the whole process is driven by the sub-atmospheric pressure gradient through the stages, generated at start-up by a steam ejector, but maintained by progressive condensation.

The strengths of this system are mainly the possibility to adopt low grade steam and benefiting from the economies of scale. These are he reasons why this technology is the most widespread throughout the world.

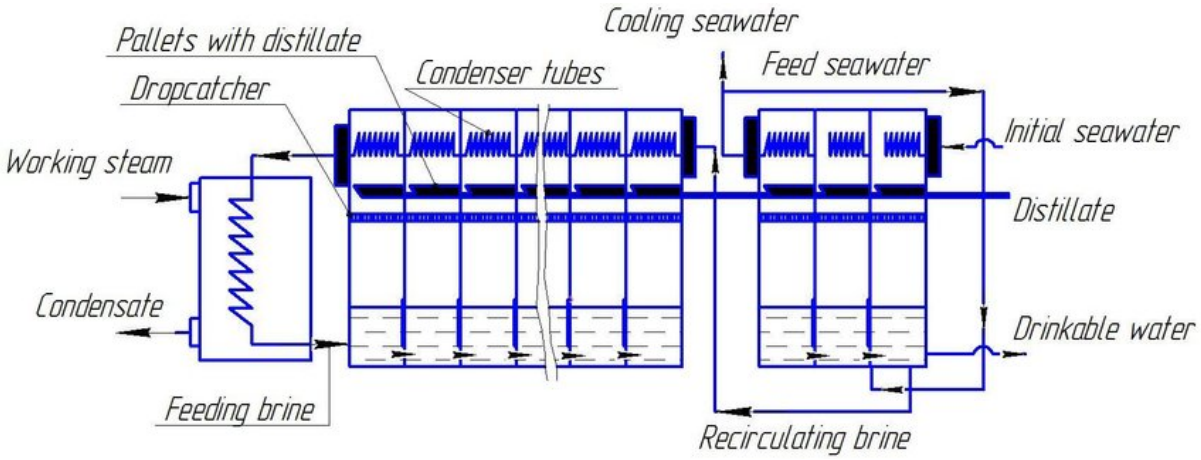

Figure 2.17: MSF plant schematic

It can be easily calculated the amount of produced distilled water with eq.2.5:

$$\frac{\Gamma_f}{\Gamma_m} = \frac{L_v}{c_p \Delta F} + \frac{N-1}{2N} \tag{2.5}$$

Where L_v is the average latent heat of vaporization, Γ_f and Γ_m the mass flow rates, expressed in $\frac{kg}{h}$, respectively of the feedwater and the distillate and N is the total number of stages. ΔF is the flashing temperature range and can be calculated as:

$$\Delta F = T_h - T_{bN} = (T_{b1} - T_{bN}) \frac{N}{N-1} \tag{2.6}$$

Where T_h is the top brine temperature, T_{bN} and T_{b1} are respectively the temperature of brine in the last and first effect all expressed in Kelvin.

2.4.3 Multieffect Distillation

Thermal desalination plants are mainly used in places with poor water quality where the RO plants would have increased operating costs and where high availability of cogenerative steam for thermoelectric plants is present [12]. MED is more effective than other thermal

desalination systems since it requires lower grade heat at approximately $70 - 80\,°C$ compared to the $120 - 130\,°C$ of MSF. Since scaling and corrosion problems were solved in the past few decades, MED has become more competitive therefore gaining more and more share of the total desalination capacity globally.

The MED process consists of a series of effects, ranging up to 16, where pure water is separated from the feed via evaporation processes. The high number of effects is essential to increase the overall efficiency of the system since thermal energy can thereby be recovered from the generated vapor to drive the successive effect therefor avoiding excessive energy rejection.

The most common MED process used is the *falling film evaporator* where the feed seawater is sprayed over the surface of heated tubes. The produced steam is then redirected to the next effect for boiling new seawater or the brine coming out of the previous effect. The maximum temperature of the system is kept at approximately $70\,°C$ to avoid scaling and corrosion issues. This in turn leads to the possibility of using alternative construction materials which lower the capital cost and enables exploiting low grade heat as means of desalinated water production.

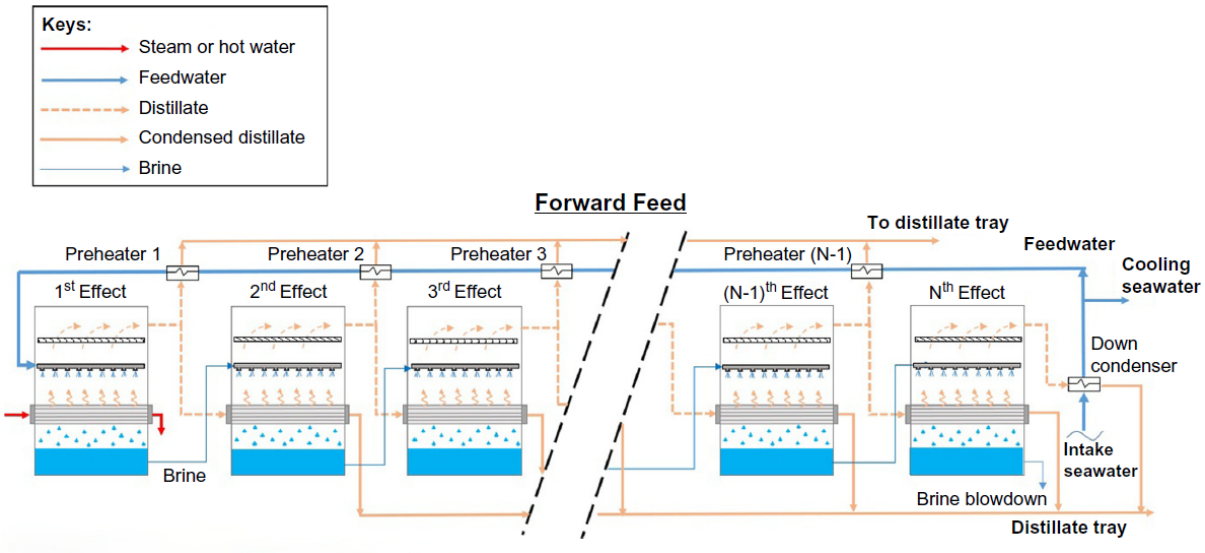

Figure 2.18: MED process configuration: Forward feed

Typical values of a MED plant consumption are $40 - 80\,kWh_{th}/m^3$ [13] for thermal energy and $1.5 - 2.5\,kWh_e/m^3$ for electrical needed by pumps and auxiliary systems.

2.5 Energy Storage

Stability, reliability and flexibility between energy supply and demand are mandatory for electrical grids to continuously work properly. The historical configuration of an electrical grid is a "$top - down$" model (fig.2.19) where a central power plant produces energy to be

then delivered to the final users.

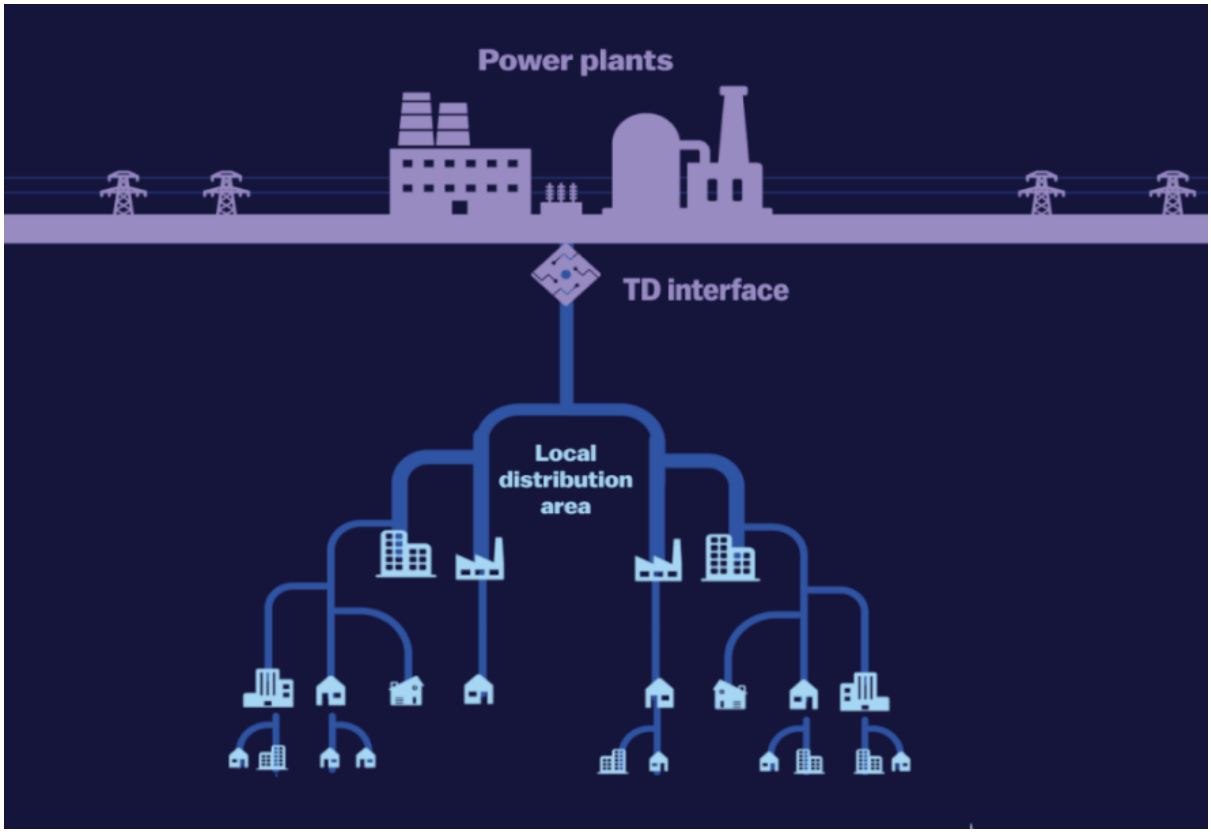

Figure 2.19: Grapical interpretation of a "$top - down$" model

Nowadays the situation has changed. Thanks to renewable technologies, users are now producers and a new balance needs to established (fig.2.20). The intrinsic variability and intermittency of these technology is the main issue we're currently facing. Energy storage systems are an attractive solution to the problem by quickly storing and then dispatching the energy surplus when needed.

Energy storage technologies are divided into two groups [14]: those that can deliver precise amounts of electricity very rapidly for a short duration(capacitors, batteries and flywheels), as well as those that take longer to ramp up, but can supply more power for longer periods (compressed air energy storage and pumped-storage hydro-power). They can further be categorized by their underlying physical phenomena to store energy such as: electrochemical, electrostatic, electromagnetic, chemical, kinetic, potential, thermal.

An effective way to display the differences between these technologies is to consider their specific energy ($\frac{W \cdot h}{kg}$) and peak power (i.e. the rapidity at which the technology is able to deliver a certain amount of energy $\frac{W}{kg}$). Figure 2.21 gives a neat graphical representation of what previously mentioned.

The main advantage of coupling renewables with storage systems is the possibility to

have "*peakshaving*" (fig.2.22). Not only this enables an increased grid stability but offers a reduction in electricity price during the peak demand [15] as well as frequency regulation. This will at last enable a higher degree of predictability of the renewable power production.

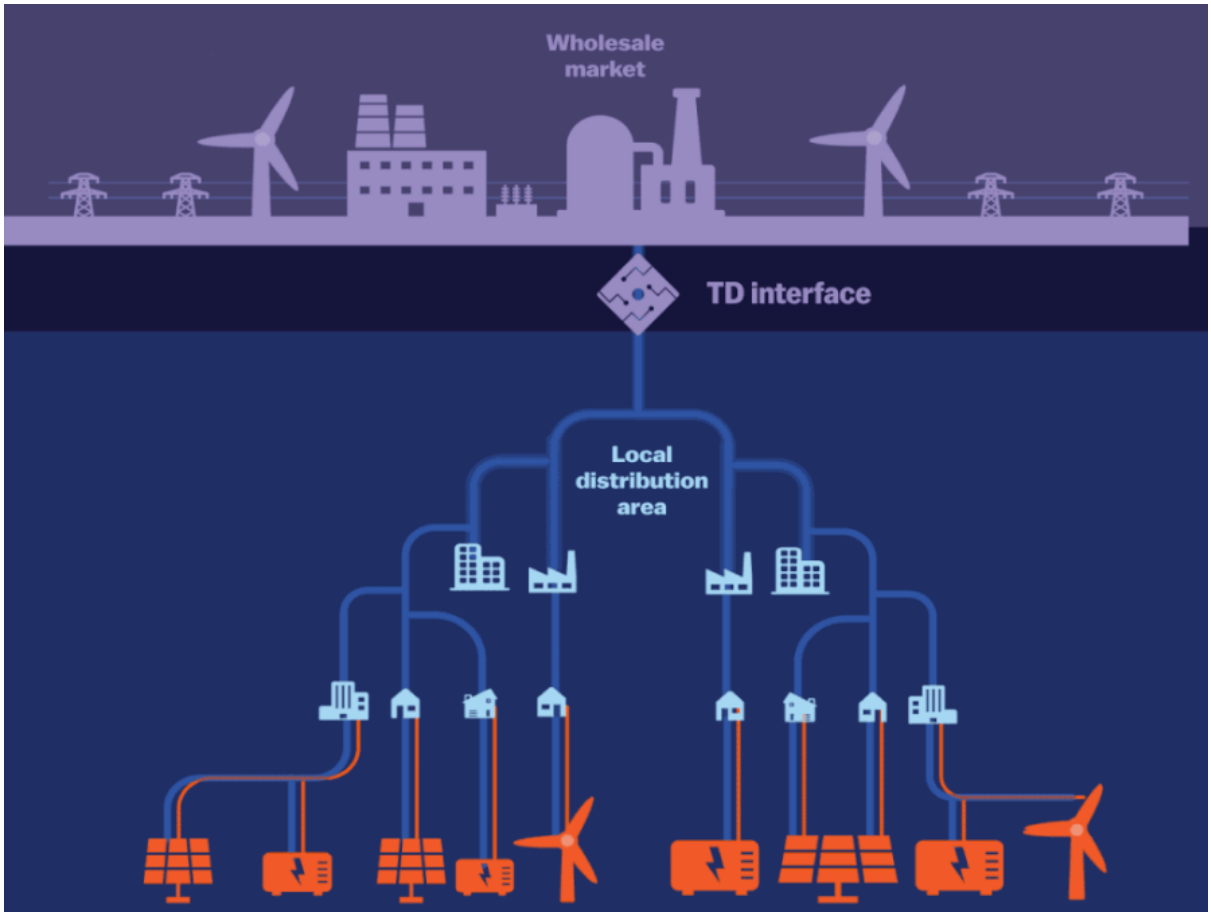

Figure 2.20: Grapical interpretation of a "$top - down$" model with renewables

Moreover battery storage systems can be used in applications such as grid stabilization via frequency regulation. To be effective in this task it is mandatory for the batteries to have a nominal power grater than 1 MW and a power/energy ratio og at least $1:1$. Instead for peak shaving applications, the capacity of the system may vary appreciably from case to case ranging from mere 10 kWh to hundreds of MWh depending on the grid dimensions and requirements.

2.5.1 Battery Storage Systems

Li-ion Batteries

Driven their rapid cost reduction and increasing energy density, lithium-ion batteries are currently the most wide used electro-chemical storage devices. Given their versatility in supplying both power and energy, they have found use in products for the everyday life

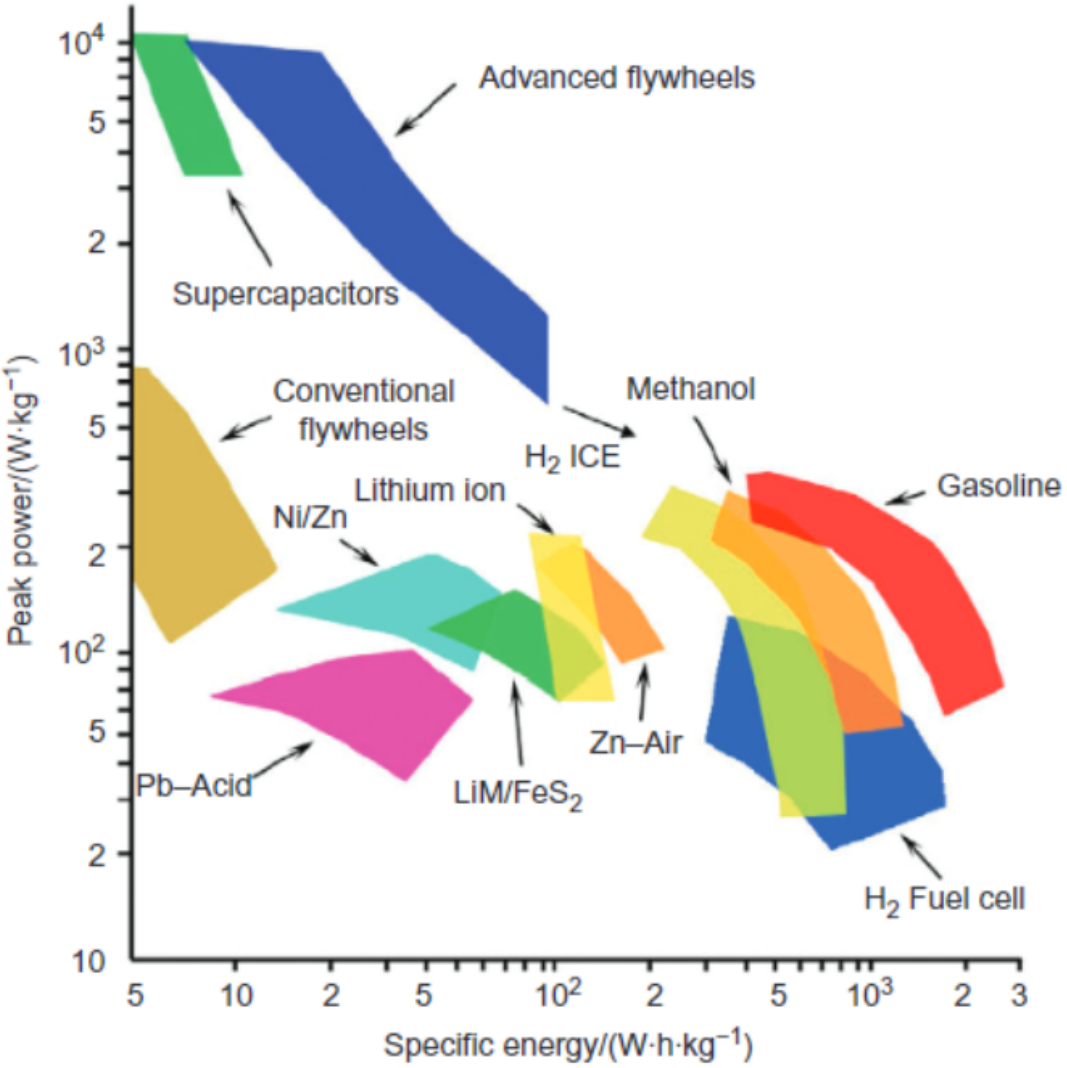

Figure 2.21: Energy density versus peak power

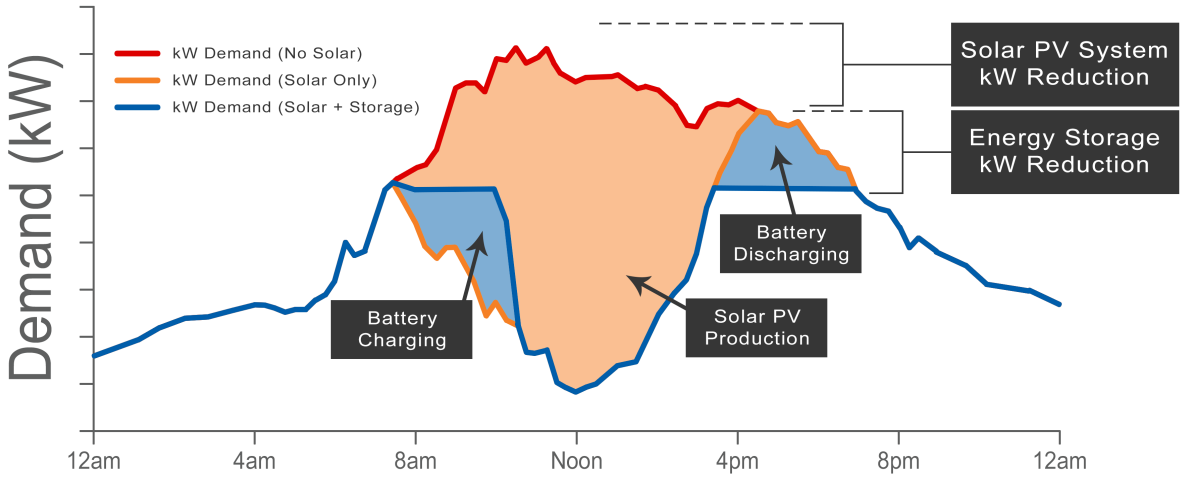

Figure 2.22: Peak shaving using battery technology

up to applications where sizes greater than $100MW$ are required.

Li-ion batteries are usually base on lithium-intercalation compounds. The basic working principle is the migration of lithium ions through the electrolyte located between anode and cathode [16]. Lithium ions are released from the anode and diffuse to the cathode during the discharge process and viceversa. Anodes are typically graphite-based compounds while the cathodes, from which the batteries performance are determined, are lithiated compounds such as $LiCoO_2$, $LiMn_2O_4$ and $LiFePO_4$. State-of-the-art li-ion batteries have energy densities ranging between $75 - 200\ \frac{Wh}{kg}$ which is not enough for grid usage. Therefore different anodes materials are undergoing intensive studies to substitute graphite with silicon being arguably the most promising. The problems related to such a technology are mainly the short lifespan of around 15 years with annual degradation and the flammability risk associated to them. The typical duration of such devices is between 0 and 6 hours therefore making them suitable for peak shaving.

2.6 Grid Frequency

Previously it has been mentioned that a high penetration of renewable energy sources into the grid can cause serious issues when dealing with frequency stability [17]. Changes in supply and demand in electricity will cause a variation of frequency namely: an increase if the supply is greater than the demand and a decrease in the opposite scenario. The margin of error in which we can have frequency variation is extremely small, in perspective also a 1% deviation over a long period can cause serious damages to equipment and infrastructure. Therefore a controller over the grid frequency is required. Managing electrical frequency falls to a country's high voltage transmission system operator which can instruct power units to turn off or on in order to keep the total frequency at 50 or 60 Hz depending on the nation. The grid frequency is directly connected to the generator speed of a power plant. A 3600 rpm and a 3000 rpm devices will be used in a 60 and 50 Hz grid respectively. In fast frequency changing scenarios like the ones envisioned for the future of the European grid, it is of utmost importance to have rapid and flexible power plant to cope with the intermittency of renewable sources. Figure 2.23 shows the different stages of frequency control. The primary regulation is the most demanding since it deals with sudden variations of the grid (i.e. wind turbine cut-off) and requires to be kept in the range ± 800 mHz during all the transient. Furthermore the steady state has to be reached within a 30 seconds margin. The load following pertains to the tertiary frequency control and is less demanding compared to the primary. Here the requirements are to match supply and demand.

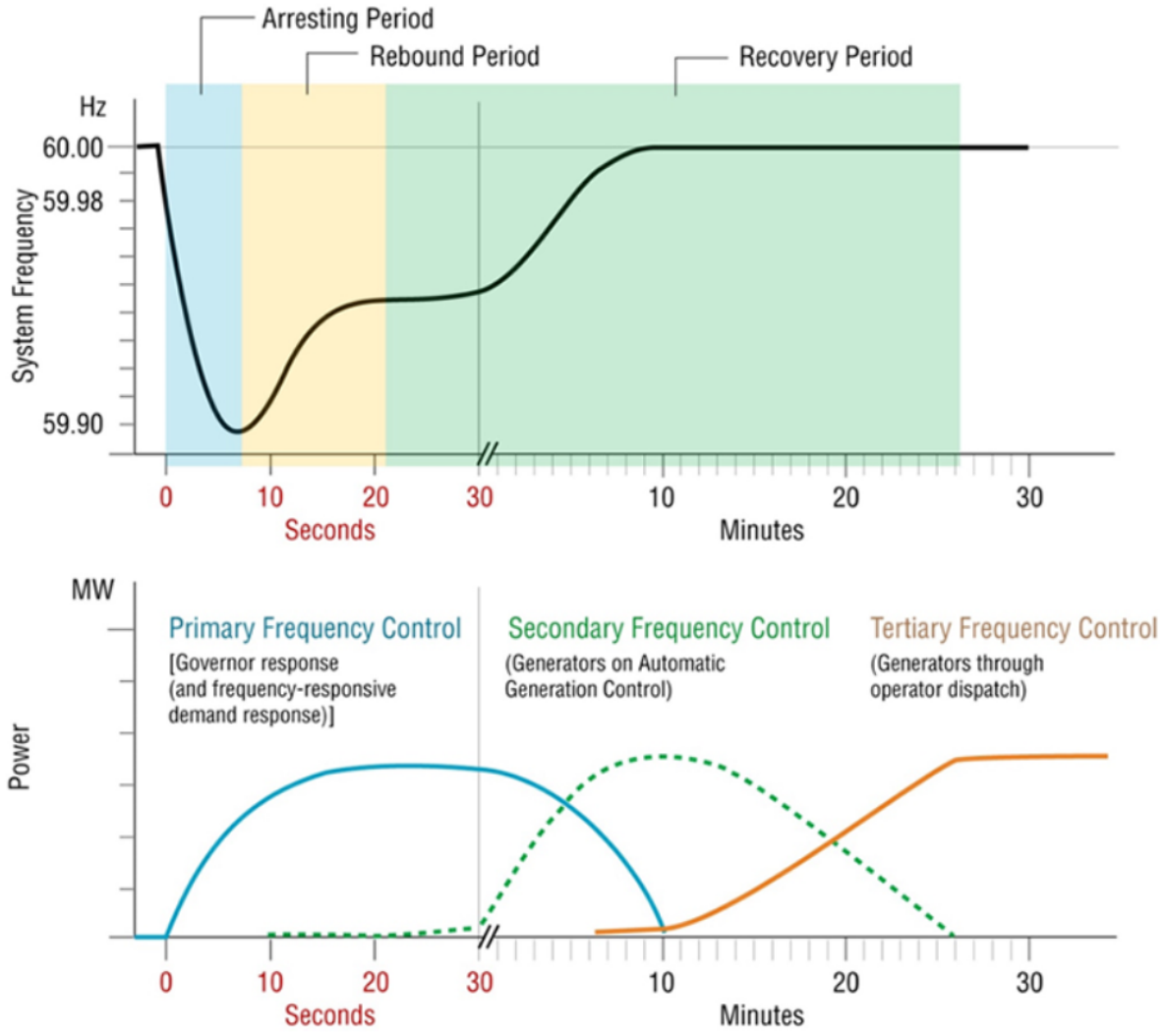

Figure 2.23: Primary, secondary and tertiary grid frequency definition

Dymola NPP Simulator

3.1 Dymola Software

The development of the power plant model was carried out using an object oriented approach, implemented into Dymola software based on the Modelica language. The advantage of this approach is the possibility to use an acausal approach. For the simulation of physical systems, this modeling inherits some important advantages compared to the more used causal approach which are:

- No a priori establishment of input and output variables
- Better description of physical components
- Modularity and reusability of the model
- Inheritance of the components (i.e. defined independently of their potential connections)
- Components represent physical parts of the plant

This results in a software capable of a multi-engineering approach given the vast selection of libraries which allow multi-field, trustworthy modeling of complex integrated engineering systems. Given the open libraries it is easy to build of modify pre-existing components to anyone's needs. Furthermore the symbolic manipulation of the components makes this software extremely intuitive to model with. These qualities are of extreme importance for the scope of this work since it is envisioned the creation of a highly modular simulator which can be easily adapted from case to case and that's why Dymola has been considered the best option.

3.2 ALFRED Nuclear Power Plant

Following the work of Ponciroli et al.[18] the development of the simulator was focused on the creation of two main blocks: the reactor core and the SG. For the connections in the primary side a modification to the ond-dimensional, equation base $Flow1DFV$ component used in the ThermoPower library had to be made to implement molten lead

flow inside the tubes. This block models the behavior to a fluid flowing in a circular pipe. Table 3.1 shows the main core design parameters.

Parameter	Value	Unit
Core		
Thermal power	300	MW_{th}
Coolant mass flow rate	25984	kg/s
Number of FAs	171	-
Pins per FA	127	-
Coolant inlet temperature	400	° C
Coolant inlet temperature	480	° C
Fuel pin		
Cladding material	15-15-Ti	-
Fuel material	MOX	
Cladding outer radius	$5.25 \cdot 10^{-3}$	m
Cladding inner radius	$4.65 \cdot 10^{-3}$	m
Pellet outer radius	$4.50 \cdot 10^{-3}$	m
Pellet inner radius	$1.00 \cdot 10^{-3}$	m
Active height	0.6	m

Table 3.1: ALFRED main core parameters

3.2.1 Core

Point reactor kinetics, one-dimensional heat transfer models and an eight-group delayed neutron precursor concentration model has been considered. The core is divided into three sub-models each modeling a specific part of the core. The model *kinetics* (fig.3.1) describes neutrons and precursors evolution via equation 3.1. Furthermore two different models have been implemented to describe the effective fuel temperatures. The first one expresses the temperature to allow for the Doppler effect T_f^D (eq.3.2) and the second T_f^{eff} (eq.3.3) needed to consider the reactivity feedback due to pellet deformation caused by thermal stresses.

$$\begin{cases} \dfrac{dn}{dt} = \dfrac{\rho_{reac} - \beta}{\Lambda} n + \displaystyle\sum_{i=1}^{8} \lambda_i c_i + S \\ \dfrac{dc}{dt} = \dfrac{\beta_i}{\Lambda} n - \lambda_i c_i \qquad\qquad i = 1 \div 8 \end{cases} \tag{3.1}$$

$$T_f^D = 0.3 \cdot T_f + 0.7 \cdot T_f^3 \tag{3.2}$$

$$T_f^{eff} = 0.5 \cdot T_f + 0.5 \cdot T_f^3 \tag{3.3}$$

The reactivity variation due to the Doppler effect can be considered via the following equation:

$$\Delta\rho \left[T_{f1} \rightarrow T_{f2}\right] \approx 1.1 \cdot K_D \left(\frac{T_{f2}^D}{T_{f1}^D}\right) \tag{3.4}$$

where K_D is the Doppler constant expressed in pcm.

The reactivity variation given by coolant density variation and from axial and radial cladding expansions have been taken considering linear equations with constant coefficients. Also a negative feedback coefficient is considered for the core volume expansion which in turn produces increased neutron leakages. For the control rods a reactivity differential curve has been adopted considering the reactivity worth of 12 rods at different insertion length. lower degree of accuracy has been given for the safety rods since they're extracted at start-up. Therefore the total reactivity of the system can be calculated as:

$$\begin{aligned} \rho(t) = \rho_0 &+ \alpha_L(T_l - T_{l,0}) + 1.1 \cdot K_D \left(\frac{T_{f2}^D}{T_{f1}^D}\right) + \alpha_{CZ}(T_c - T_{c,0}) + \alpha_{WZ}(T_l - T_{l,0}) \\ &+ \alpha_{CR}(T_c - T_{c,0}) + \alpha_{WR}(T_l - T_{l,0}) + \alpha_{FZ}(T_c - T_{c,0}) + \alpha_{Dia}(T_{l,in} - T_{l,in,0}) \\ &+ \alpha_{Pad}(T_{l,out} - T_{l,out,0}) + A_{CR} \cdot sin\left(B_{CR} \cdot h_{CR} + C_{CR}\right) + D_{CR} \\ &+ A_{SR} \cdot \frac{(h_{SR} - x_{SR})}{LSR} \end{aligned} \tag{3.2}$$

Where the terms of eq.3.5 are in order the initial reactivity margin, the effect due to lead density, Doppler effect, axial cladding expansion, radial wrapper expansion, axial fuel expansion, diagrid expansion, pad effect, control rod contribution and safety control rod distribution.

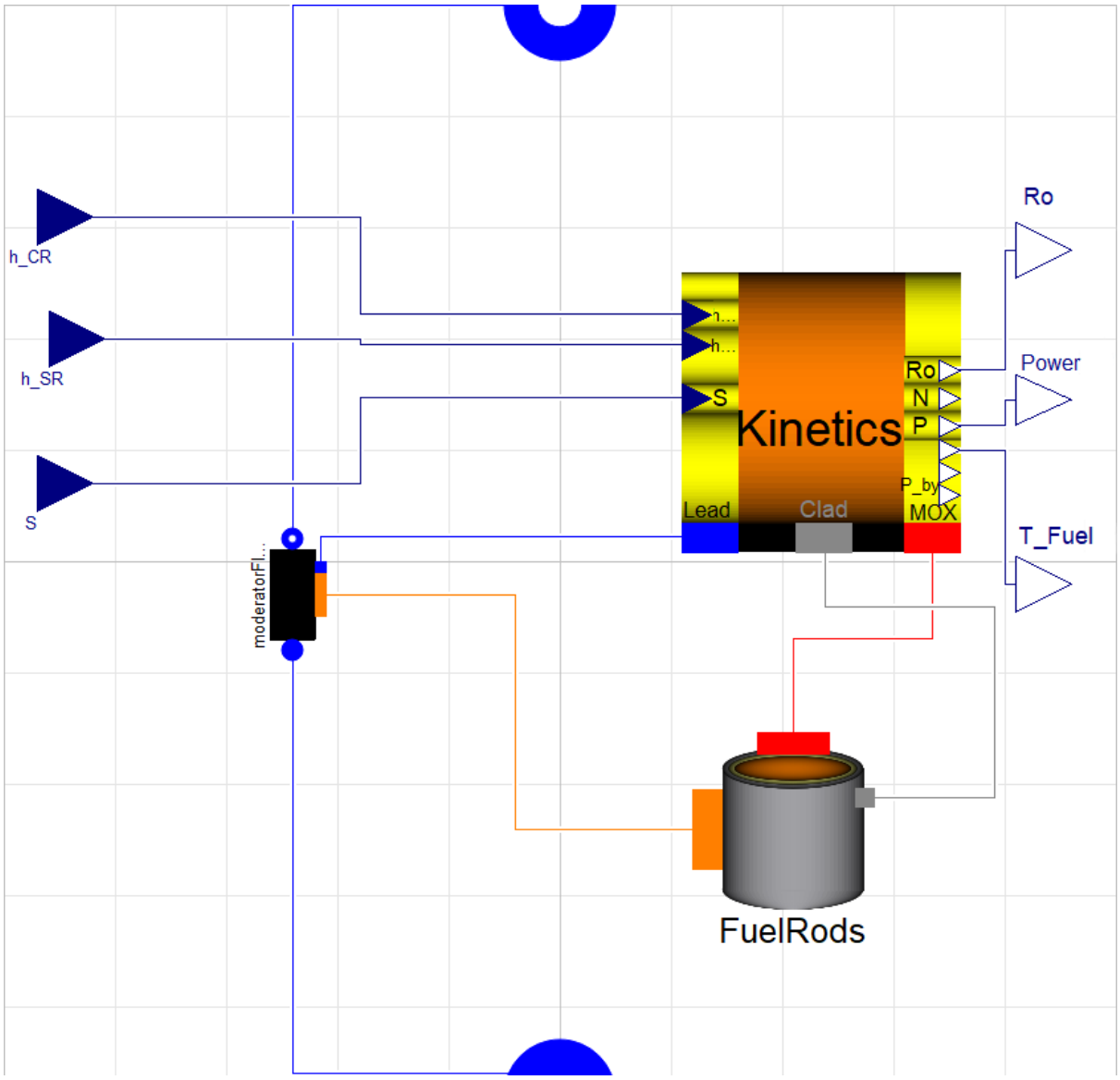

Figure 3.1: Dymola core model

The component *Fuel Rods* describes the thermal behavior of the fuel pins. A time-dependent Fourier equation is applied. The fuel pin is discretized in five radial zones, three for the fuel pellet, one for the helium gap and one for the cladding. The fuel equations is the following:

$$\rho_f c_f \frac{\partial T_f}{\partial t} = \frac{1}{r}\frac{\partial}{\partial r}\left(r k_f \frac{\partial T_f}{\partial r}\right) + q''' \tag{3.3}$$

For the Helium gap we consider steady state and considering that no power is produced in this section the equations will be:

$$\frac{1}{r}\frac{\partial}{\partial r}\left(rk_g\frac{\partial T_g}{\partial r}\right) = 0 \tag{3.4}$$

And finally the time-dependant equation governing the cladding behavior will be:

$$\rho_c c_c \frac{\partial T_c}{\partial t} = \frac{1}{r}\frac{\partial}{\partial r}\left(rk_c\frac{\partial T_c}{\partial r}\right) \tag{3.5}$$

Longitudinally the equations can be discretized by a user-defined value.

The third component *LeadTube* models the single-phase liquid flow of molten lead through cylindrical pipes with heat transfer from the fuel pin boundary. The physical properties of the fluid are all considered temperature-dependent. To describe the dynamics of pressure and mass flow rate eq.3.6 and eq.3.7 have been adopted.

$$A\frac{\partial \rho}{\partial t} + \frac{\partial \Gamma}{\partial x} = 0 \tag{3.6}$$

$$\frac{\partial \Gamma}{\partial t} + A\frac{\partial p}{\partial x} + A\rho g\frac{\partial z}{\partial x} + \frac{C_f \omega}{2\rho A^2}\Gamma|\Gamma| = 0 \tag{3.7}$$

While eq.3.8 was used in the description of the heat transport within the fluid.

$$\rho A\frac{\partial h}{\partial t} + \rho A v\frac{\partial h}{\partial x} - A\frac{\partial p}{\partial t} = \omega\Phi \tag{3.8}$$

To evaluate the one-dimensional heat transfer between lead and fuel pins placed in triangular lattice, the Ibragimov-Subbotin-Ushakov correlation [19] as seen in eq.3.9 was used.

$$Nu = 4.5 + 0.014 \cdot Pe^{0.8} \tag{3.9}$$

3.2.2 Thermal Inertia and Transport Phenomena Modeling

The description of thermal inertia of the lead side was carried out by modelling the hot and cold lead pools of the plant (fig.3.2) which are responsible for the most part of the thermal inertia of the system. For the transport phenomena outside of the core, the same model of *Lead Tube* was modified in such a way to neglect thermal dispersion.

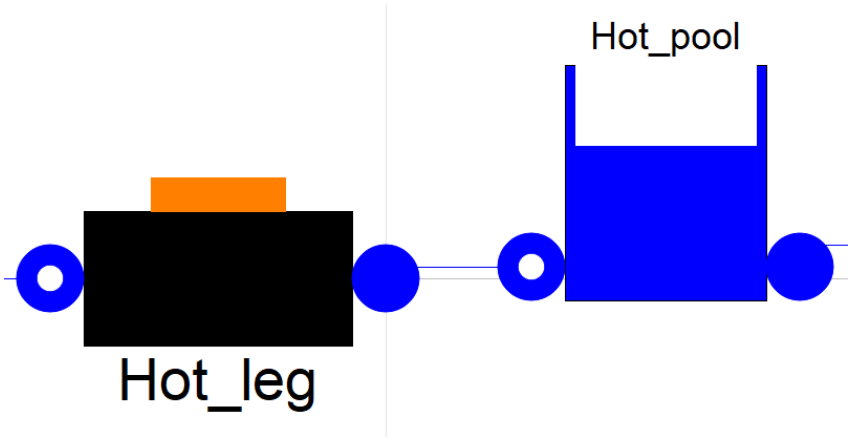

Figure 3.2: Dymola *Hot Leg* and *Hot Pool* model

3.2.3 Steam Generator

Concerning the SG model, a simplified one-dimensional model has been adopted as shown in fig.3.3. A counter-current configuration was easily implemented with the *Counter Current* block attached to the *Lead Side*. For the *Water Side*, the Dittus-Boelter for single-phase and the Chen correlation (updated from the Dymola library *ThermoPower*) for two-phase heat transfer were considered. As for the core, also for the *Lead Side* of the SG the Ibragimov-Subbotin-Ushakov correlation for the heat transfer of single-phase molten metals was used [19]. To be precise the SG block models the effect of eight bayonet type SGs which is the number envisioned in ALFRED nuclear power plant. Thus we are simulating one SG only with a power of $300MWth$. Table 3.2 sums up the nominal parameters of this technology

To better describe the heat transfer inside the SG, different wall interfaces between water and lead were implemented by adopting suitable conductive elements. The thermal resistances were computed with the Fourier equation thus enabling us to evaluate the effect of the inner and outermost tube as well as the helium gap on the overall thermal performance of the system.

Parameter	Value	Unit
Thermal power	37.5	MW_{th}
Feedwater inlet temperature	335	$°C$
Feedwater outet temperature	450	$°C$
Steam pressure	180	bar
Length of heat exchange	6	m
Number of tubes	510	-

Table 3.2: Single bayonet SG parameters

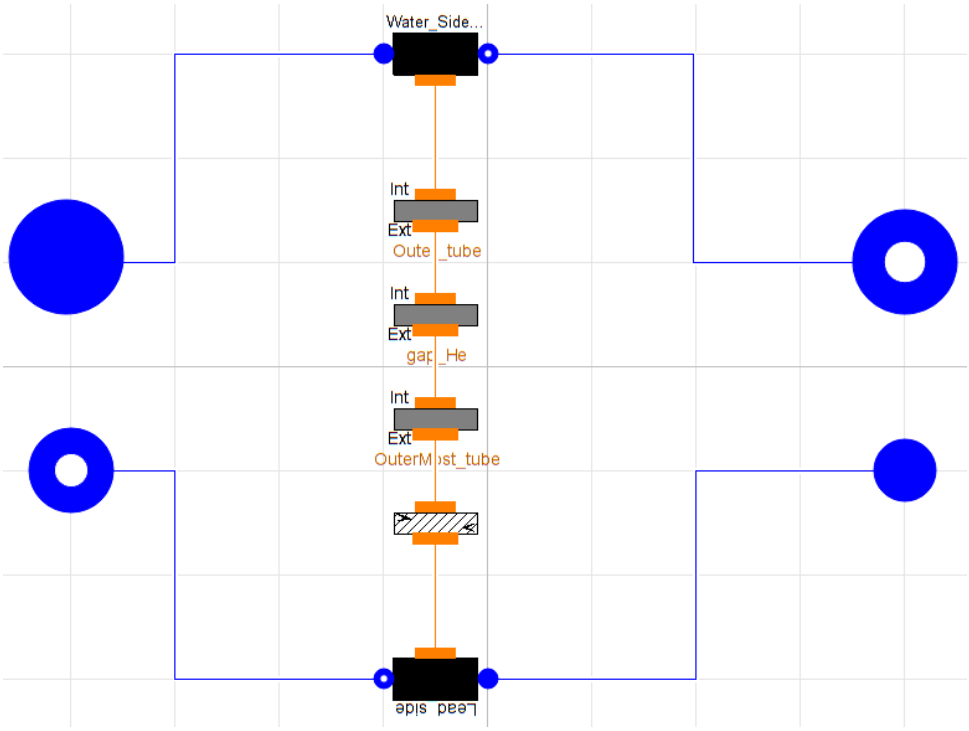

Figure 3.3: Dymola model of the Bayonet SG

3.2.4 Turbine

The simplified model of the *Steam Turbine Unit* found in the *ThermoPower* library in Dymola was used to simulate a high and low pressure stage. The mechanical and isoentropic efficiencies of both stages were calculated to deliver a maximum power of 130 MW_e in nominal conditions (i.e with *Bleed*1 valve opened and *Bleed* valve closed as in fig.3.4).

The model is extremely flexible on choosing the desired pressure of the extracted steam. This enables the study of different co-generation scenarios. In our case, the pressure was

set to 0.5 bar thereby letting us use saturated steam at approximately 80 $°C$ useful for a MED desalination plant while for MSF we should use higher temperatures of roughly 120 $°C$.

The *Bypass* is nominally closed and is opened only in low power conditions such as start-up thus avoiding jeopardizing the turbine integrity. It is also used to change the turbine mass flow rate in the case that no cogeneration is required and also suitable for pressure control.

Finally the admission valve shown as $kvValve$ in fig.3.4 can be used to control the mass flow rate entering the turbine. At the inlet the steam is superheated hence the relationship between the mass flow rate at the inlet is approximately proportional to the admission valve coefficient and the inlet pressure as expressed in eq.3.10:

$$\Gamma \approx k_v p \tag{3.10}$$

3.3 Model Testing

Starting from nominal full power steady state operation, the reactor dynamics were investigated via transient initiators. Both step insertion and extraction of the control rods as well as an increase in the secondary mass flow rate were studied.

A careful evaluation of the possible mass flow rate extracted from the turbine low pressure stage was carried out by varying both $Bleed\ Valve$ and $Bleed\ Valve1$.

3.3.1 Control Rod Step Insertion and Extraction

The dynamic response of the system to a variation of the control rod height of ±5 cm was undertaken. This is of primary importance to evaluate the correct transient behavior and time constants of the system.

At 3000 seconds the control rods are inserted while at 7000 second they're brought at their initial position. With no further external input the core automatically balances out the excess and defect of reactivity thanks to its intrinsic negative feedback phenomena between neutronics and thermo-hydraulics as shown in fig.3.5.

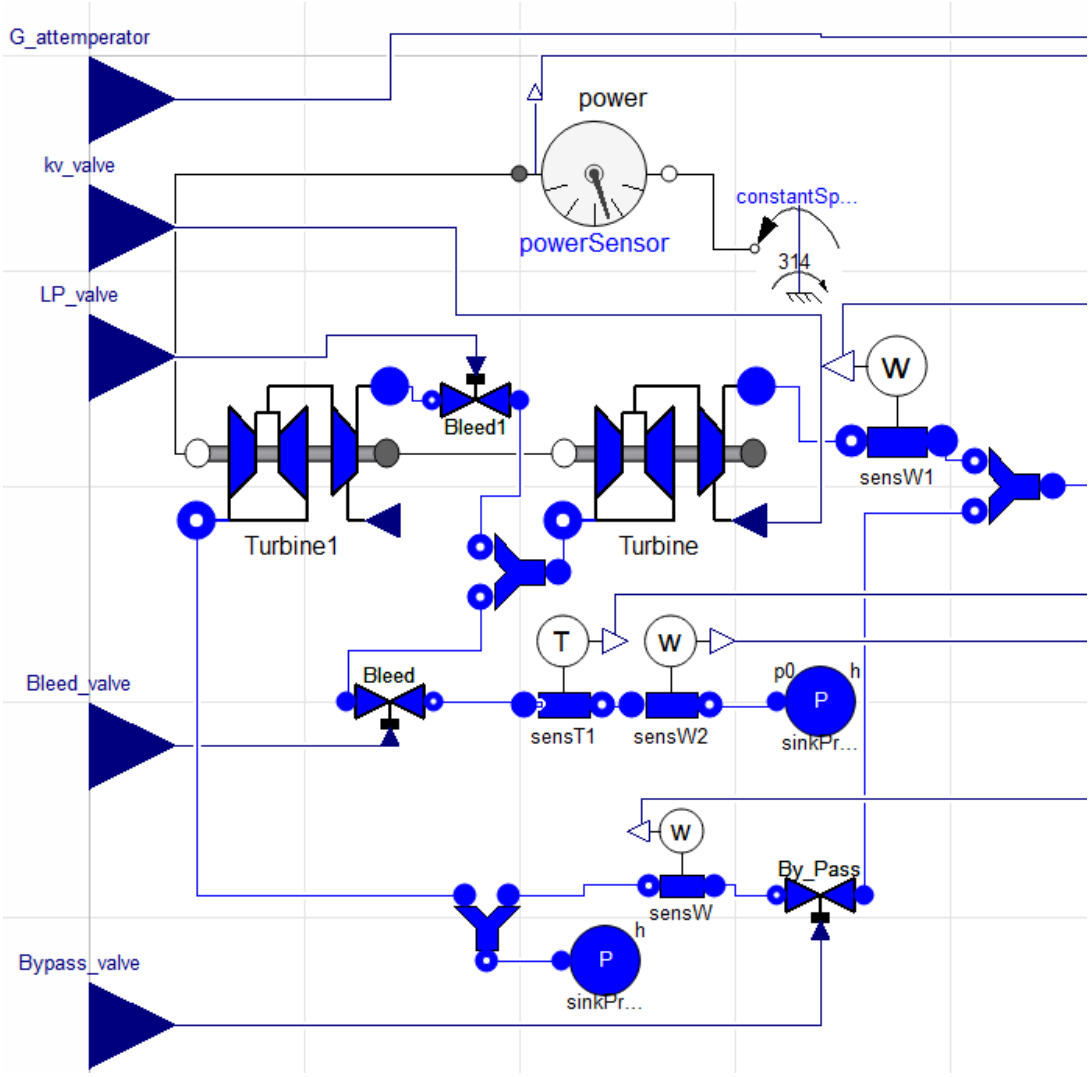

Figure 3.4: Dymola model turbine group with extraction valve

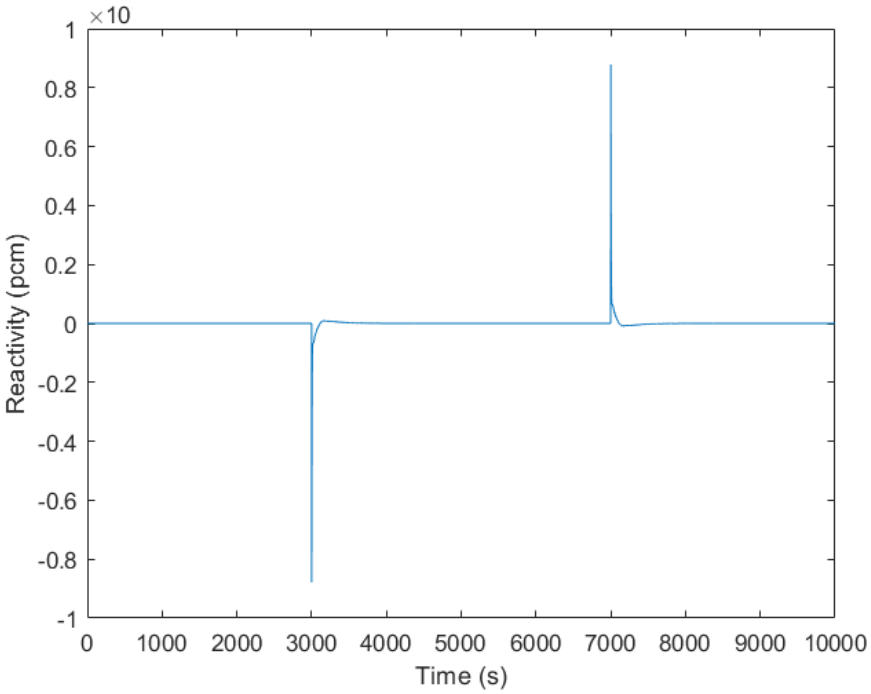

Figure 3.5: Reactivity transient by control rod height variation

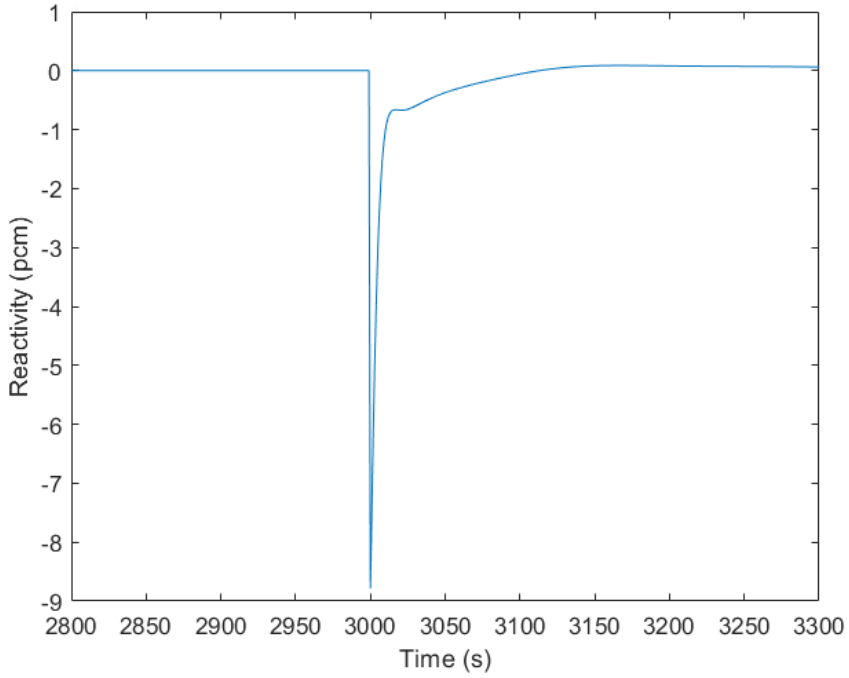

Figure 3.6: Reactivity transient close up by control rod height variation

The thermal power closely follows the reactivity by suitably adjusting itself. Indeed the control rods insertion will lead to a decrease of the power level and a withdraw will give the opposite effect as it can be seen in fig.3.7. This in turn will lead to a drop of the temperature level of both water and lead with a consequent reduction in mechanical power production (fig.3.8 and fig.3.9).

It is important to keep an eye on the steam temperature since an excessive increase or decrease could bring to damaging the turbine permanently. As an example a harsh reduction in steam temperature could bring, if not taken into account, to a water droplet production in the low pressure stages of the turbine thus leading to serious damages to the system.

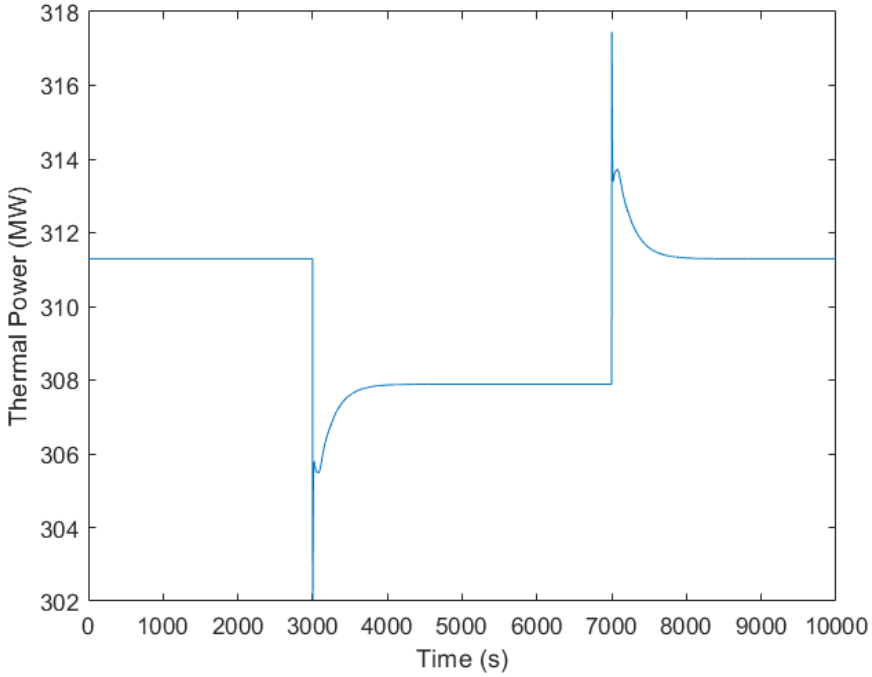

Figure 3.7: Thermal power transient by control rod height variation

In nominal power production the model is in good agreement with ALFRED's design parameter with a relative error lower than 4% calculated with eq.3.11:

$$err_{\%} = \frac{P_{simulation} - P_{design}}{P_{design}} \cdot 100 \tag{3.11}$$

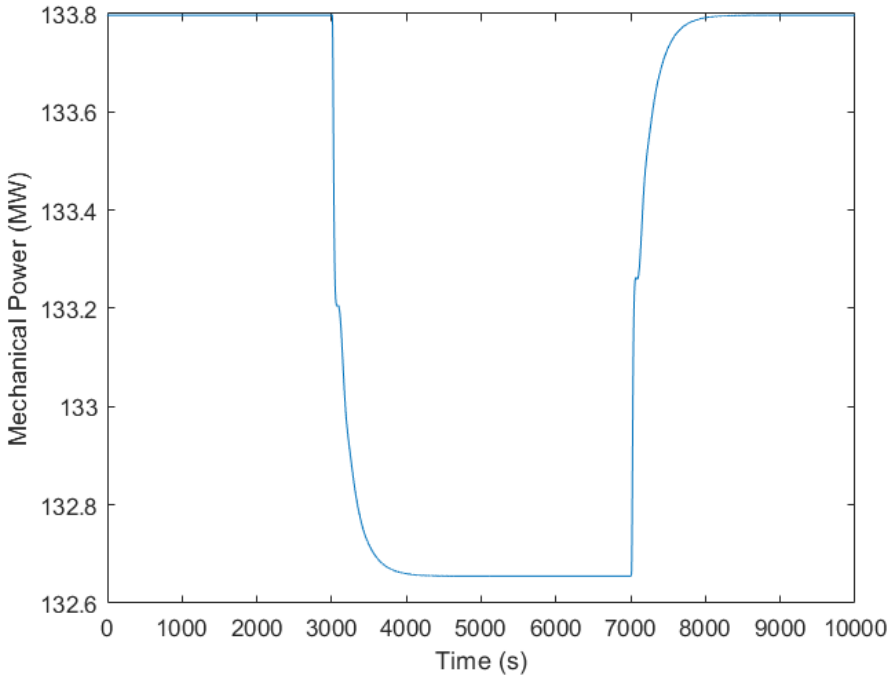

Figure 3.8: Mechanical power transient by control rod height variation

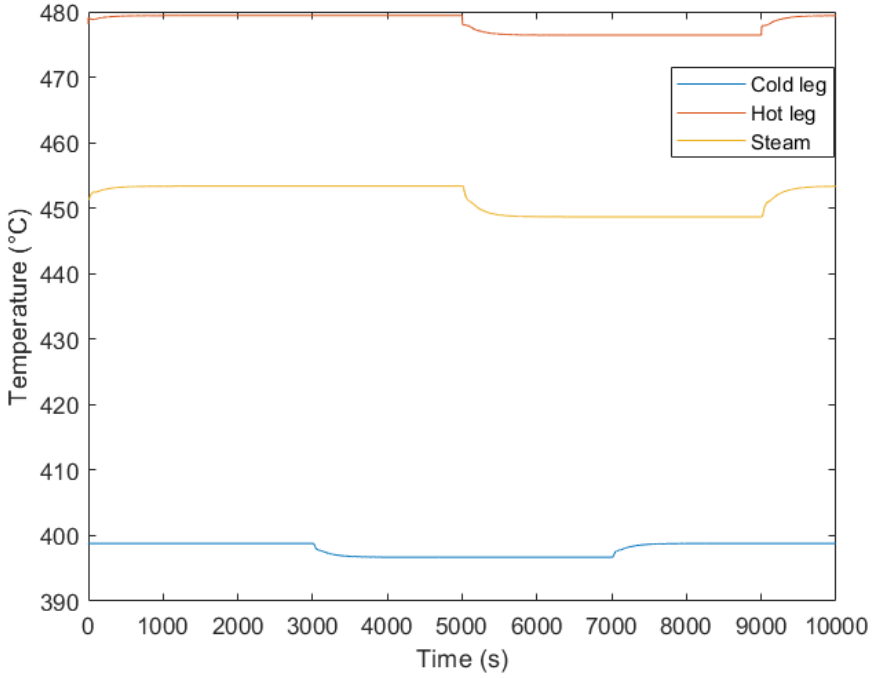

Figure 3.9: Temperature transient by control rod height variation

3.3.2 Water Mass Flow Rate Ramp Increase

Studying the behavior of a lead cooled fast reactor to a variation of water mass flow rate (fig.3.10)on the secondary side is of particular interest since it could be used as a control variable to regulate the *Cold Pool* minimum temperature that has to strictly be kept over $400\,°C$ especially throughout power transients [20]. The effect related to an increase in mass flow rate will start by having an impact firstly on the SG that will then be followed, via feedback with the core, by a power and lead temperature variation.

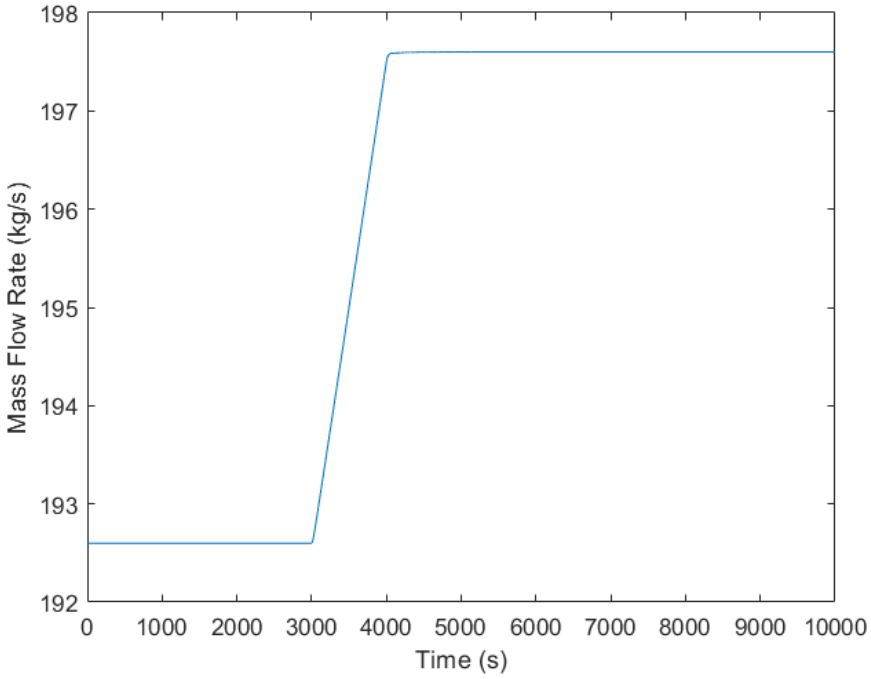

Figure 3.10: Water mass flow rate increase transient

Such increase in water mass flow rate will consequently improve the heat exchange capability of the SG thus bringing to a decrease in the average lead and water temperature and a rise in thermal and mechanical power output (fig.3.11 and fig.3.12).

As for the control rod insertion simulation, the transients have to be kept with within certain ranges to maintain the structural integrity of the system since the temperature drops shown in fig.3.13 could pose a problem if not suitably controlled. Fig.3.14 shows that an increase in mass flow rate leads to a sensible increase in the secondary side pressure that has to be avoided with suitable control strategies to maintain the integrity of the system. On the other hand also a reduction in mass flow could sensibly alter the parameters of the system with an increase in temperature levels for both lead and water and a reduction of pressure also to be strictly kept under control.

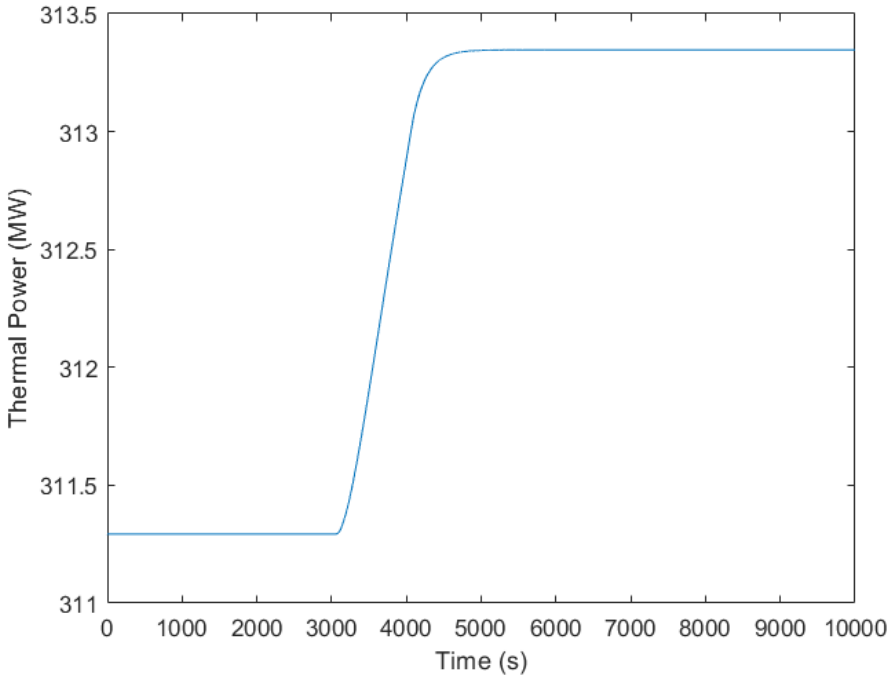

Figure 3.11: Thermal power variation to a ramp increase in water mass flow rate

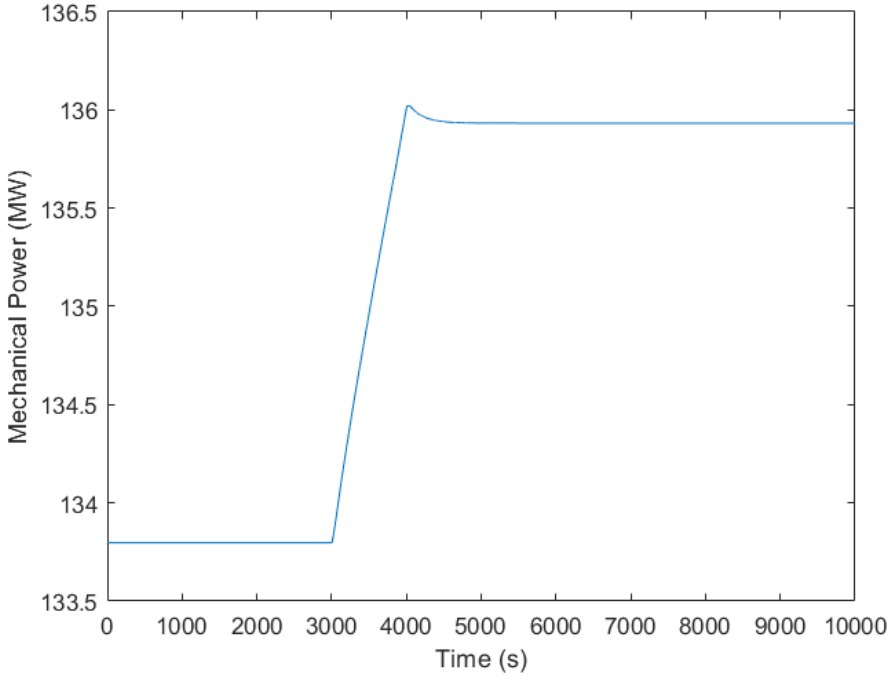

Figure 3.12: Mechanical power variation to a ramp increase in water mass flow rate

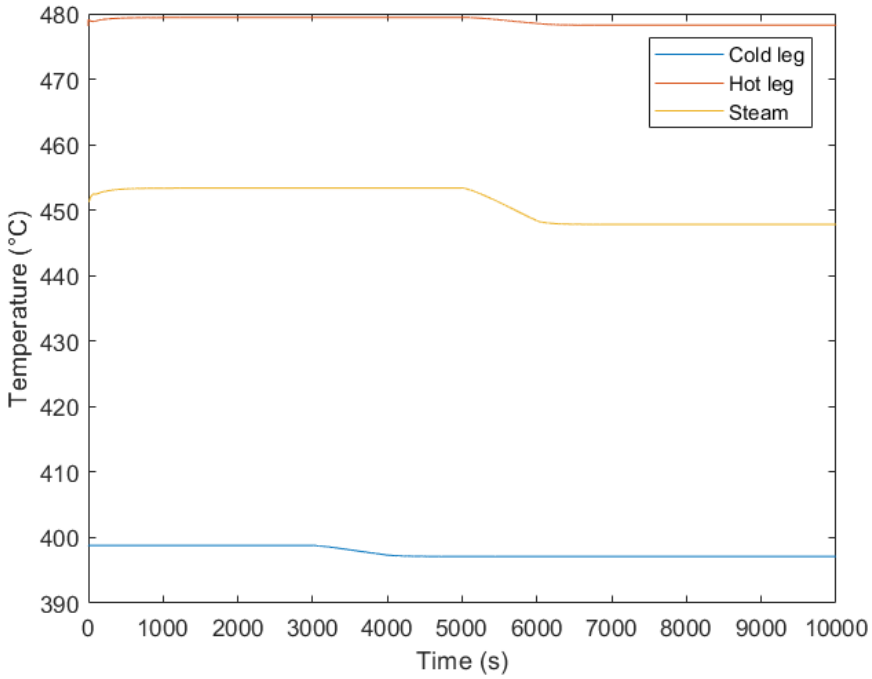

Figure 3.13: Temperature variation to a ramp increase in water mass flow rate

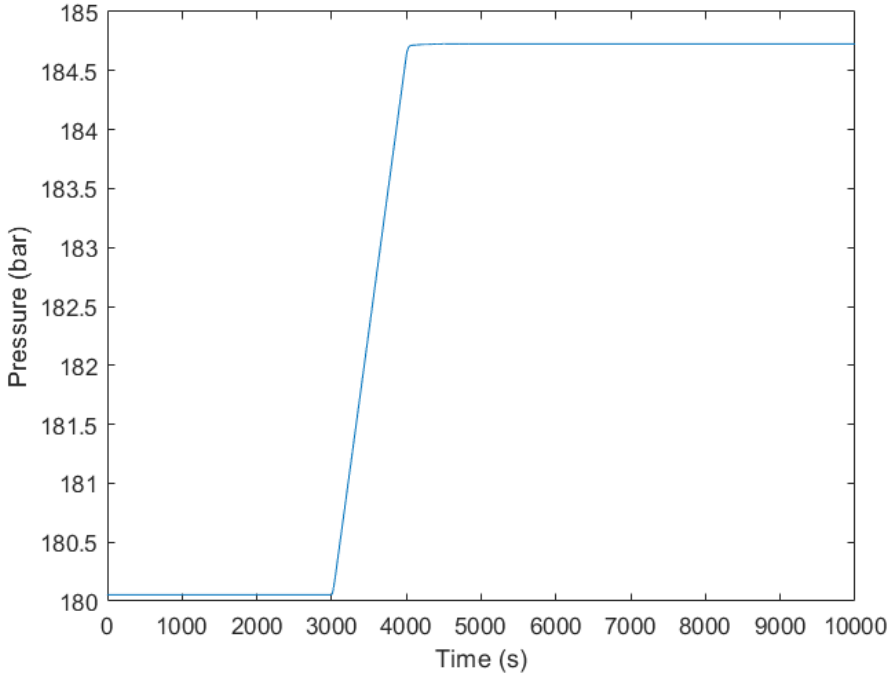

Figure 3.14: Pressure variation to a ramp increase in water mass flow rate

3.3.3 Turbine Steam Extraction

Given the high temperatures and pressures reached by the steam, ALFRED power plant could be suitably modified to enable various cogeneration options. By using the turbine modifications shown in fig.3.4, the steam extraction was carried out (at the end of the high pressure block) at a pressure of 0.5 bar thus giving a temperature of the extracted steam of roughly 80 $°C$. These values have been chosen for both the possibility of district heating and for thermal desalination in particular for MED systems.

The simulation was carried out by completely opening the extraction valve denominated $Bleed\ Valve$ in fig.3.4 at 1000 seconds and subsequently at 1500 seconds by closing the low pressure stage valve called $LpValve$ leaving it only at a 2% opening giving us an extracted mass flow rate of roughly 14 kg/s. Indeed temperature, thermal power level and turbine mass flow rate remain untouched since the extraction only changes the mechanical power output and it is confirmed in fig.3.15,fig.3.16, fig.3.17 and fig.3.18.

The efficiency of the plant was also taken into account to see the overall reduction generated by steam extraction. As seen in fig.3.19 we obtain a roughly 1.5% decrease that was calculated as:

$$\eta = \frac{P_{mech}}{Q_{in}} \tag{3.12}$$

With Q_{in} the thermal produced by the reactor and P_{mech} the mechanical power produced. Another important parameter for a cogeneration plant is the utilization factor (fig.3.20) defined as:

$$ut = \frac{P_{mech} + Q_{ut}}{Q_{in}} \tag{3.13}$$

Where Q_{ut} is the useful heat extracted from the complete condensation of the steam and was calculated as:

$$Q_{ut} = \Gamma_{ex} \left(h(T_{ex}, p_{ex}) - h(x = 0, p_{ex}) \right) \tag{3.14}$$

With x being the steam quality and h the hentalpy calculated at the outlet of the extraction and when completely condensed (x=0).

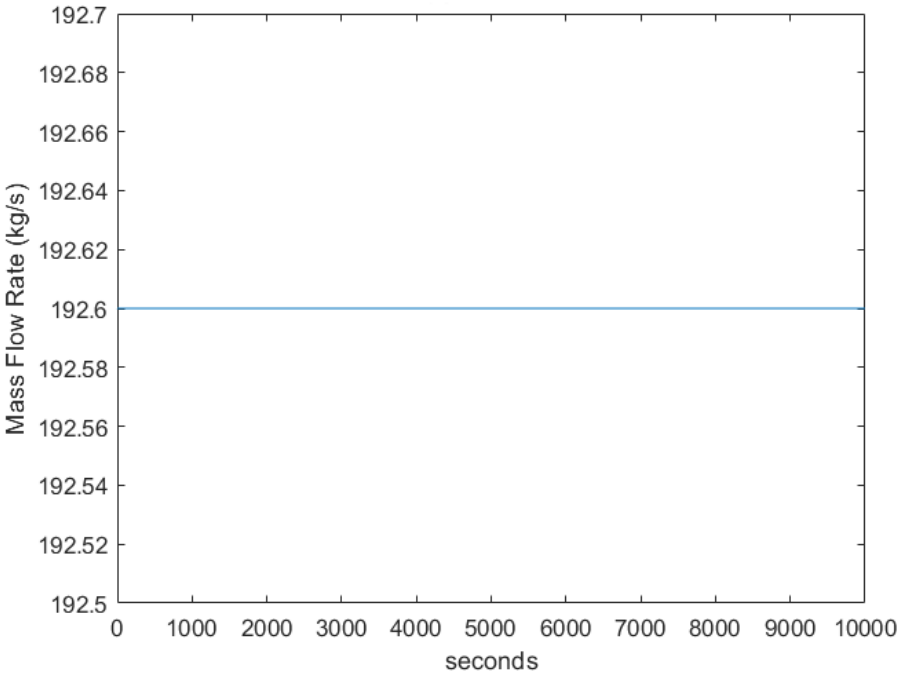

Figure 3.15: Turbine inlet mass flow rate

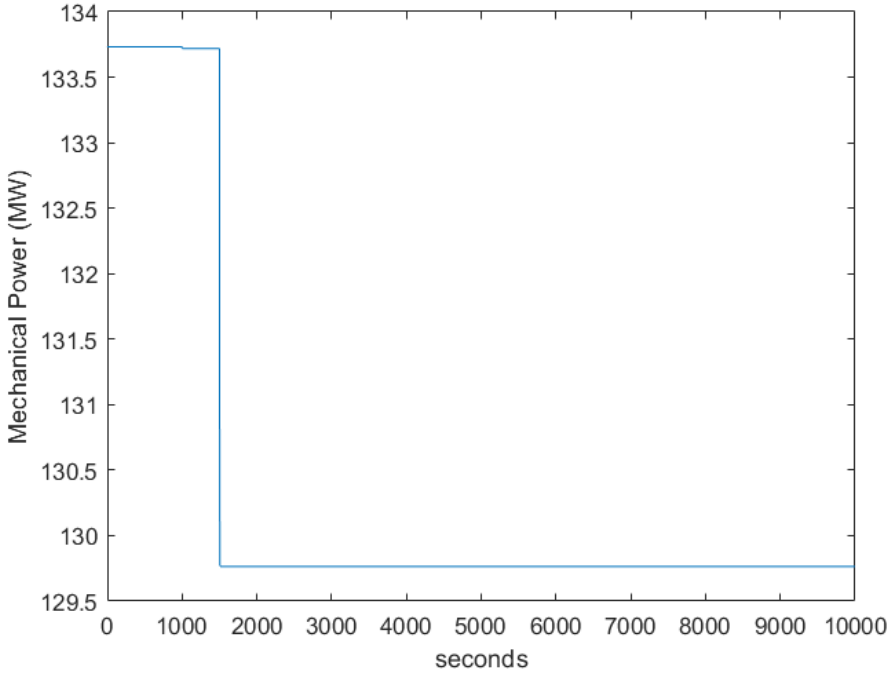

Figure 3.16: Mechanical power variation given by steam extraction

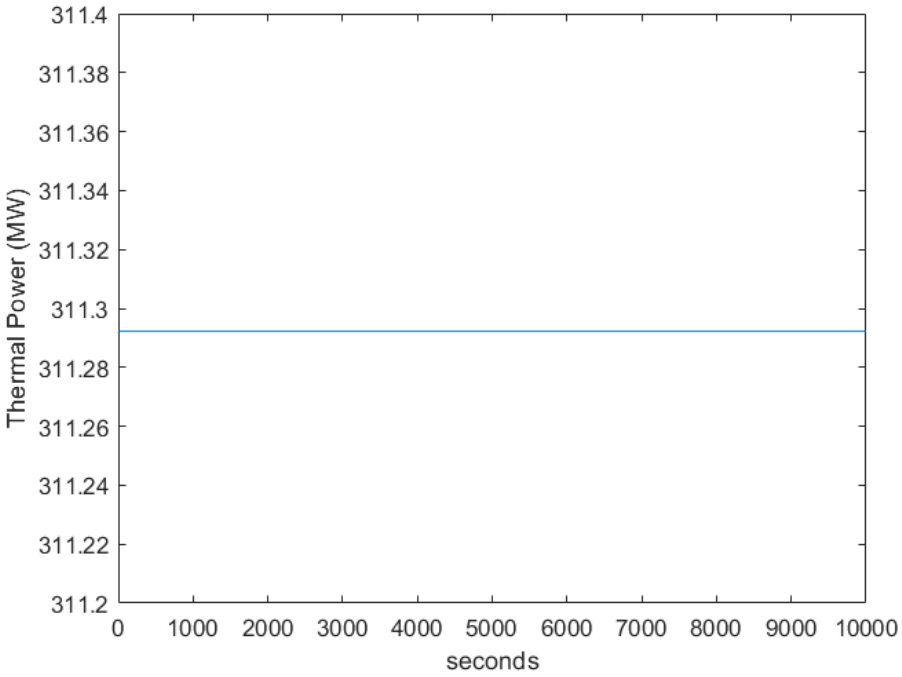

Figure 3.17: Thermal power not being affected by the steam extraction

Finally some interesting considerations have to be made on the influence of both valves. As previously mentioned, the $Bleed\ Valve$ was completely opened at 1000 seconds but, taking as an example fig.3.19 and fig.3.21, just a negligible effect on both efficiency, mass flow rate and power can be noticed. Contrarily to the above stated valve, the $LpValve$ is the major contributor to the steam extraction.

It is of extreme importance to understand that the former valve is necessary to have a proper steam extraction but only the latter influences the final output. Thus we will show in the following chapter how this behavior was exploited to simplify the control mechanism of the plant in terms of cogeneration.

3.4 Considerations

A complete simulator of ALFRED nuclear power plant was carried out on the Dymola software given the advantages it has compared to other programs. Both updates and modifications on the work of Ponciroli et al.[18] where performed to bring the model to the newest version of the program and to enable the turbine group to have steam extraction for cogeneration scenarios.

Tests involving control rod insertion and withdraw, ramp increase in water mass flow rate in the secondary loop and characterization of the extraction valves were performed. The results are in good agreement with both the design parameter and the characteristic times of the plant envisioned.

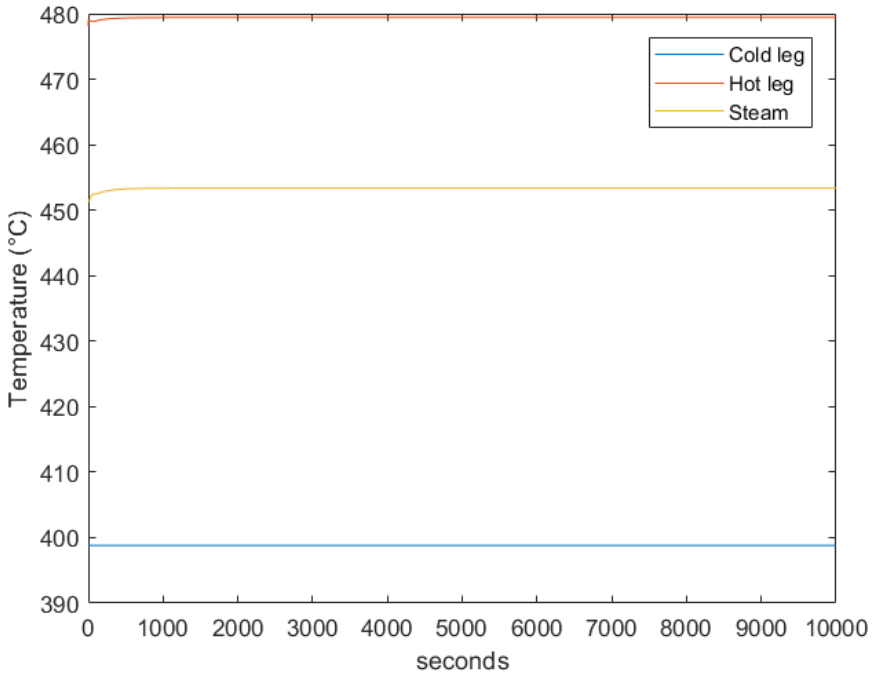

Figure 3.18: Temperatures not being affected by the steam extraction

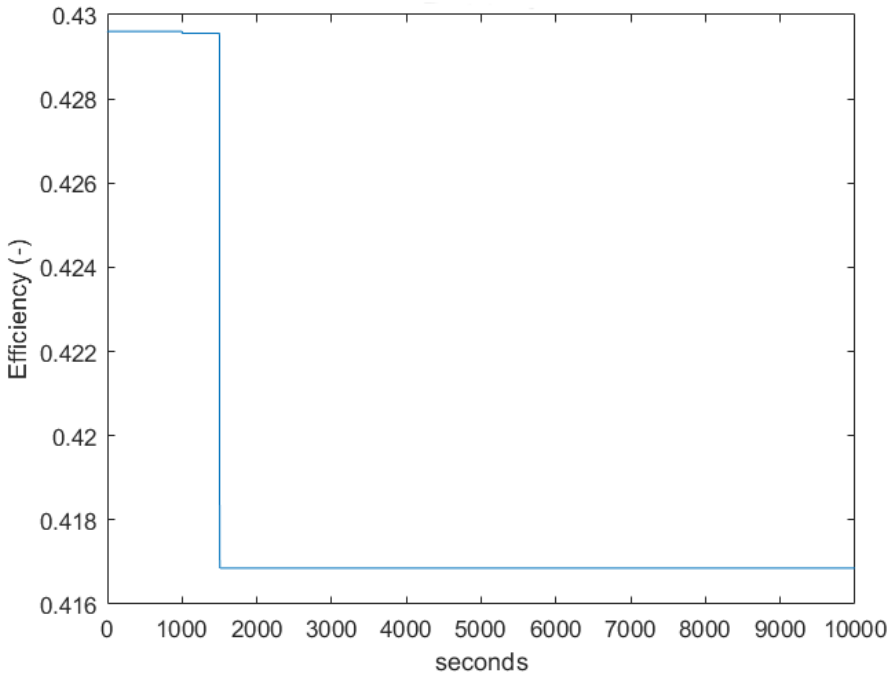

Figure 3.19: Efficiency variation given by steam extraction

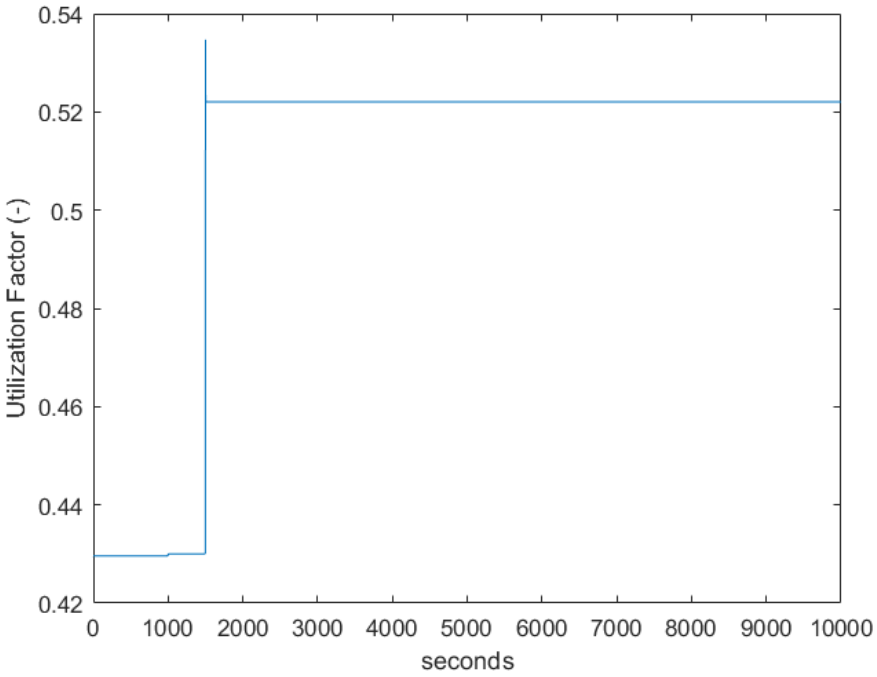

Figure 3.20: Utilization factor increase given by the Q_{ut}

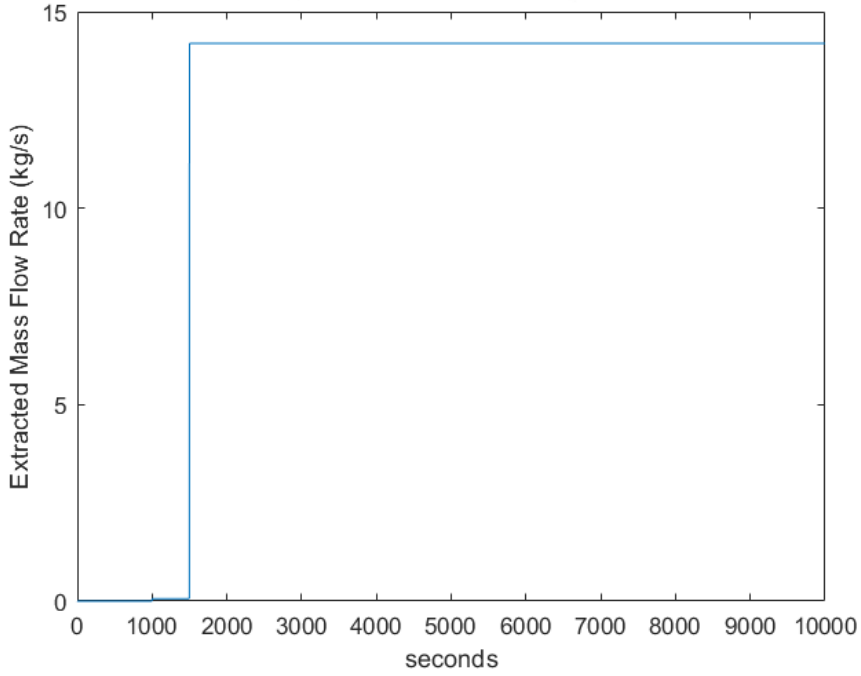

Figure 3.21: Mass flow rate of the extracted steam

Simulink Library Development

4.1 Plant Controller

Since the final goal is the development of a model capable of simulating different electrical grid scenarios with diverse renewable and cogeneration technologies, it is of primary importance to develop a controller for the reactor capable of keeping the nominal parameters constant, enable steam extraction for cogeneration and perform primary frequency regulation.

Compared to the LWR, where the control is performed by varying the thermal power output of the reactor, a different strategy has to be defined for ALFRED since the thermal capacitance of the bayonet tube SG is much lower compared to that of a U-tube giving the system slower time constants and making the aforementioned strategy not feasible for load following . Thus the flexibility of the latter goes missing in an LFR. Furthermore, particularly slow dynamics (approximately 1500 s) characterize our reactor given the lead reduced speed and large thermal inertia. To overcome this limitation, the control strategy developed by Ponciroli [20] has been adopted. This control strategy enables the decoupling of the primary loop from the balance of plant and it works solely on the steam entering the turbine by suitably venting the excess steam directly to the condenser. In addition, a *constant pressure* operation mode has been adopted since more suitable for the SG operation compared to a *sliding pressure mode* since it avoids thermal and mechanical stresses as well as rapidly varying the power production to follow the grid demand. It is also of upmost importance to keep the lead lowest temperature constant to 400 $°C$ to avoid possible freezing of the coolant and embrittlement of the components. An additional controller has been added to the aforementioned strategy to enable steam extraction at the inlet of the low pressure stage. This controller works on varying the opening of two valves, namely: the extraction valve and the low pressure valve, which are suitably regulated to enable steam extraction for for the required cogeneration power . Therefore, both feedback and feedback-feedforward controllers have been developed and tuned so to have the desired behavior of the system. Table 4.1 sums which controller loop has been adopted for every controlled variable.

Control variable	Controlled variable	Loop
Control rods height	Thermal power	Feedback
Bypass valve	SG pressure	Feedback
Turbine admission valve	Mechanical power	Feedback+ Feedforward
Feedwater mass flow rate	Cold leg temperature	Feedback + Feedforward
Turbine low pressure valve	Cogeneration thermal power	Feedback

Table 4.1: Pairings between input and output variables for the control strategy

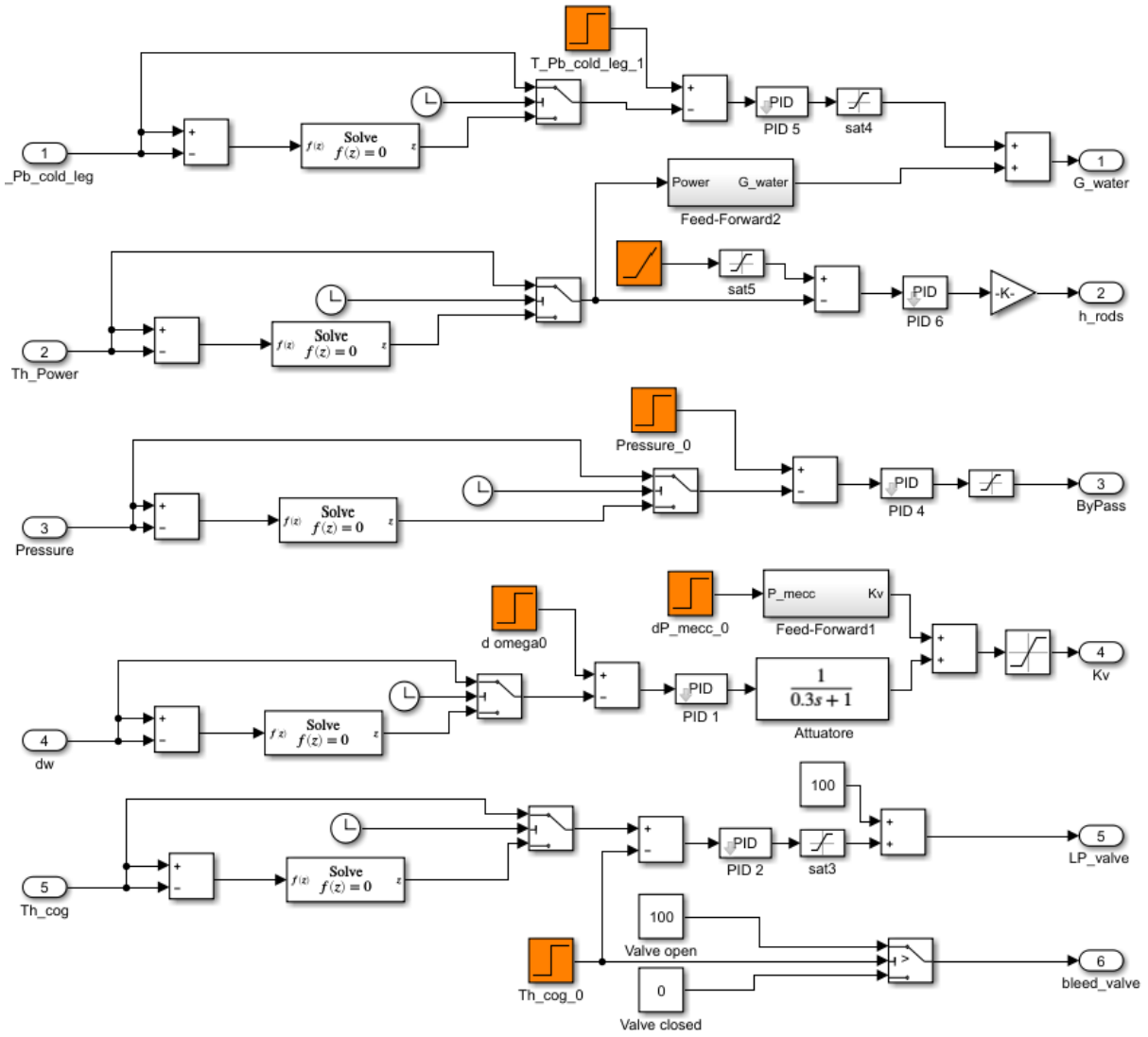

Figure 4.1: ALFRED power plant controller

The creation of the controller itself was carried out in the Simulink environment after importing inside of it the Dymola model. Using Simulink over Dymola for building PID controllers gives important advantages such as higher degree of flexibility and the possibility to choose the appropriate solver for the model. Especially with Simulink a variable step solver has been adopted for the whole model improving the overall performance and enabling to use one solver for both the FMU (functional Mock-up Unit) equations and the Simulink model itself. As a second note it is not possible to simulate a complete three-phase grid on Dymola while it is easy in Simulink thanks to the library $Simscape Power Systems$.

In fig.4.1 a detailed overview of the whole controller is shown. Two important aspects of this system have to be highlighted. The first pertaining the steam extraction controller. As stated in subsection 3.3.3, even though it is of primary importance to consider the $Bleed Valve$ during steam extraction, the only two positions in which this valve is effective are completely opened and completely closed. Thus it is mandatory to consider it in the control of the extraction for cogeneration but it will not directly affect the feedback loop which is uncoupled from it. The second aspect is related to the PID controller assigned to the mechanical power. This is used for primary frequency regulation by suitably adjusting the mechanical power via an opening signal sent to the admission valve. Therefore we're adjusting the mechanical power given the value of grid frequency. This was tuned in such a way to obtain the desired droop value which is defined as:

$$\sigma = -100 \frac{\Delta f / f_0}{\Delta P / P_0} \tag{4.1}$$

with f_0 and P_0 respectively the nominal frequency of the grid (50 Hz) and nominal power of the reactor (130 MWe). The droop value σ has to be kept in the range $4 - 5.7\%$ for NPP [21]. Thus the general form of the controller can now be calculated as:

$$R(s) = \left[\frac{1}{\sigma}(1 + s\tau)\right]\left(\frac{1}{1 + sT_a}\right) \tag{4.2}$$

With the second term being the dynamics of the actuator with T_a being its characteristic time constant and is equal to $T_a = 0.2 - 0.4\,s$ and $\tau = 0.4\,s$. This approach is sufficient to guarantee a stabilization to a new steady state in case of external perturbations. Fig. 4.2 shows the complete power plant simulator with controller and heat exchanger for cogeneration implemented.

The heat exchanger calculates the heat transferred with an external MED desalination plant. It uses the energy balance shown in eq.3.14 and, given that the hentalpies are set, it needs only the extracted steam mass flow rate as input.

The entire plant then has to be connected to a static synchronous grid so to let us study the primary frequency regulation capability of the system. In fig.4.3 the plant is

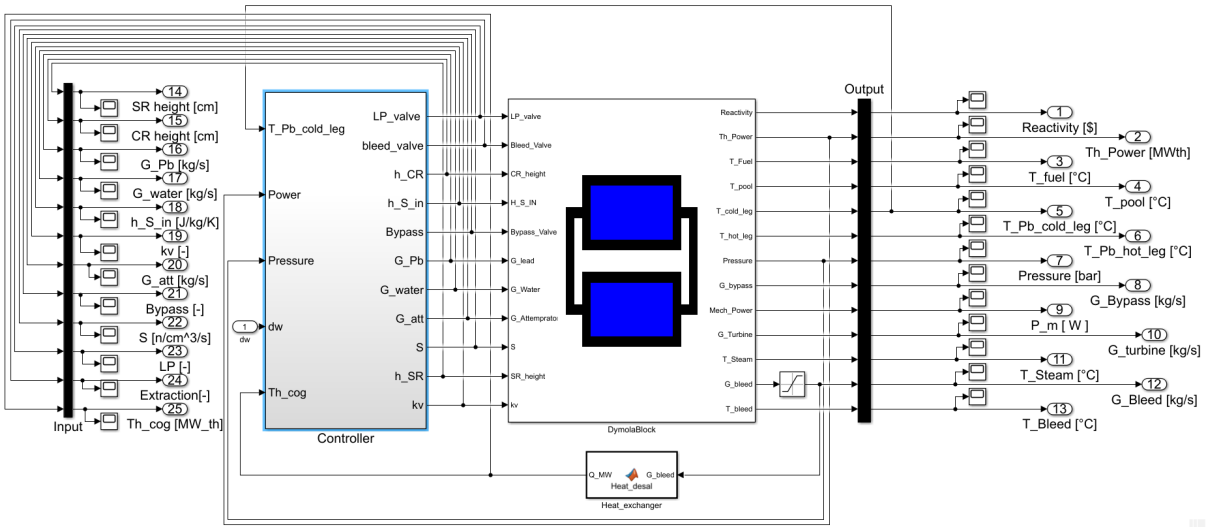

Figure 4.2: ALFRED power plant and controller

connected to a constant three-phase RLC load to keep the electrical power output at 130 MWe. The rotor speed variation is the input for the frequency regulation.

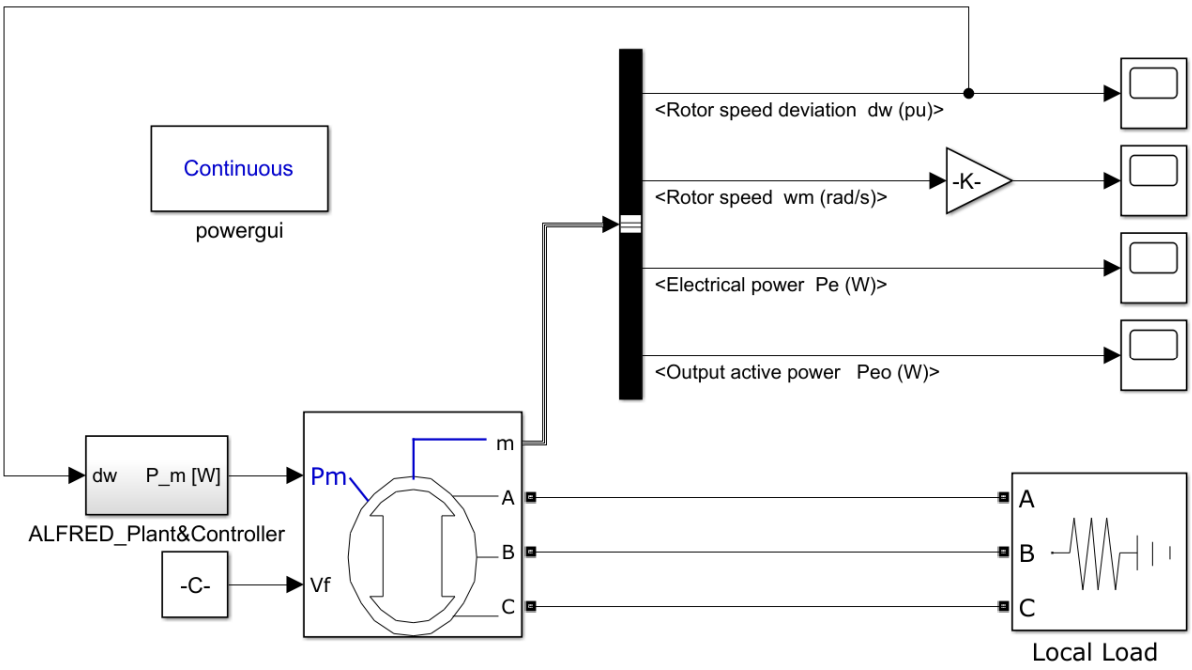

Figure 4.3: ALFRED power plant connected to a static grid

4.2 Controller Testing

In this section, the controller capabilities will be tested by studying two scenarios. The first related to a thermal power increase while keeping the load constant. This can show

us the limits of the controller in regulating mechanical power, grid frequency and other parameter. The second will study the possibility of steam extraction connected to the demand of a determined amount of heat.

4.2.1 Reactor Thermal Power Increase

The simulation follows a hypothetical request of increasing the reactor thermal power at 2000 s from 311.4 MWe to 320 MWe. All the other control variables are required to be kept constant. From fig.4.4 we can see that the reactor brings itself to the desired power. This was done by suitably withdrawing the control rods.

The mechanical power has to remain constant for how the grid is built and the frequency must arrive at a 50 Hz steady state condition. To do so the controller must work on the turbine admission valve. Fig.4.5 verifies that the controller is able to keep the mechanical power fixed by working on the $kvValve$ (fig.4.6).

With fig.4.7 we can ultimately see that the frequency is kept under control and with a transitory that doesn't exceed the range $49.2 - 50.8$ Hz [22] considered as the safety threshold for grid stability.

Given that both the pressure (fig.4.8) on the secondary loop and the cold temperature (fig.4.10) of the lead are fixed, an increase in power will directly influence the hot leg therefore increasing the average lead temperature. To keep the cold leg at constant temperature the controller has to increase the water mass flow rate in the secondary loop thus rising the pressure which is counterbalanced by an opening of the bypass valve (fig.4.11). This can also be verified by fig.4.9 which has to be maintained constant to have the same power output.

During this simulation the steam extraction for cogeneration wasn't considered therefore all the parameters pertaining it were at nominal value.

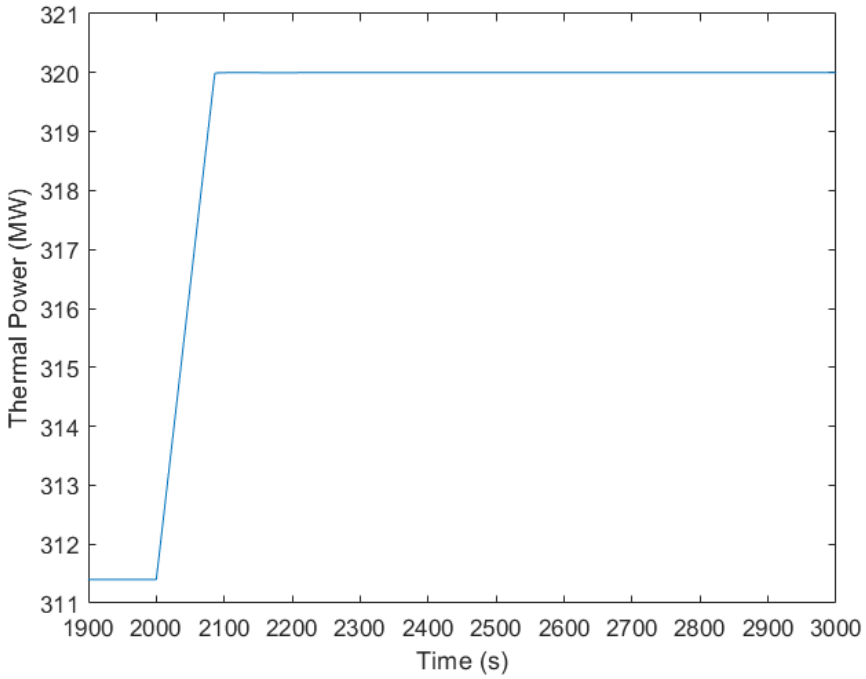

Figure 4.4: ALFRED power plant increase in thermal power

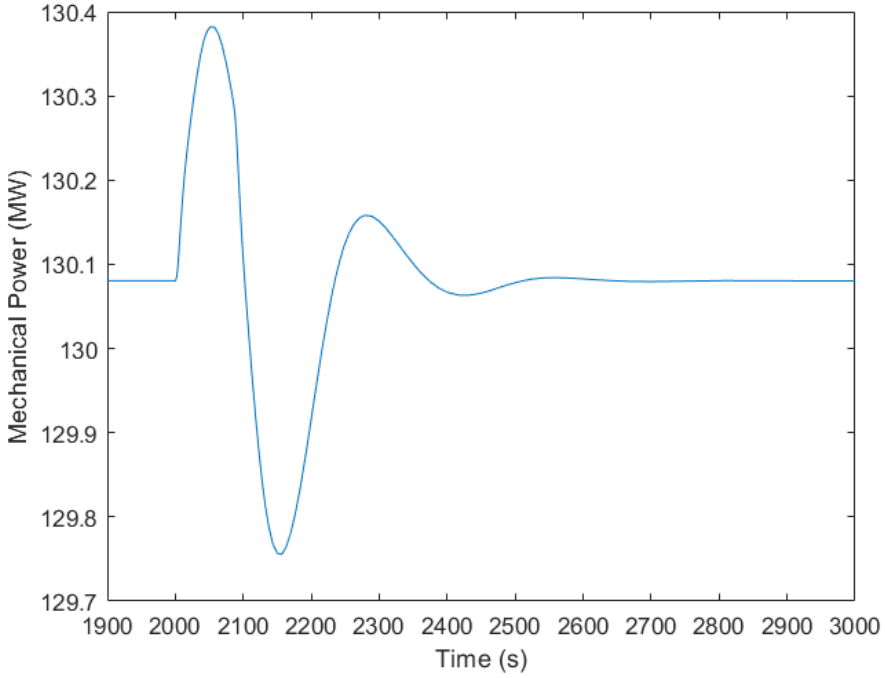

Figure 4.5: Mechanical power control

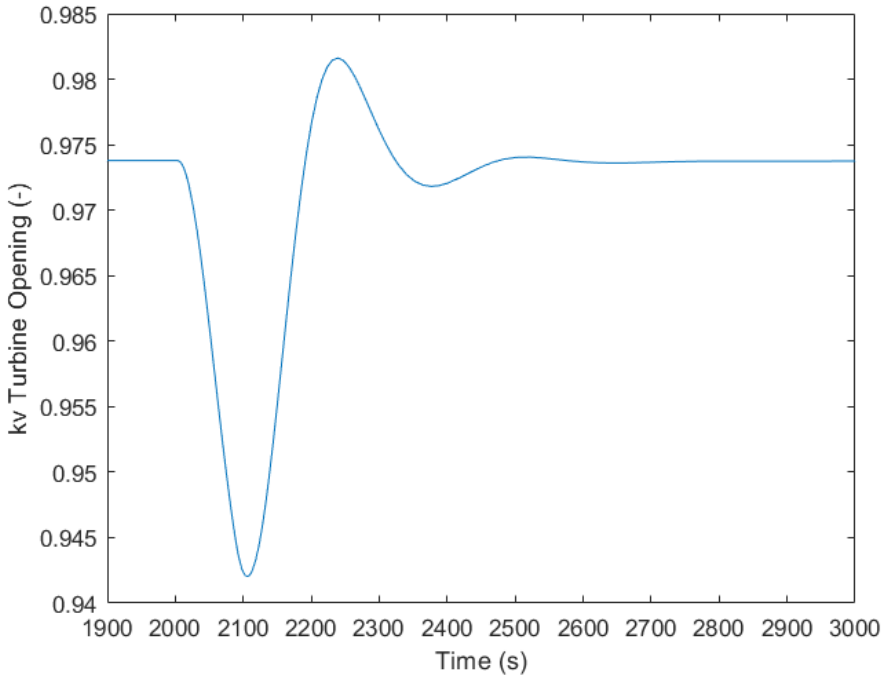

Figure 4.6: Turbine admission valve

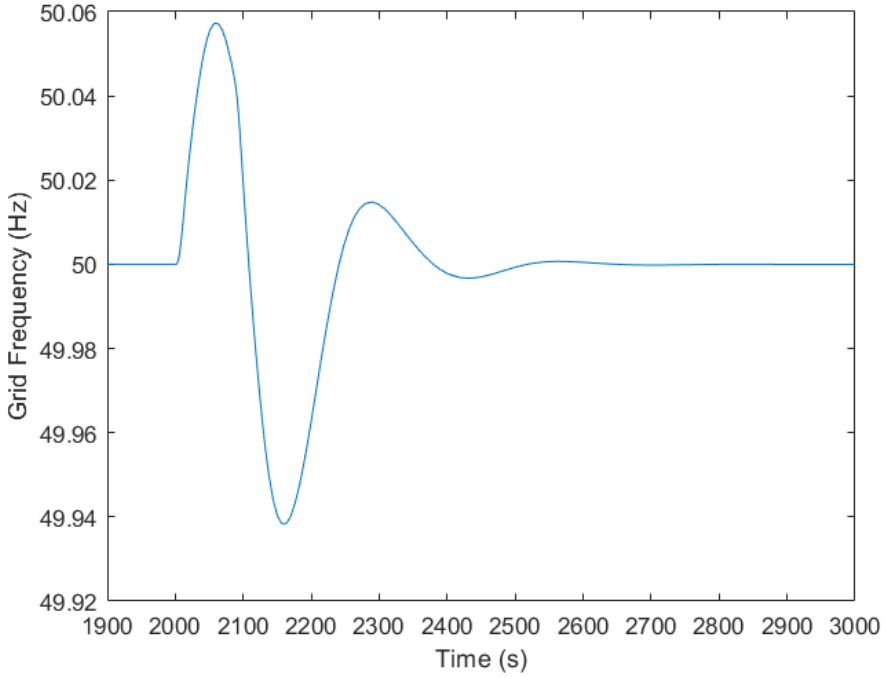

Figure 4.7: Grid primary frequency

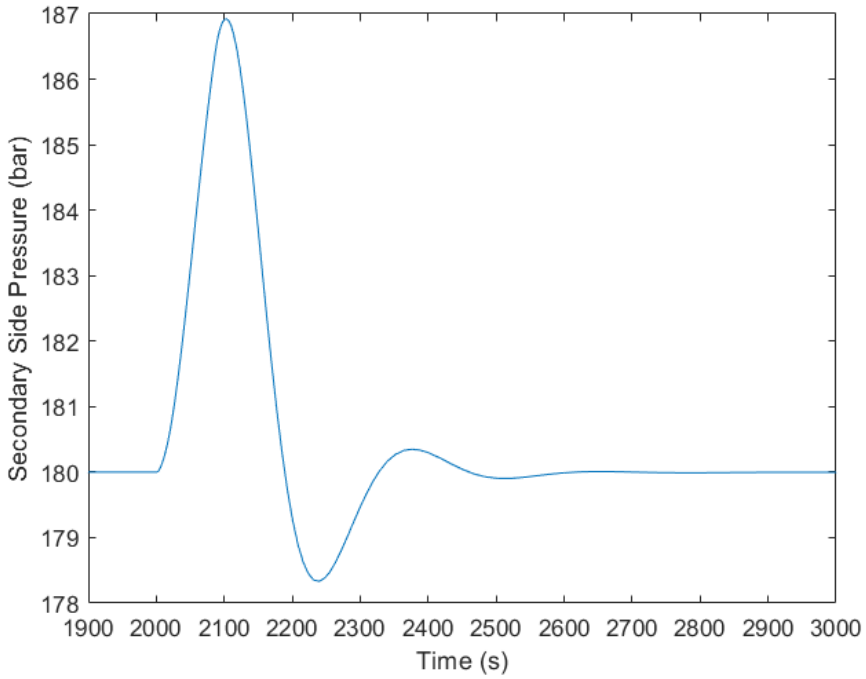

Figure 4.8: Pressure of the secondary loop during the transient

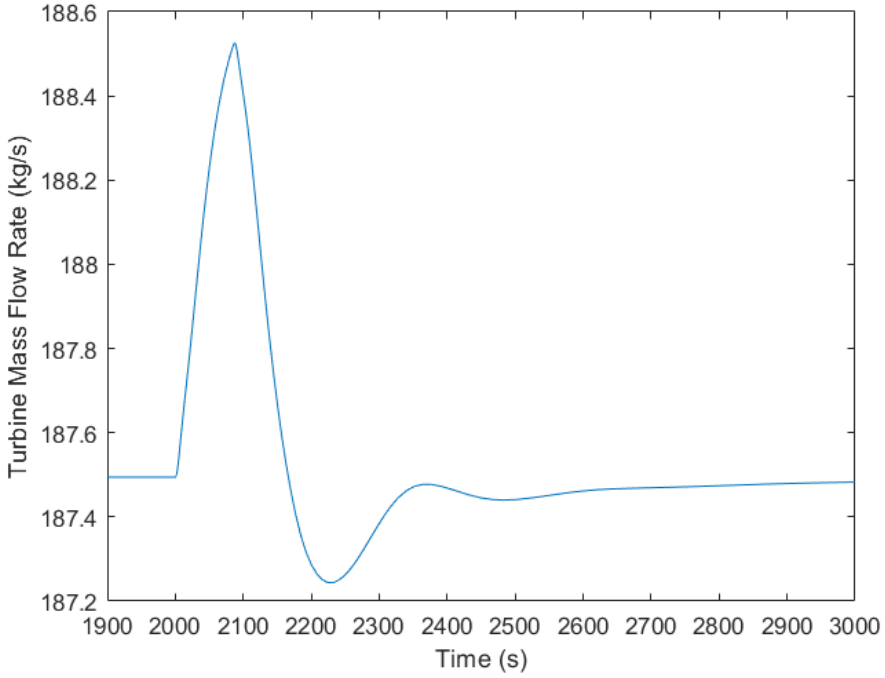

Figure 4.9: Turbine inlet mass flow rate

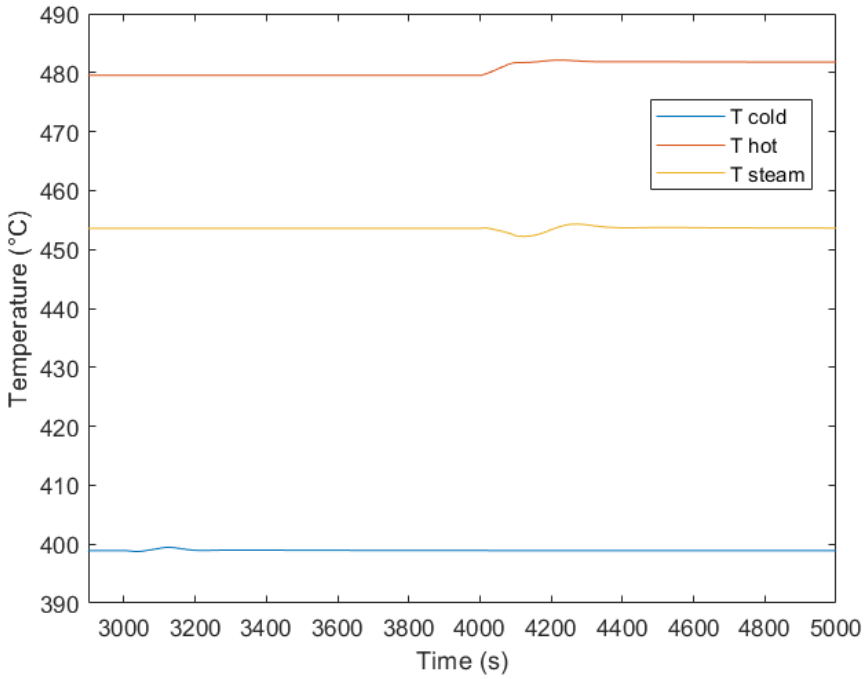

Figure 4.10: Temperature of the primary and secondary loop during the transient

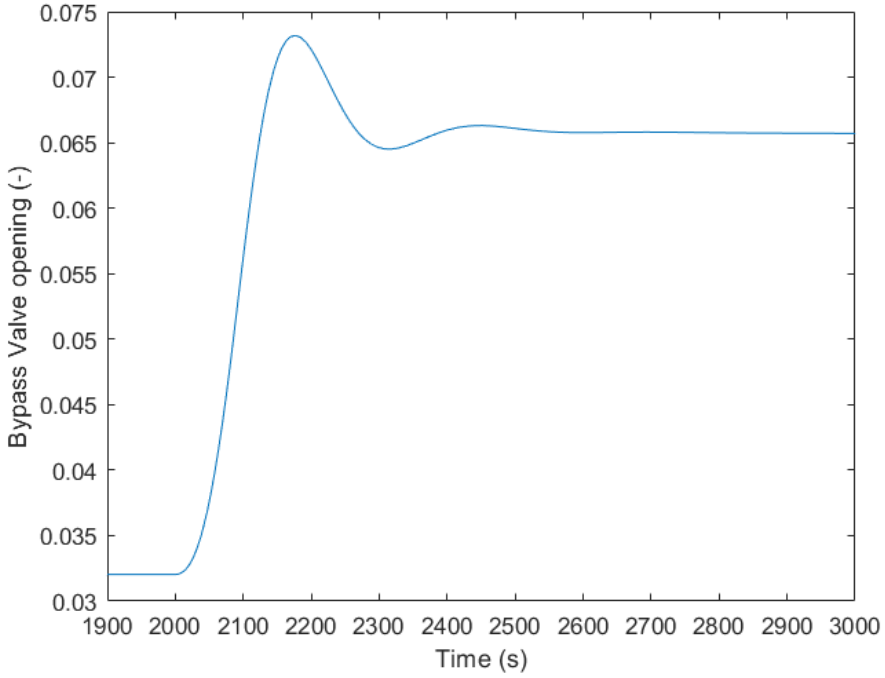

Figure 4.11: Bypass valve during the transient

4.2.2 Cogeneration Control

The scenario studied simulates a reduction of 5 MW_e in the grid consumption that is followed by keeping the nominal thermal power constant and extracting enough steam to have a suitable load follow via cogeneration. Furthermore the rapid change in grid power will create an unbalance in the grid frequency that will be stabilized by adjusting the turbine admission valve.

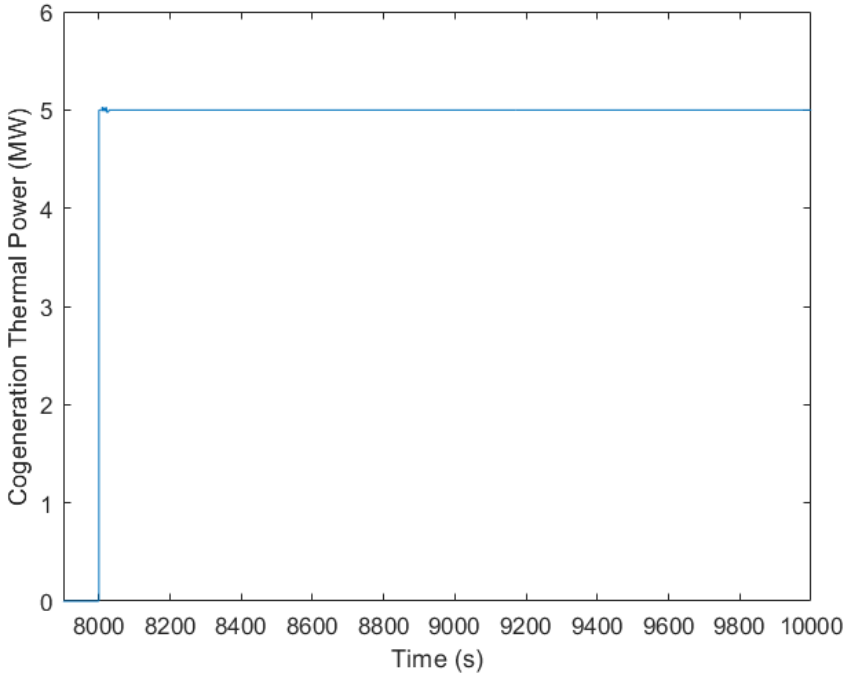

Figure 4.12: Thermal power for cogeneration

The cogeneration control was set to obtain 5 MWth (fig.4.12) which require only roughly 2.2 kg/s of low pressure steam to achieve this result (fig.4.13). The system has been set to extract slightly super-heated steam at a pressure of 0.5 bar and temperature $80\,°C$ so to enable the use in a MED desalination plant. A second version could have been built where steam was extracted at $120\,°C$ to also employ MSF technology but following considerations will show the superiority of the former technology over the latter.

As before mentioned, the turbine admission valve will have the goal of adjusting the mechanical power in a suitable way to regulate the primary frequency of the grid. In particular the results show that the admission valve needs to close to reduce furthermore the power production since 2.2 kg/s of steam extraction are not sufficient to follow the load correctly and a bigger decrease in electrical power production is required. An alternative to the admission valve would have been that of producing more heat for cogeneration, therefore reaching the desired electrical power output, which would lead to less stress on the valve which would only be used for primary frequency regulation

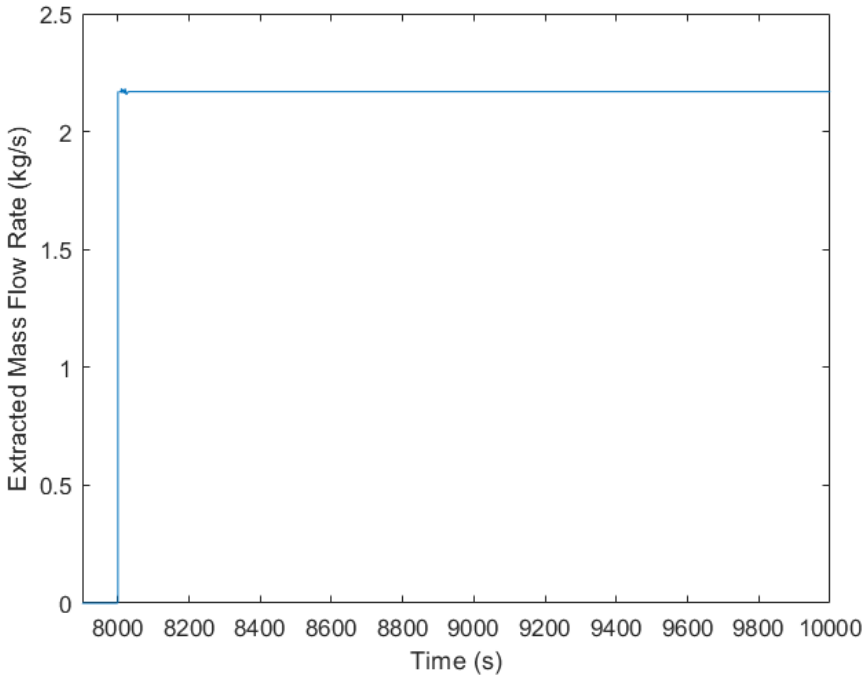

Figure 4.13: Steam extraction flow rate for cogeneration

Fig.4.14, as expected, shows that the admission valve closes to reduce the steam flow entering the turbine and enables to stabilize the grid frequency (fig.4.15). Also in this case the frequency safety threshold is respected.

Directly proportional to the admission valve is the turbine mass flow rate at the inlet which receives nearly a 5 kg/s decrease to keep up with the electricity demand(fig.4.16). The results in fig.4.17 are satisfying since the mechanical power lowers to steady state operation of 125 MWe after a short transient. It has to be mentioned that the valve new steady state is at 95 % opening. This means that, even though we're following the load via cogeneration, the primary frequency regulation control will bring inevitably to reduction in steam usage with consequent loss of revenues. A before mentioned this could be avoided partially by finding the right cogeneration heat extraction and making the valve work only on the frequency regulation.

Finally, the thermal power (fig.4.19), the pressure in the secondary loop (fig.4.18) and the cold leg temperature (fig.4.20) are kept under reasonable values during the transient and then go back to their nominal values.

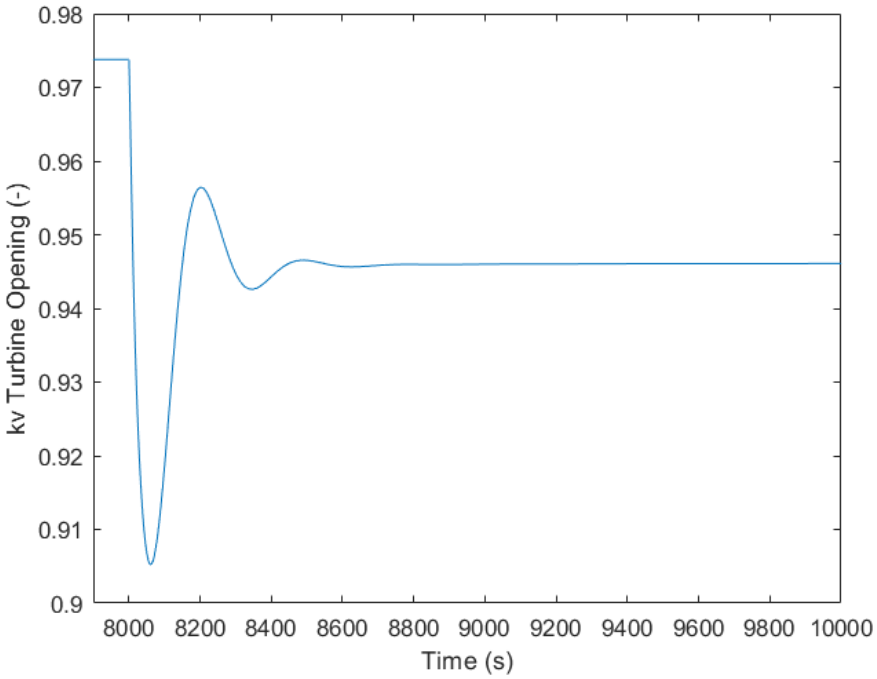

Figure 4.14: Turbine admission valve

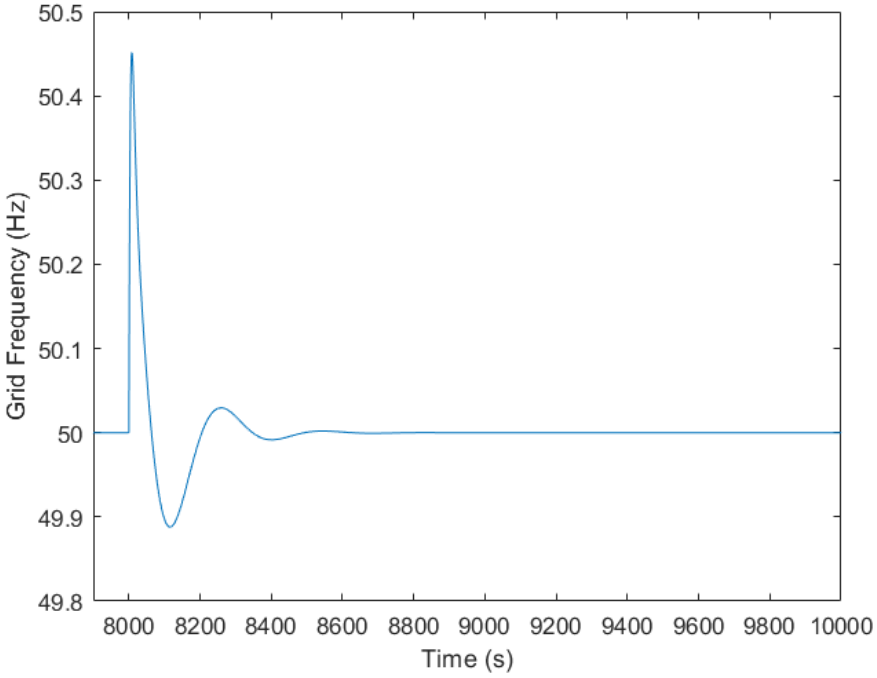

Figure 4.15: Grid frequency

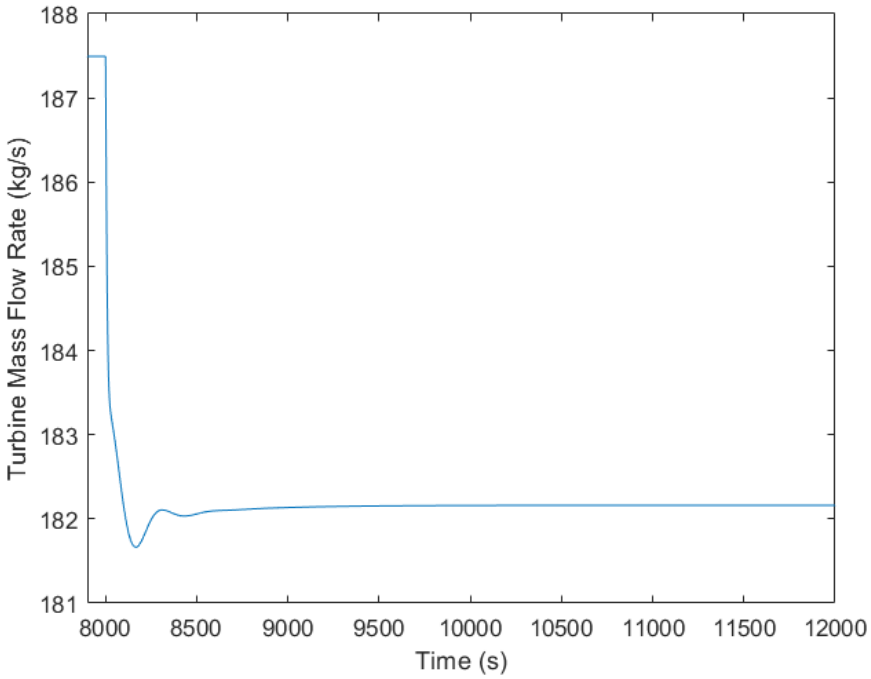

Figure 4.16: Turbine inlet mass flow rate

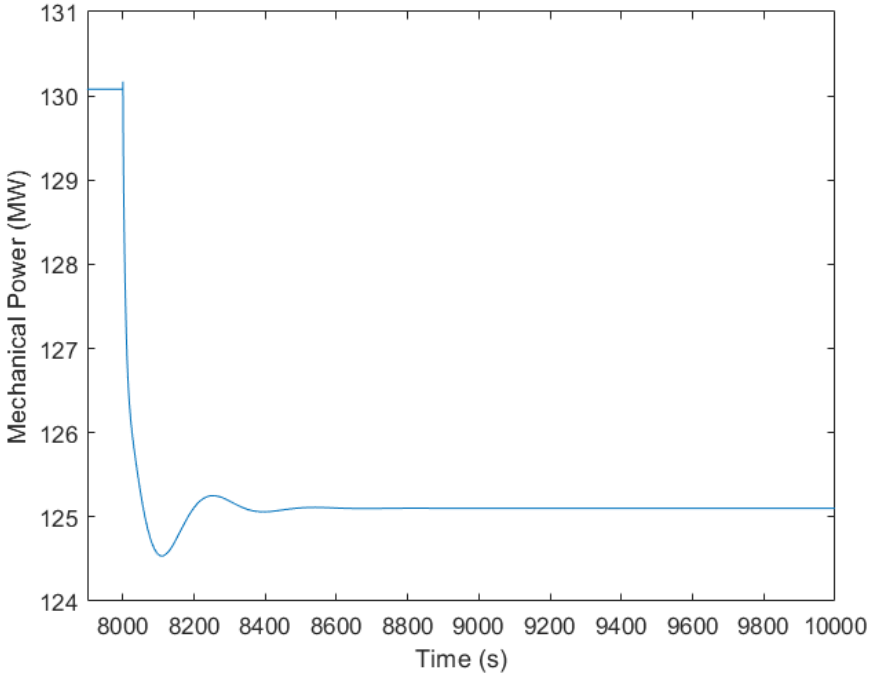

Figure 4.17: Mechanical power production

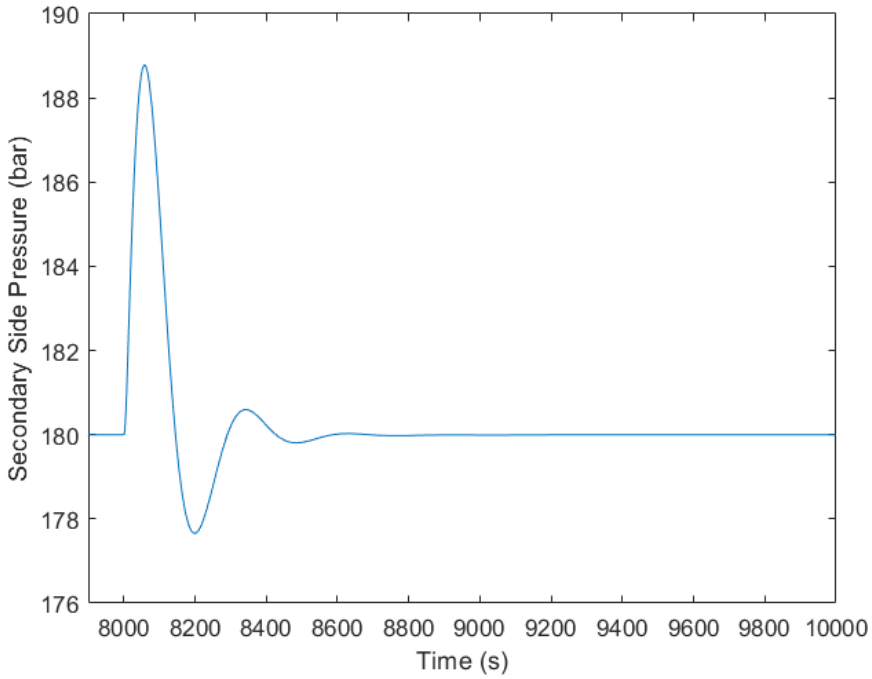

Figure 4.18: Secondary loop pressure

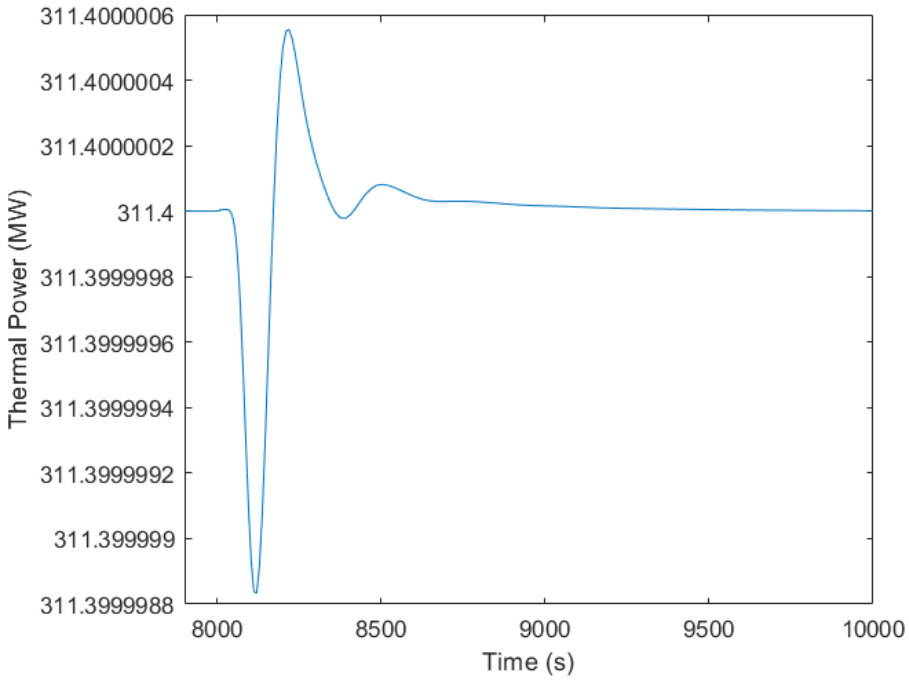

Figure 4.19: Core thermal power

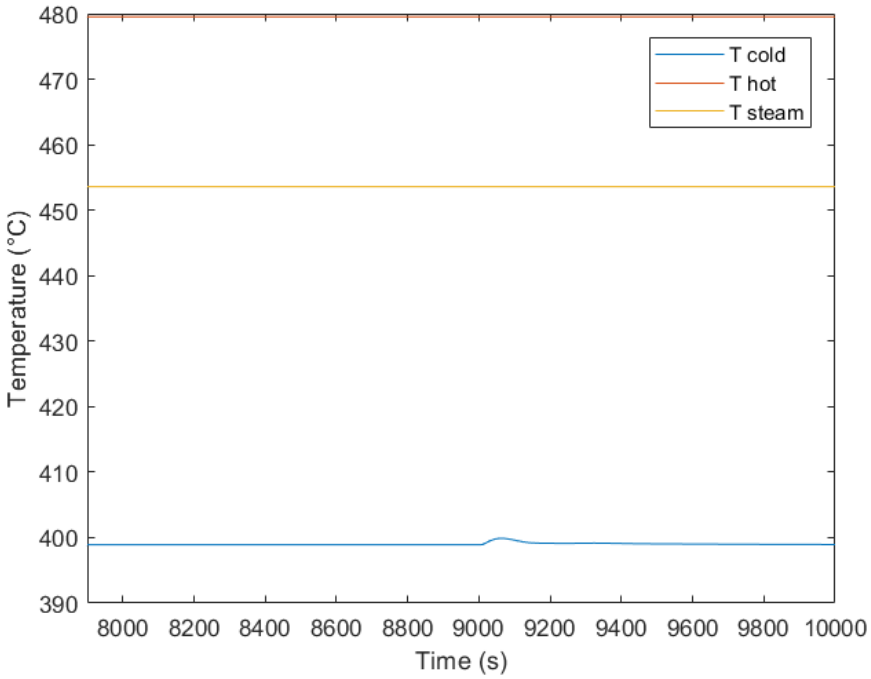

Figure 4.20: Temperatures of the primary and secondary loop

4.3 Desalination Plant Models

Simple models pertaining MSF, MED and RO have been developed and simulated singularly to verify the usefulness of these plants. For thermal desalination the developed algorithm uses as input the heat transferred from high-quality steam extracted from the low pressure turbine stage. It is therefore essential to evaluate the GOR of each plant so to then calculate the require heat for a certain daily capacity of the plant[23]. The equations adopted are the following:

$$GOR_{MED} = 0.8 \cdot \frac{MTB - T_{ls}}{ATD} \tag{4.3}$$

$$GOR_{MSF} = \frac{\Delta h|_{T_{im}}}{c_p \left(T_{ih} + T_{be}\right)} \cdot \left(1 - \exp\left(\frac{cvm \cdot T_{ov}}{\Delta h|_{\frac{MBT+T_{ls}}{2}}}\right)\right) \tag{4.4}$$

Thus we can obtain the total heat required for desalination with:

$$Q_{des} = \frac{W_{th} \cdot 3600}{GOR \cdot 24} \Delta h|_{T_{ls}} \tag{4.5}$$

With W_{th} the capacity of the thermal desalination plant.

An electrical energy requirement has also to be considered for these plants. To this aim the specific electricity consumption (SEC), expressed in megawatts, is calculated.

$$SEC_{MED} = 1.5 + 0.1\,(GOR - 10) + \frac{IFR \cdot IP}{9866 \cdot IPE} \tag{4.6}$$

$$SEC_{MSF} = 2.7 + 0.2\,(GOR - 8) + \frac{IFR \cdot IP}{9866 \cdot IPE} \tag{4.7}$$

For te RO only electricity consumption is present. This can be calculated as the sum of the electrical consumption of: the high-pressure pump (HPP), seawater pump (SP), the driving booster pump (DBP) and other expenses (OE).

$$SEC_{RO} = HPP + SP + DBP + OE \tag{4.8}$$

Taken all into account the various block were developed and tested. Table 4.2 shows the comparison between MSF and MED. The difference between the two systems are noticeable, the MED consumes less electricity for the same input heat and produces more fresh water. It is also important to consider that MED need steam at a temperature in the range $70 - 80\,°C$ and it is higher at about $120\,°C$ for MSF. Thus the former is much more suitable than the latter in a cogeneration option since the steam extraction will influence less the overall power plant efficiency.

Desalination Plant	Required electrical energy (MWE)	Capacity (m^3/day)
MED	6.78	4160
MSF	12.69	3910

Table 4.2: Capacity and required heat of MSF and MED plant for a 10 MWth input

For the reverse osmosis a direct comparison with the other technologies is difficult since it doesn't use thermal energy. Still, from the simulations, 1 MWe is sufficient to produce 5847.2 $\frac{m^3}{day}$, far superior to the thermal counterpart. At a first glance the use of RO plants seems preferable to thermal systems since it permits a simplification of the power plant (by avoiding the need of steam extraction) and increased capacity but, as

stated in chapter 2.4, in situations of high water salinity, the operation and maintenance cost of this system increase to such an extent to justify moving to a thermal plant.

Note that the results were obtained considering probable values for water salinity and other boundary conditions. Therefore the results are highly case specific and can be evaluated by changing the parameters in the code.

Interestingly, RO plants can be used as a direct alternative to battery storage systems since the aim would be the same, redirecting the electricity during the low demand hours. Thus a techno economical evaluation is required to determine whether it is more fruitful to store energy or to produce desalinated water.

4.4 Battery Energy Storage System, Solar and Wind Farm Models

For the model of battery, solar panels and wind turbines, the library developed and verified by Mathworks group [24] has been used and suitably modified to work in a 50 Hz grid instead of a 60 Hz one. The advantage of this library compared to other options was the simplicity of the blocks that directly enabled a connection to a three-phase grid without needing to add inverters, buck boost converters etc.

The *Solar Farm* block requires as input the solar irradiance (W/m^2) and can be customized by choosing the efficiency of the panels and the total area covered by the farm. The parameters shown in table 4.3 were chosen to have a theoretical maximum elecricity production of the farm of 10 MWe. The model calculates the power output of the panel as a simple product between efficiency and irradiance. The power calculated is then converted to the specific voltage and therefore current required directly into three-phase configuration.

Technology	Efficiency $(-)$	Area (m^2)
PV	10 %	10000

Table 4.3: Solar farm

The *Wind Farm* block need as input the wind speed in m/s and necessitates the nominal power, nominal wind speed and maximal or $cut-off$ wind speed to be specified. The parameters in table 4.4 were chosen taking into account a value slightly higher than the average wind speed in Milan ($2-3$ m/s [25]). This model is subdivided into two blocks, a controller and the power production itself. The power is calculated as in eq.2.3 considering it as proportional to the cube of the wind speed. The power coefficient is kept constant. A simple controller is used in a Boolean manner by disconnecting the turbine in case the top speed of the wind reaches the cut-off value.

Nominal power (MWe)	Nominal wind speed $\left(\frac{m}{s}\right)$	Maximal wind speed $\left(\frac{m}{s}\right)$
10	5	15

Table 4.4: Wind farm

Finally the *Energy Storage* model requires the grid frequency and voltage, the capacity and power and charge/discharge controls. As input the power entering/exiting the system is needed. The capacity considered is pretty high for this system (table 4.5). The reason behind this choice is merely connected to the fact that a complete charge or discharge made the overall simulation run-time sluggish. This block is composed of an under/overcharge controller which constantly check that the state of charge (SOC) of the system doesn't exceed a predetermined threshold in which case the power entering/exiting the battery will be interrupted. The other part is a SOC calculator given the capacity and power of the system. The calculated power required (or delivered) by the system is then sent to a $Three-phase\,dynamic\,load$ block which converts the input into a three-phase signal that can be used in conjunction with the rest of the grid.

Technology	Capacity (MWh)	Power (MW)
Li-ion	100 %	5

Table 4.5: Battery storage system

4.5 Considerations

In this section the controller developed by Ponciroli [20] was modified to enable the cogeneration control for the plant. Furthermore different desalination plants (RO, MED and MSF) were modelled and studied. The reverse osmosis technology shows clear advantages over the thermal counterpart since is of more simple use when coupled with a power plant and is extremely more efficient. The problem of this technology is related to the high increase in O&M costs when dealing with high concentrations of salts in water. In this case a thermal method becomes an attractive alternative. As for thermal desalination the best candidate for coupling with our plant was found to be the MED technology given it's lower operational temperature, which give a higher utilization factor, and better efficiencies of fresh water production. Moreover the photo-voltaic and wind farm, as well as the battery energy storage system block have been discussed and will be used in the next section in the complete grid model.

Two scenarios were envisioned to study the capabilities and limits of the controller: first an increase in reactor thermal power and one studying the load follow by cogeneration option. the capabilities of the controller to set the reactor to its nominal values and to keep the grid frequency stable have been satisfying.

It has to be kept in mind that in all the simulations the admission valve, starting from nominal conditions, was opened at roughly 97.5% coherently with the French experience where, to enable the required frequency control, the magnitude of variation under primary frequency control is set at ±2% nominal power [26]. Thus we are reducing the total amount of mechanical power produced by the reactor to keep the grid stable. This is of extreme importance for a techno-economical feasibility evaluation of the plant since the overall availability is sensibly reduced therefore reducing considerably the profits the NPP can make.

Complete Grid Model

5.1 Final Model Assembly

Since we want to study the influence of a high penetration of renewable energy sources into a representative European grid, it is necessary to define a suitable grid candidate to simulate, which in this case is the Milanese one of which energy demand and meteorological data are given. The scenarios that will be studied pertain one a pure electrical components system and one a thermal cogeneration system. For the former both base load and load follow reactor configuration will be studied while only base load for the latter. For the purely electrical systems a preprogrammed charge/discharge battery control strategy will be adopted while for the reverse osmosis plant the excess electrical production will be redirected to it. The capabilities of these systems will be studied separately and coupled together. For the thermal system scenario a preprogrammed thermal cogeneration during the night hours will be used for a MED desalination plant. These scenarios want to show the physical feasibility of these load follow strategies from a physical perspective, such as less overall thermomechnical stresses on the plant. Furthermore it is of particular interest to see which solution will require less help from the external grid for primary frequency stabilization and load following. Finally, having all the components verified, a representative model of the Milanese grid was constructed. Two main versions have been created, the first related to only electrical systems in fig.5.1 (i.e batteries and RO plant), the second based on thermal cogeneration systems in fig.5.2 (i.e MED and district heating).

The grid consists of a 220 kV and a 20 kv section. The reactor is considered being distant 20 km from the medium tension utility while the rest of the grid is connected via a 80 km line. The value of the network's resistance over reactance ratio has been set to 7 which is typical of a 220 kV transmission line [27]. The network in considered fully meshed with a 2 GW power production, therefore it can compensate for power unbalances.

In the electrical only simulations that will be proposed, the reactor will operate both in *Base Load*, where the regulation will be left to the outer network and *Load Follow* configuration where the reactor will try to stabilize the grid and vary the mechanical power output acordingly with the demand. The remaining portion of the demand will be covered by a combination of grid, solar, wind and batteries. For thermal cogeneration a simple preprogrammed *Load Follow* strategy will be used.

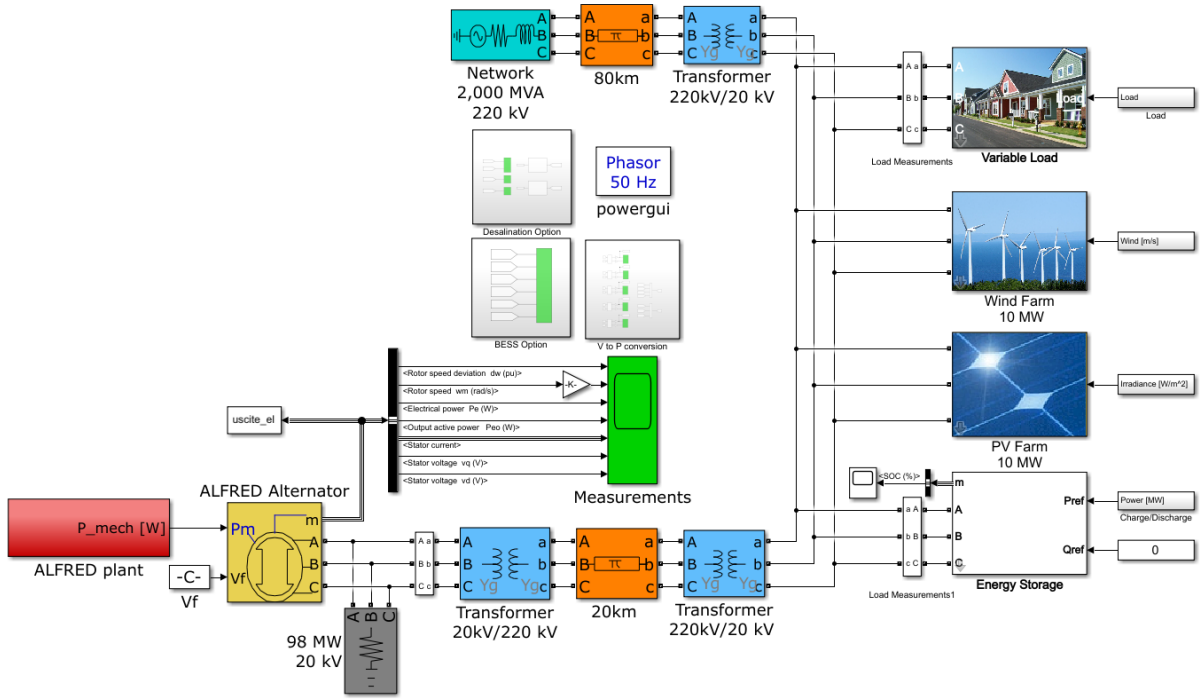

Figure 5.1: Entire grid model for electrical systems only

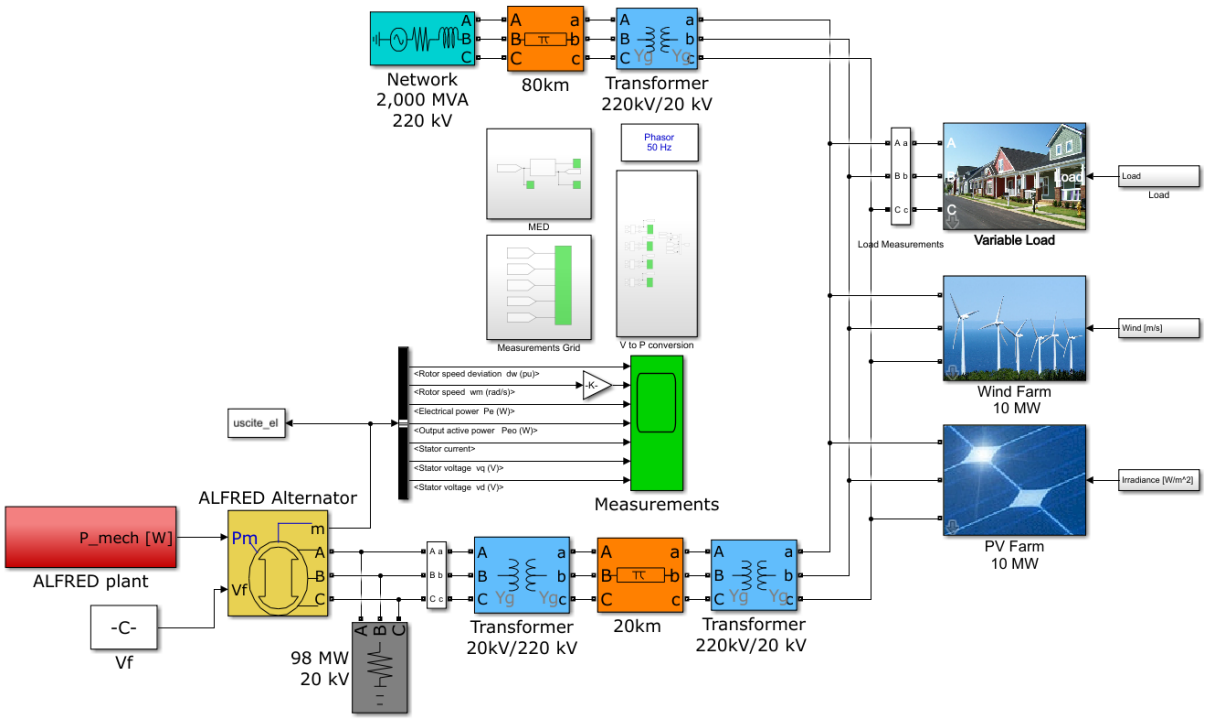

Figure 5.2: Entire grid model for thermal cogeneration systems

As for the blocks pertaining solar and wind farm, the inputs that have been used are the data relative to the 13^{th} July 2020 for energy demand, solar irradiance and wind speed taken on an hourly basis. A *Variable Load* block has been added to account for the daily load variation.

In the cogeneration model, the battery storage system has been removed since during low demands period the surplus in electrical production is converted to heat thus making the batteries useless for load follow. Still, lower capacity high power batteries could be used as an alternative to the reactor for frequency regulation thus keeping the reactor working at 100% nominal power.

The model shown in fig.5.1 will in parallel run more scenarios. This is able since it will calculate the effect of the battery storage system and the RO plants separately and in conjunction both for *Base Load* and *Load Follow* . The same thing will not be done for the thermal cogeneration model in fig.5.10 since the battery pack is not present therefore being able to study only a *Load follow by cogeneration* scenario.

5.2 Grid with Battery Storage System

As for the battery option, it is mandatory to chose a charge/discharge control to enable optimal energy capacity for the required peak shaving and grid stability, since the power output of the batteries can't be adjusted in real time to follow the load. Therefore a correct control strategy choice for batteries can improve the load following capabilities of the system at a reduced capacity of the battery pack. In this simulation, a preprogrammed *Time Controlled* charge/discharge method has been proposed where during night time the batteries get charged and during the day discharged [28]. More sophisticated and predictive methods could be implemented to improve the overall system performance and reduce the required capacity of the batteries. Fig.5.3 shows the single contributions of each plant. The battery storage system was set to discharge condition near the point where the *Load* curve becomes greater than *ALFRED* power plant production. Of course the time when this will happen can't be known in advanced but it can be approximated with good precision by looking at the data from the day before. To be noted that the plot shows only the variable part of the energy demand in fact fig.5.1 and fig.5.2 show a 98 MW static load attached to the reactor.

The results are significant when compared to the standard case with no batteries installed (fig.5.4). The storage system, even with the simplest control method possible, is able to effectively reduce the gap between the two curves (fig.5.5). Better control methods would only reduce the gap even more enabling better results.

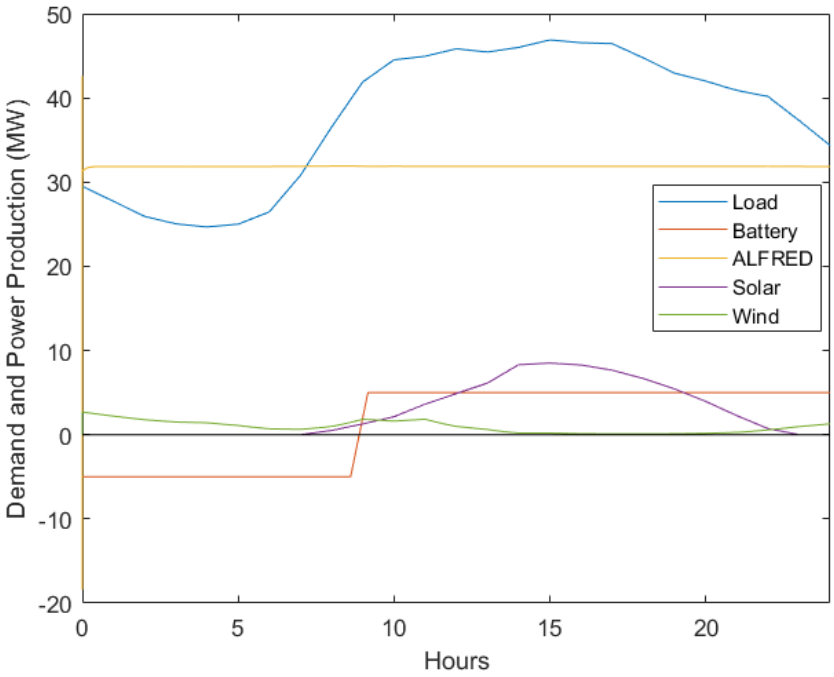

Figure 5.3: Electrical demand and separate contributions of every energy device

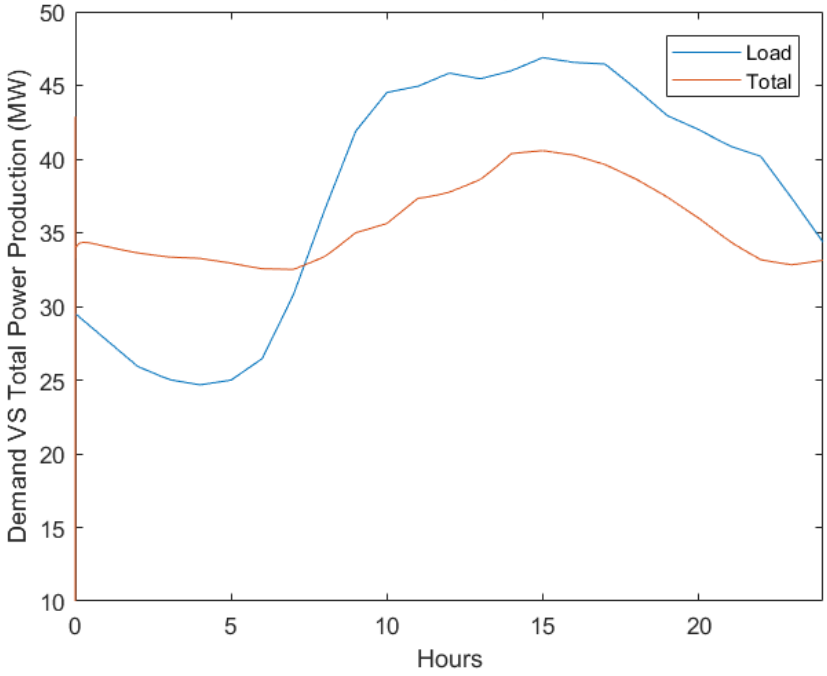

Figure 5.4: Electrical demand VS. Total energy produced without battery storage system

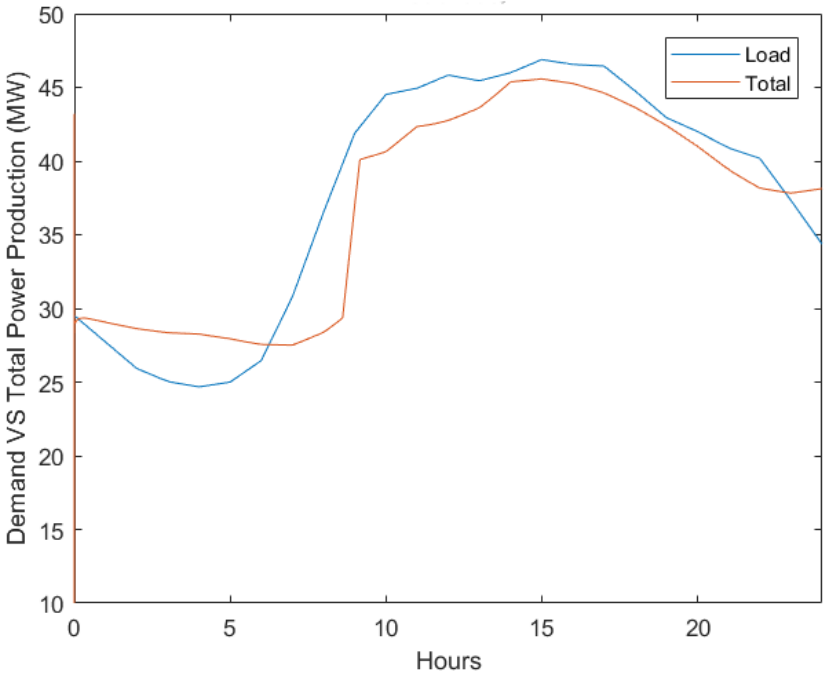

Figure 5.5: Electrical demand VS. Total energy produced with battery storage system

5.3 Grid with Reverse Osmosis Plant

An alternative to the storage system is redirecting the excess electricity production to an RO desalination plant. Fig.5.6 shows the capacity of the plant, which is the output of the desalination block, during the various hours of the day for the case without batteries. Thus the difference between the two curves in fig. 5.4 in this case is canceled when we have a surplus in electricity production (red line greater than the blue) but remains untouched when the electricity demand is higher than what is being generated. A third alternative could be coupling batteries with a smaller RO plant in such a way to reduce even more the gap between the two curves at the cost of lower daily fresh water production (fig.5.7).

All the aforementioned results are valid alternatives from a technical feasibility. Which option is the best is extremely case specific. For example, considering a geographic region with plenty of easily accessible fresh water,the installment of a desalination plant would be useless and the main goal would be to follow the load. On the other hand, places with scarcity of fresh water would probably choose the option of only using desalination. Technically speaking, although feasible, working at partial load with a desalination plant is not advantageous from an economical point of view therefore when considering the maximum capacity of the plant it would be more convenient to build a smaller one which on average works at higher capacity.

In all the electrical scenarios aforementioned, the physical parameters of the reactor remain constant thus it was deemed uneccessary to show them.

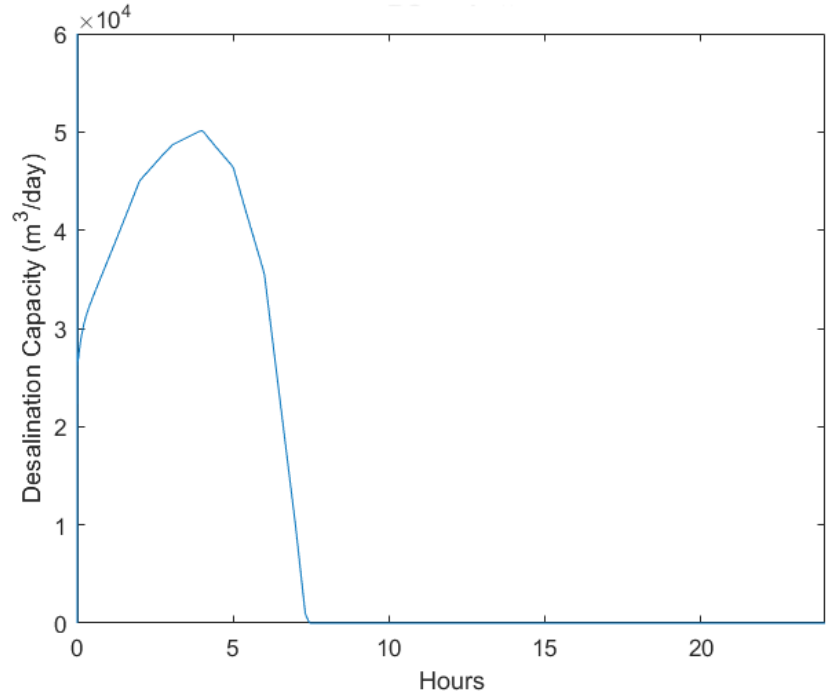

Figure 5.6: Capacity of the RO plant during the day

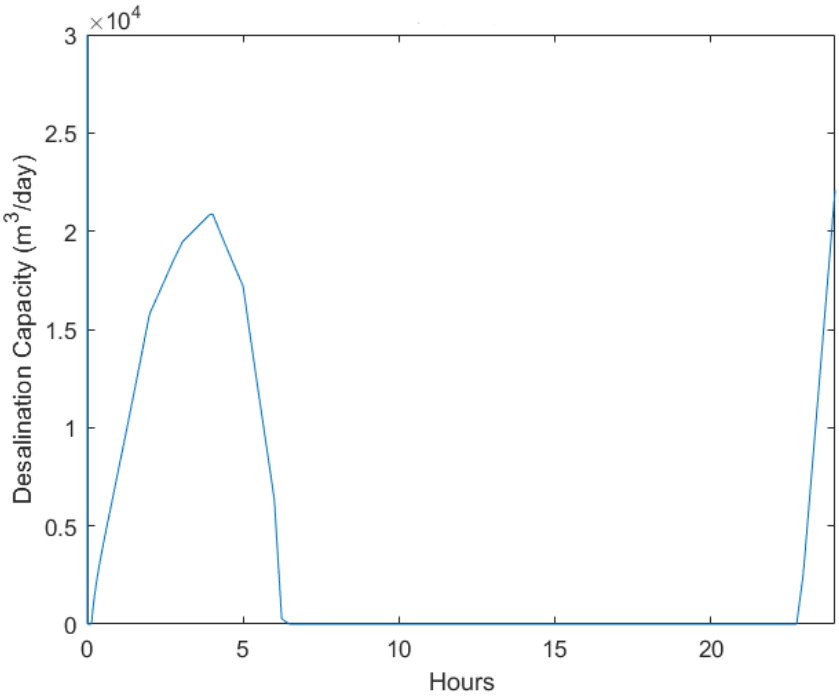

Figure 5.7: Capacity of the RO plant during the day with batteries

5.4 Grid with MED Plant

For the thermal systems a production of 15 MWth of heat for an MED plant will be studied. The MED was used instead of the MSF because of the advantages it has when coupled with a power plant compared to the latter. A pre-programmed load follow strategy [3], as for the batteries simulation, has been adopted. Compared to RO a simpler control has been used since the controller developed doesn't relate the electricity production directly to the steam extraction for cogeneration.

From fig.5.8 we can see that, during the cogeneration, the reactor mechanical power decreases of about 3 MWe while the total load decreases of about 10 MWe. This can be explained by fig.5.9 which shows the electrical power that also has to be redirected to the desalination plant which is of about 7 MWe. What just mentiond shows how much more difficult is to follow the load with this type of system compared to the RO but is the only one capable of desalinating waters with extremely high salt concentrations. Of course as for the latter technology, the capability of load follow during the daily peaks is absent.

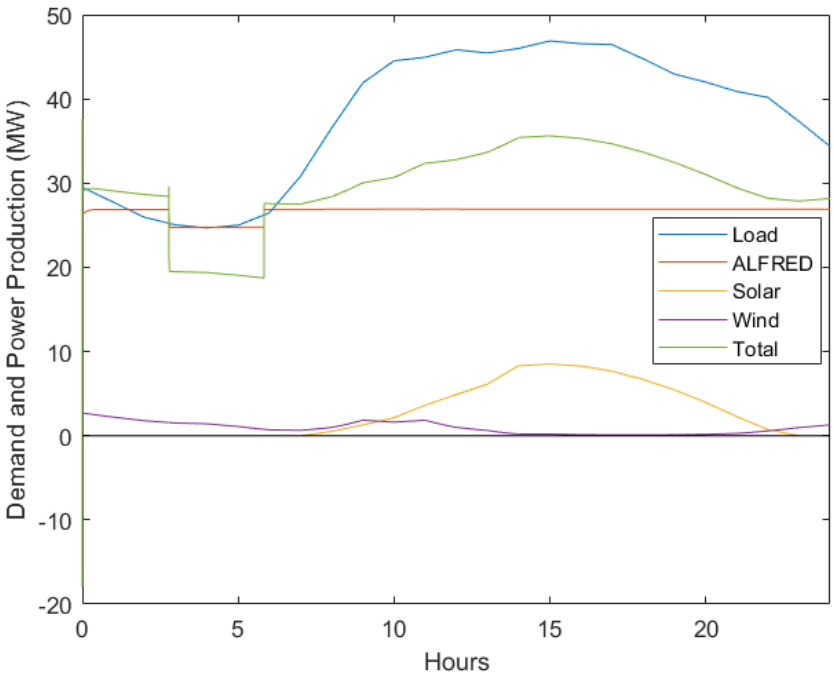

Figure 5.8: Eergy demand and total energy production

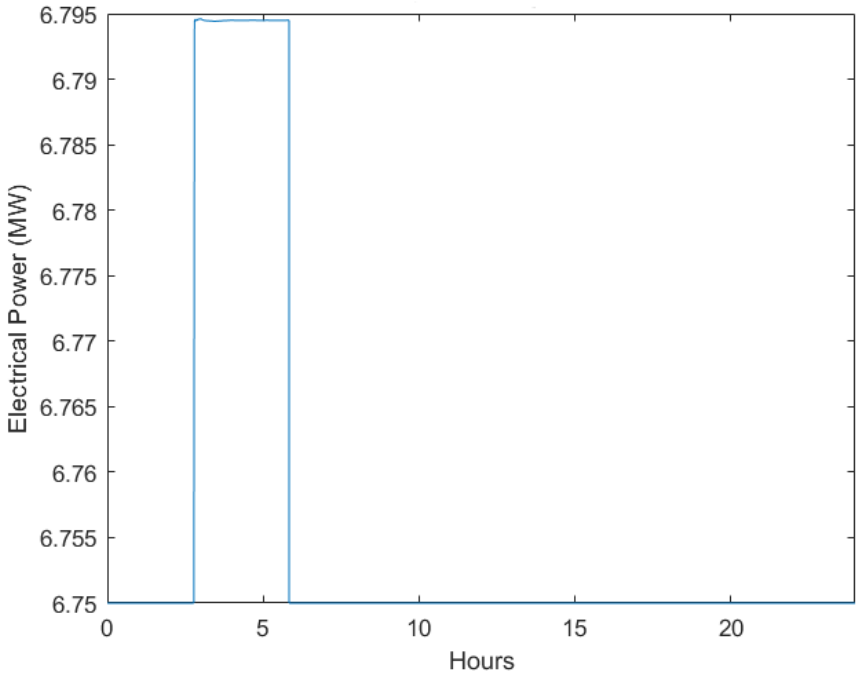

Figure 5.9: MED electrical energy requirement related to a 15MWth input

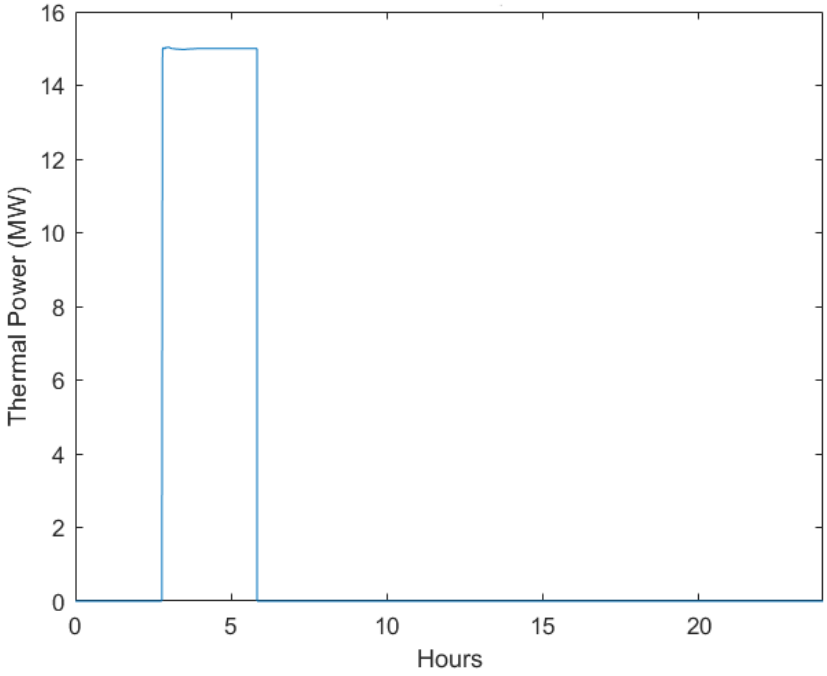

Figure 5.10: MED heat input

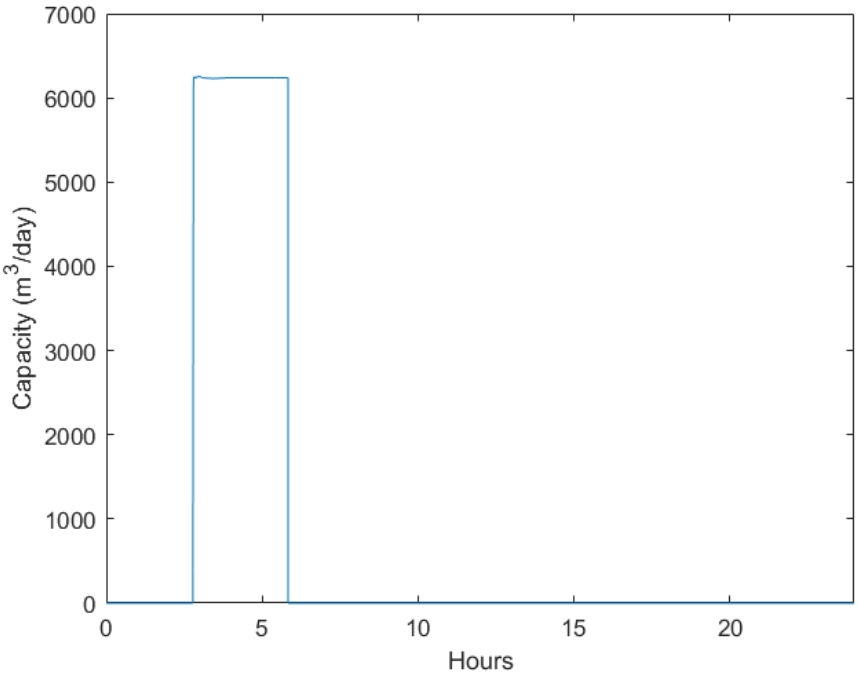

Figure 5.11: MED capacity

5.5 Reactor Load Follow

5.5.1 With Battery Energy Storage System

The last simulation will deal with managing the following of the electrical demand by varying the reactor mechanical power. This can be accomplishes thanks to the controller that connects the grid frequency variation to the turbine admission valve that can rapidly and effectively change the power generated by the turbine unit. Indeed, in the plant secondary loop, the pressure and temperature controller will need to work in tandem with the frequency controller to maintain the the nominal values of the plant. As an example, the admission valve closure will reduce the flow rate entering the turbine which in turn will increase the pressure of the secondary side that will be dealt by the bypass valve which will suitably vent the excess steam.

The first macro group of scenarios that will be shown regards a load following with battery storage system configuration. Again, a preprogrammed charge/discharge strategy has been adopted starting from a lower state of charge of 5% compared to 40% of the previous simulations. This choice will lead to a battery power cut-off at around 17-18 p.m and then starting the charging again at 22 p.m (fig.5.12). The sum of all power contributions given in figure 5.13 shows us that the demand and supply curves are closer compared to the other scenarios. Moreover the reactor is capable of keeping the grid stable throughout all the day. An important perturbation in the grid happens when the battery abruptly cuts off at 17 p.m (fig. 5.14) which is still perfectly handled by the plant

as seen in the close up in figure 5.15 since the frequency still remains well within the safety margins. Moreover this rapid transient will bring little stress to the plant itself as it can be seen in figure.5.16 the pressure remains basically constant with spikes during the inversion from charge to discharge, during the cut off and during the recharge of the battery. These spikes are controlled with no problems by the controller, as it can be seen by the close up on the first peak in figure 5.17 the highest value is only 1 bar over nominal parameter which can be dealt with. Still it is not suggested to let the reactor alone deal with these kind of fast changes in grid frequency since in the long run it could lead to higher O&M costs.

As for all the previous cases studied, also here it will be analyzed the desalination option to cover the surplus energy production. Again RO is the technology used. Compared to the previous cases we can see here that the reactor keeps a gap between supply and demand which is much smoother compared to the previous RO capacities studied making it simpler to define the optimal dimensions of the system. The temperatures have not been shown since little to no variation had been found during the transients.

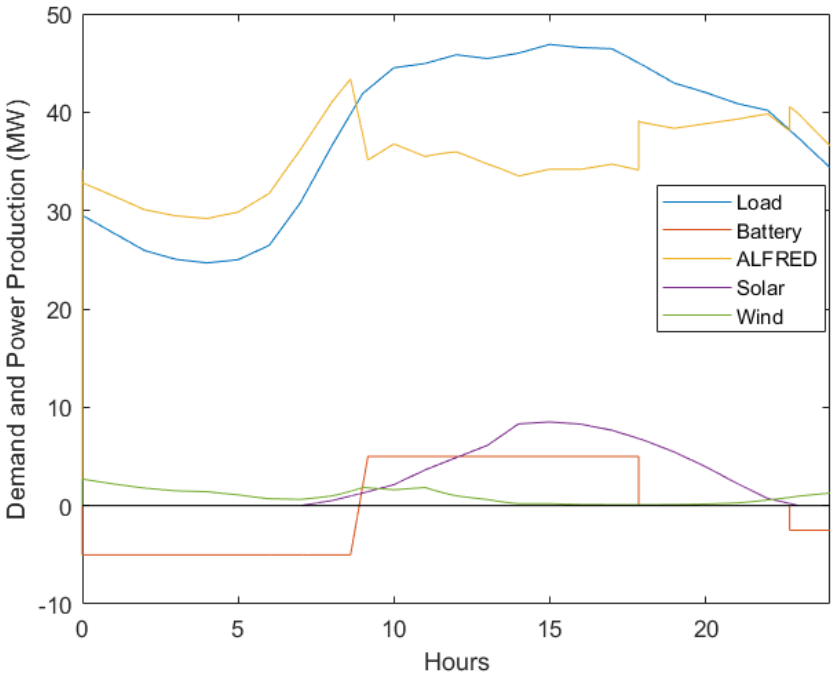

Figure 5.12: Reactor load components

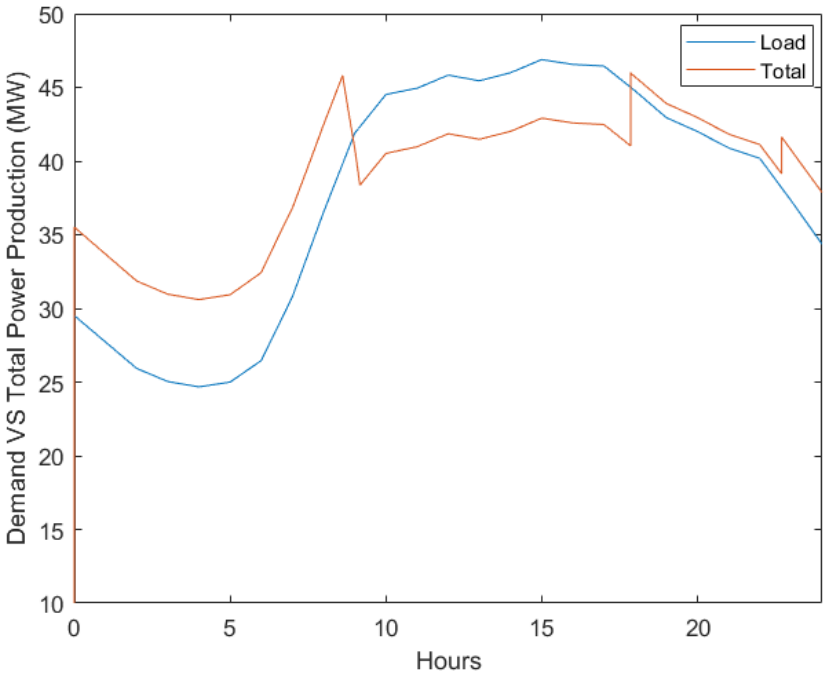

Figure 5.13: Reactor load following with battery pack

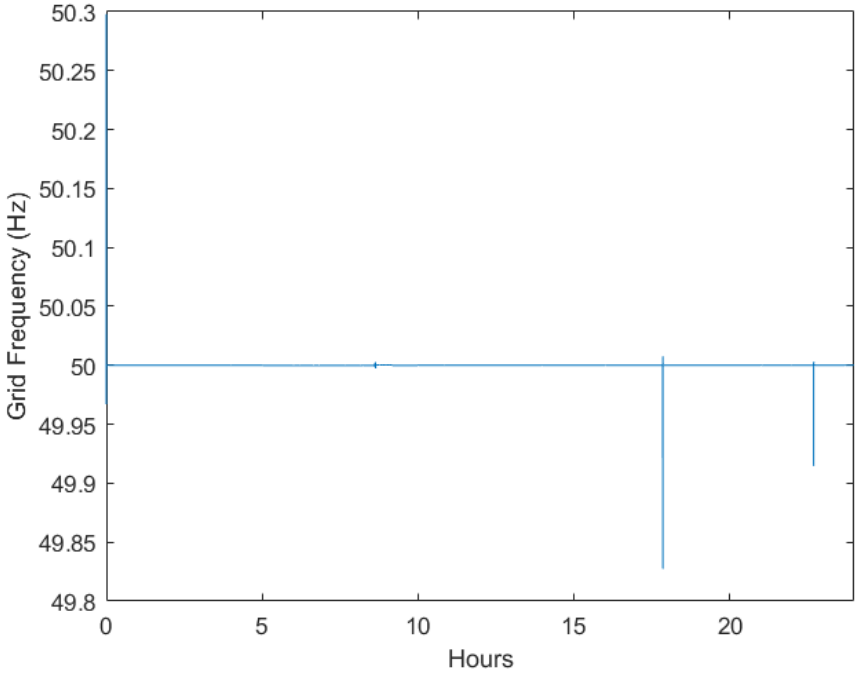

Figure 5.14: Grid frequency during the reactor load follow with battery pack

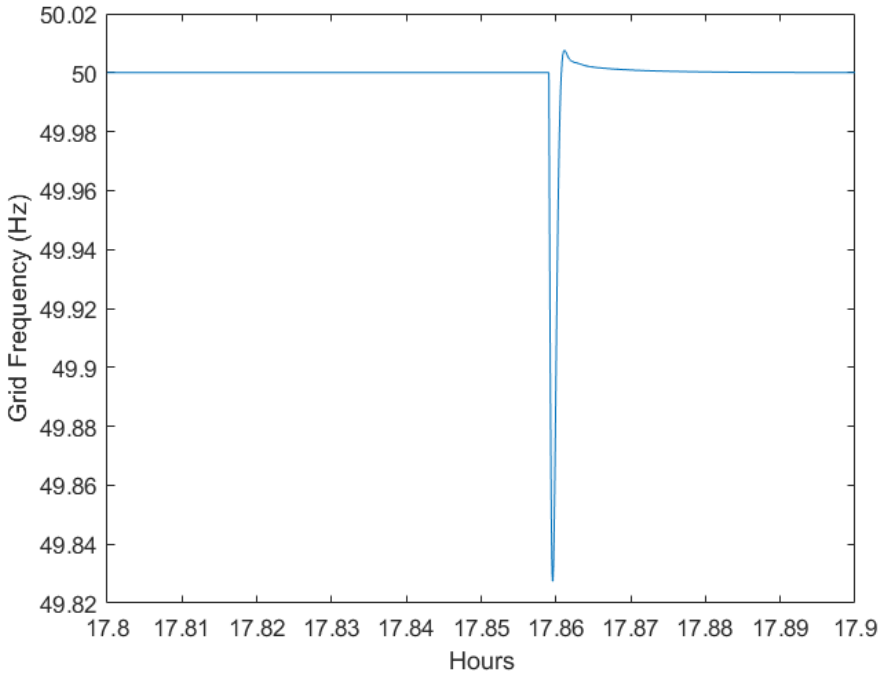

Figure 5.15: Grid frequency close up at 17 p.m

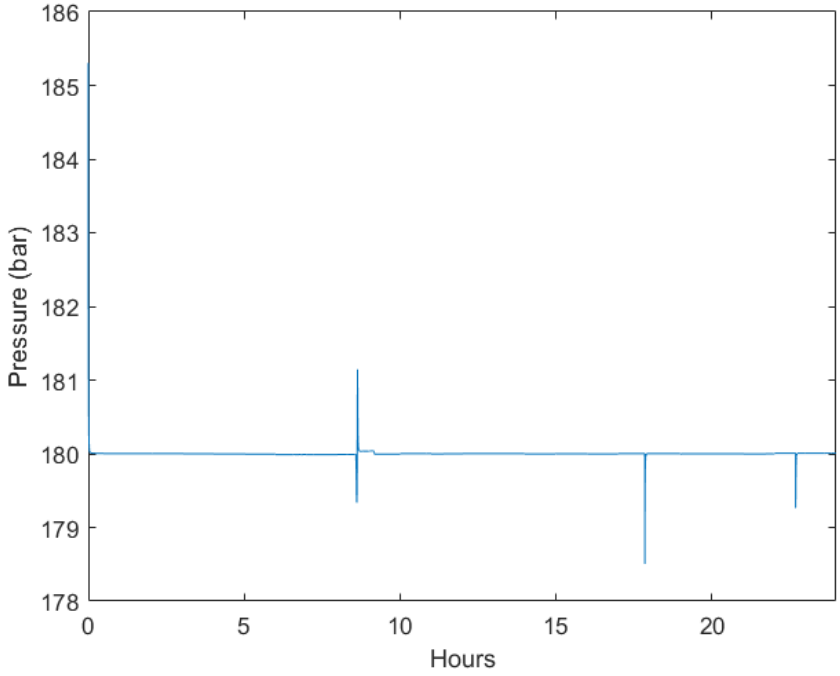

Figure 5.16: Plant pressure

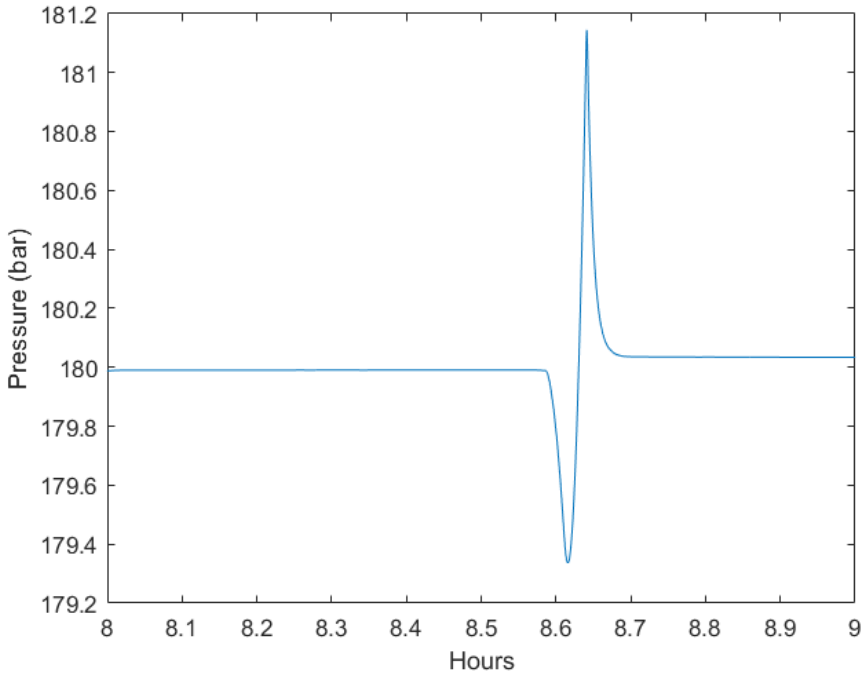

Figure 5.17: Plant pressure close up

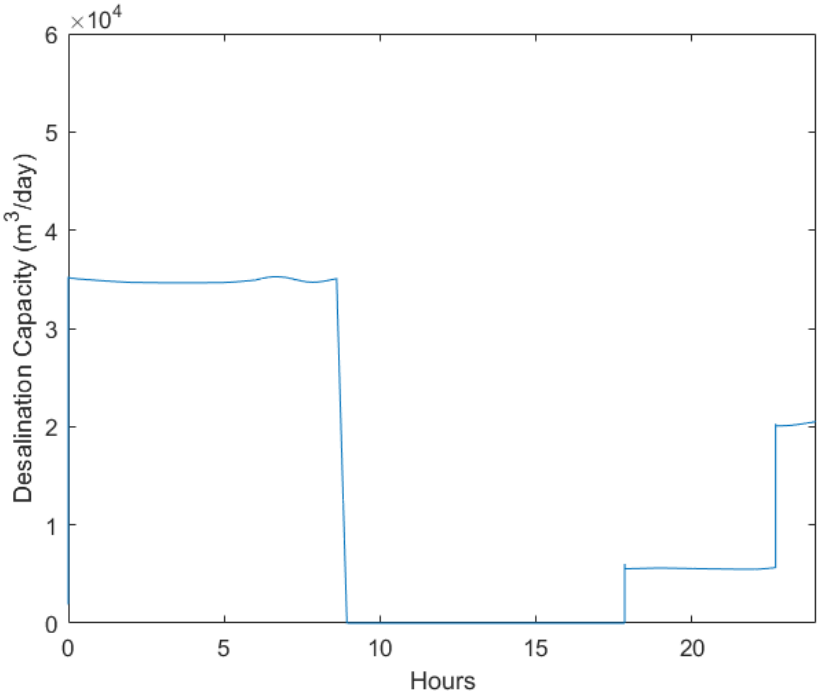

Figure 5.18: Reverse osmosis capacity with reactor following the load and battery pack

5.5.2 Without Battery Energy Storage System

Finally the case of pure load following, without battery storage system, has been taken into account. Figure 5.19 that this option is much better suited for load following from a technical stand point. In contrast to the base load case, here adding batteries actually degrades the performance of the system. In this scenario, neither spikes in frequency nor in the system pressure have been identified. A reverse osmosis plant would also benefit from this type of load follow. In fact, as seen in figure 5.18, the extra production of electricity is substantially constant which in turn leads to constant daily plant capacity. Therefore it makes it easy to find the optimal plant dimension if results are considered on a yearly average. It has to be reminded that throughout all of these simulations the primary system of the reactor remained substantially untouched and every regulation was carried out on the secondary loop to minimize the thermomechanical stresses on the core.

Even though at first glance this option seems to beat the other scenarios, it has to be taken into account that the capacity factor of this configuration is considerably lower compared to the others given the load following nature. Therefore this strategy, whilst having its own advantages, could be confined to case specific applications where grid stability is more of an issue, like in rural or isolated areas, not certainly in the European grid.

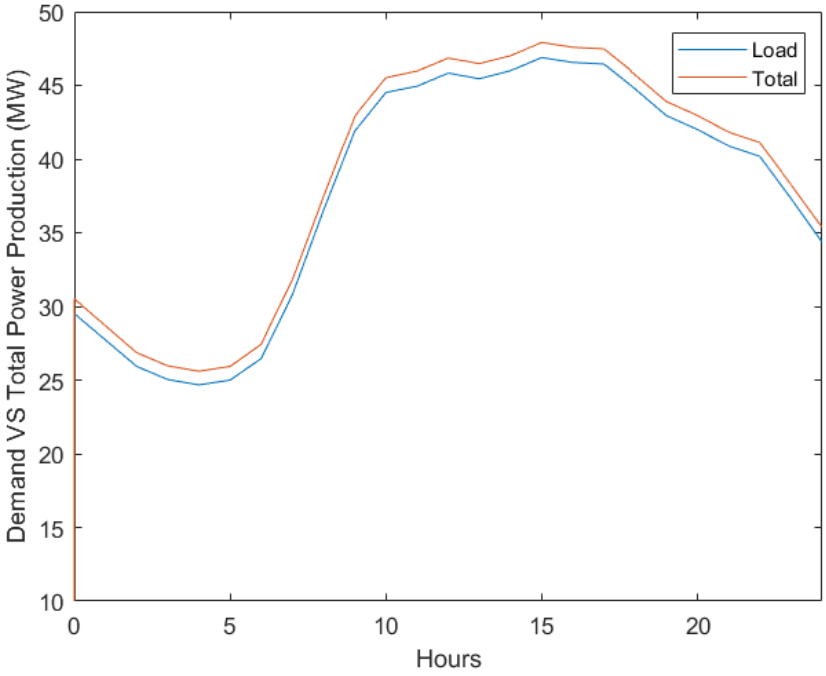

Figure 5.19: Reactor load following with no battery pack

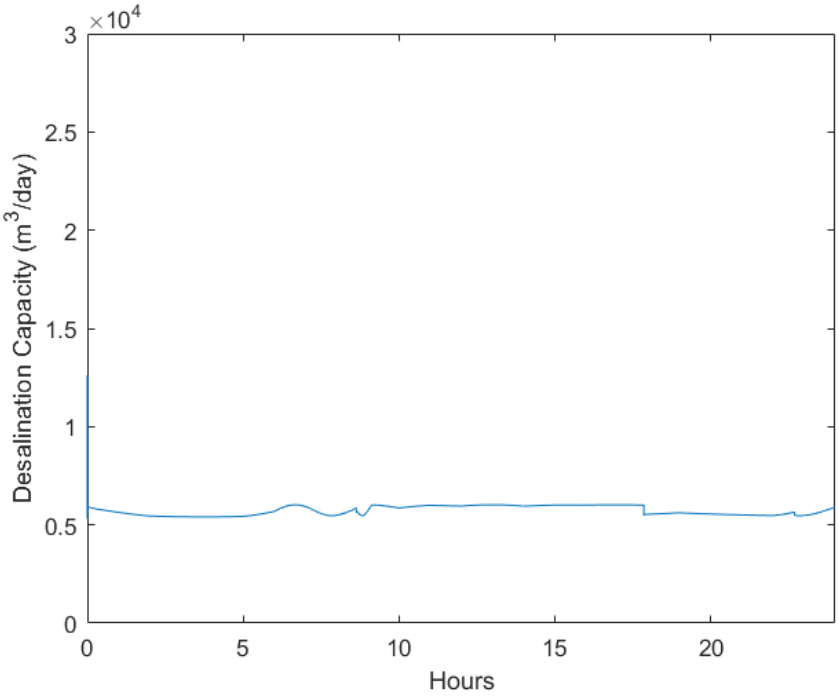

Figure 5.20: Reverse osmosis capacity with reactor following the load and no battery pack

5.6 Considerations

Two grid models have been developed (one regarding only electrical systems and one capable of thermal cogeneration) and simulated using real life data for energy demand, solar irradiance and wind speed. Various scenarios for load follow were taken into consideration. For reactor in base load configuration these options were:

- By redirecting the excess electrical power to an RO desalination plant (*Dynamic Load Follow* [3])
- By reducing the mechanical power output via thermal cogeneration for MED desalination plant
- By using a battery storage system with a pre-programmed charge/discharge control strategy for peak shaving
- By coupling battery and RO technologies

And for the reactor in load following configuration the scenarios considered were:

- Reactor follows the load alone
- Reactor follows the load coupled with a battery pack with a pre-programmed charge/discharge control strategy

- Reactor follows the load and redirects the excess electricity to an RO plant
- Reactor follows the load coupled with batteries and RO

The battery option has shown to be the most suitable for load following when coupled with a base load configuration for the NPP while resulted the worst when the plant was in load follow configuration. The RO results in the easiest way to produce fresh water both from a control and technical perspective since no modifications to the turbine in the power plant are needed. The main drawbacks,for this technology, are economical since it's not suitable for high concentration salt water. By integrating the capacity data shown in fig.5.6, fig.5.7, fig.5.11, 5.18 and 5.20 we can find the total water produced by each system during the day. Table 5.1 sums the results obtained.

Scenario	Water production (m^3)
RO with batteries	$4.1 \cdot 10^3$
RO without batteries	$1.2 \cdot 10^4$
RO load follow with batteries	$5.73 \cdot 10^3$
RO load follow without batteries	$1.49 \cdot 10^4$
MED	$7.9 \cdot 10^2$

Table 5.1: Total fresh water produced in the various scenarios

As we can see the MED plant has the worse performance and as expected the capacity in the coupled batteries and RO system, both in base load and load follow configuration of the plant, is reduced compared to the only RO option. To these results a techno-economical evaluation is of upmost importance to understand which strategy of the ones aforementioned is actually the best. It is expected that the answer will be case specific depending on where the coupled system will be located.

Conclusions

Within this thesis work the development of an extremely modular and versatile simulation environment to study the behavior of different reactor technologies coupled with diverse cogeneration options has been developed. A strong penetration of renewable energy systems has been envisioned considering the current global trend therefore adding the problematic of load following and grid stabilization to the whole system. Given the high complexity of an NPP, a pre-existing model of ALFRED reactor was modified within the *Dymola* environment to enable the cogeneration option. The free dynamics of ALFRED power plant were studied for transients pertaining: control rod insertion and withdraw, ramp increase in water mass flow rate on the secondary side and steam extraction for the low pressure stage of the turbine. The results are in good agreement with the expected physical behavior of the system. The model has then been imported into Simulink where a PID controller for the entire system was built. The capabilities of said controller are, within the physical constraints of the system:

- Deliver the required thermal power
- Keep the pressure constant at 180 bar
- Maintain the cold leg temperature to the set-point of 400 $°C$
- Deliver the needed cogeneration heat
- Adjust the mechanical power given the grid frequency variation

Three control strategies, two for the purely electrical systems and one for the thermal cogeneration, were then adopted both aiming at keeping the thermal power of the reactor at nominal levels. In case of coupling with purely electrical systems two configurations of the reactor were studied namely: a base load and a load follow mode. To these two configuration then, the addition of a reverse osmosis plant, of a battery energy storage system, or both coupled was implemented. For the RO the excess electricity during the night hours was redirected for the production of fresh water. For the BESS a time based charge/discharge control approach was adopted. Instead for the thermal systems, a reduction in mechanical power output of the plant was made possible by enabling the withdraw of heat for industrial applications via steam extraction. This strategy enters in the *load follow by cogeneration* type which is nowadays considered an economically

and technically more viable solution to the classical load following by varying the thermal and mechanical power output of the reactor. For this purpose, models of RO, MED and MSF desalination plants were developed and tested. Results show a clear superiority of the reverse osmosis over the other technologies given the lower electrical input and higher capacity. At the same time a thermal desalination systems is needed for high salt concentration waters. It was shown a clear advantage in using MED over MSF given the lower operational temperatures and higher capacities per MWth obtainable by the former. Thus a higher utilization factor is achievable by the coupled system MED and ALFRED.

Finally a complete three-phase grid model was developed with a 10 MWe photo-voltaic and a 10 MWe wind farm plus a variable load block to simulate the typical daily load curve using real data. To study the different solutions for load following a battery energy storage system based on Li-ion technology was implemented as an alternative to cogeneration. Eight scenarios were taken into account considering two different developed models: one pertaining solely electrical systems and one considering thermal cogeneration. The scenarios are the following.

- Reactor in base load configuration and peak shaving with battery storage system
- Reactor in base load configuration and redirecting excess electricity to the RO plant
- Reactor in base load configuration and coupled batteries and RO
- Load follow by cogeneration of 15 MWth for MED plant
- Reactor in load follow configuration alone
- Reactor in load follow configuration and excess electrical production sent to RO plant
- Reactor in load follow helped by BESS
- Reactor in load follow with coupled RO and BESS

The figure of merit considered was how much electrical energy the grid had to daily introduce in the system to compensate for the demand not covered (figure 6.1). It has to be highlighted that of the eight scenarios, only five are shown. This is because the coupled RO and battery pack scenarios have the same results of the battery only configuration given that the same amount of electricity is required from the grid. The results show a clear advantage of using the battery storage system coupled with RO when dealing with a reactor in base load configuration. In this situation both fresh water and good load following are achieved. The option pertaining only RO is not as suitable as the one just discussed given the inability of this configuration to follow the load during the peak hours. On the other hand this is the best solution in terms of daily water production since it has the highest capacity between the two base load configurations. If instead we consider load follow configuration, the results show exactly the opposite. In fact, in the current configuration, the best coupling is that of the reactor with the RO only, without the use of

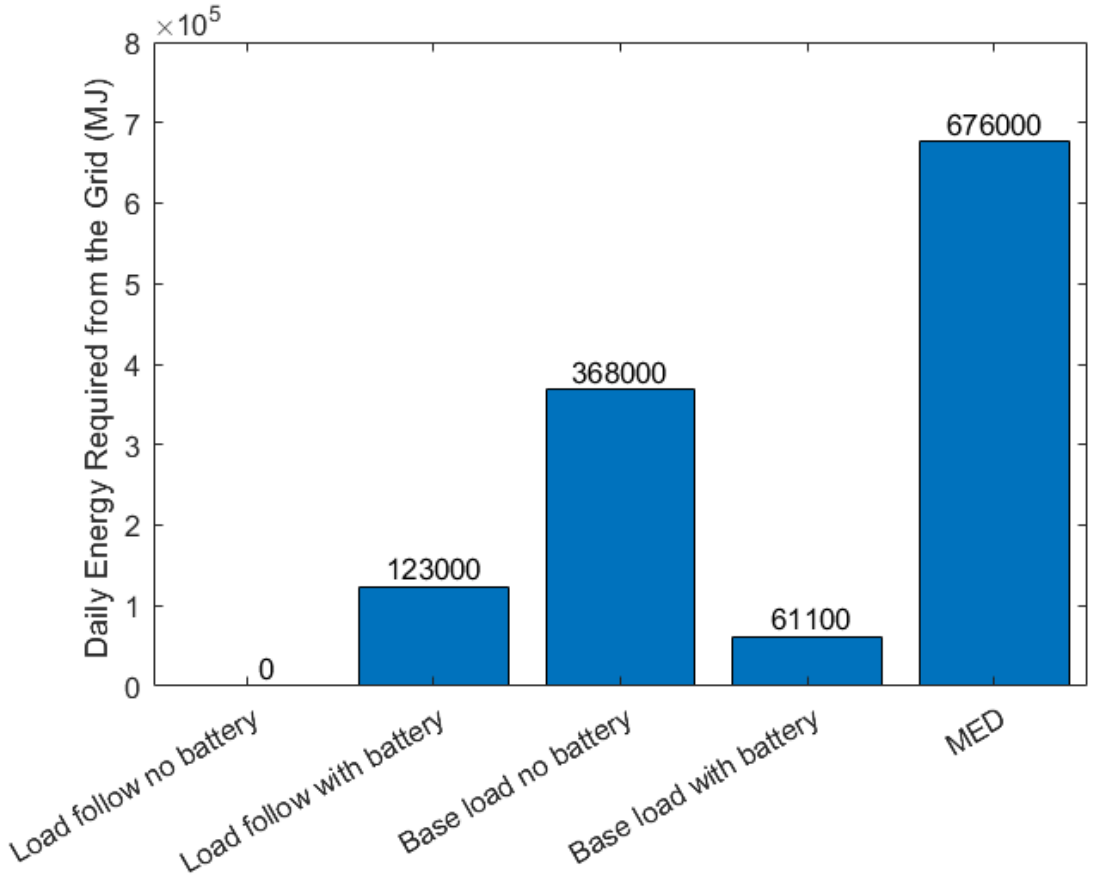

Figure 6.1: Electrical energy taken from the grid to compensate the demand

battery that in this case tend to complicate load following and grid stability. Furthermore in this situation the electricity sent to the RO is basically constant enabling a better usage of this plant . The thermal cogeneration option seems more suitable only in the case where MED is the sole option available as in high salinity waters. It has to be noted that the steam extraction for thermal utilization inherently brings two complications to the system. First a technical one related to the modification of the turbine to enable steam extraction itself. Second, it can be easily seen in the MED simulation that a good control strategy for load following is inherently more difficult since not only we need to know the final electrical output of the reactor, but to this it has to be subtracted the electrical power required by the desalination system to work which is itself function of the input heat. Therefore the simplicity of the only electrical system is substantial from a control and technical point of view with respect to a thermal cogeneration option. At the same time thermal processes and technologies are of primary importance and most of the times are the only options for industrial and civilian applications thus a more refined control strategy for these kind of system has to be envisioned. As a final result, in terms of load follow and grid stability, the reactor in load follow configuration coupled solely with the reverse osmosis desalination plant is the clear winner. Unfortunately this is only a technical result. In fact this scenario is the one were the reactor has the worst capacity factor given it working mostly at partial load. This in turn results in an important loss

of revenues for the plant owner therefore probably making it not an economically viable solution in a fully meshed grid like the European one. On the other hand, in remote locations where grid stability and fresh water production are of utmost importance, this configuration could be an attractive solution. Thus a technical analysis alone, like the one carried out during this work, is not sufficient to show which solution is the best overall (which will nevertheless be case-specific), answer that could be given after an economical evaluation.

To briefly recap the libraries, developed within this thesis work, have been summarized in figure 6.2. It is envisioned in the future to widen the libraries created in the simulation to consider other heat requiring industrial processes such as hydrogen and bio-fuel production etc. With these technologies, novel reactor types can be studied to highlight which nuclear plant is the most suitable for certain applications thus finding the optimal coupling between systems.

The end goal of this simulator is that to use the results of the various scenarios modelled as inputs for a techno-economical evaluation therefore understanding not only the technological feasibility of the hybrid systems but also the optimum for eash case.

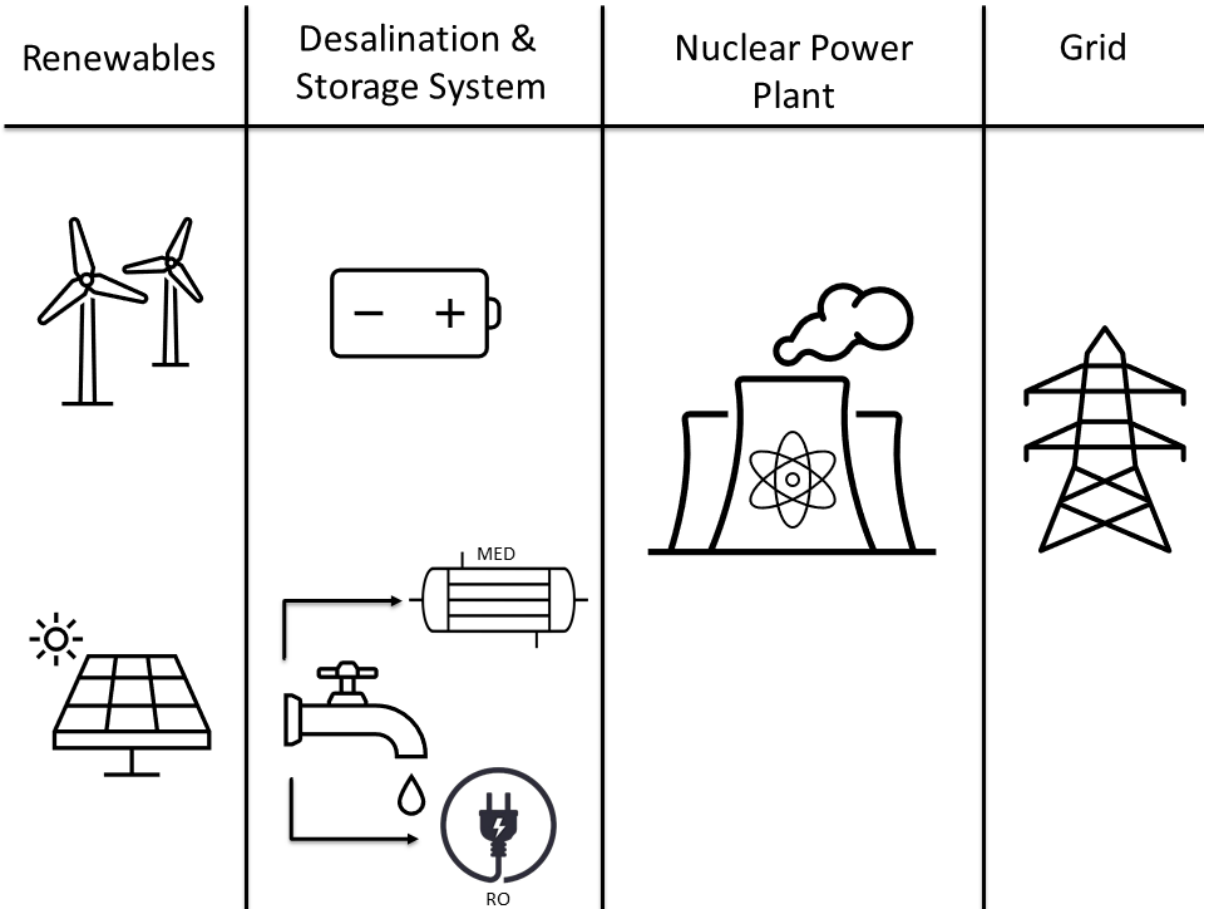

Figure 6.2: Libraries developed within the thesis work

Bibliography

[1] P. Agreement, "Paris agreement," in *Report of the Conference of the Parties to the United Nations Framework Convention on Climate Change (21st Session, 2015: Paris). Retrived December*, vol. 4, p. 2017, HeinOnline, 2015.

[2] A. Lokhov, "Technical and economic aspects of load following with nuclear power plants," *NEA, OECD, Paris, France*, vol. 2, 2011.

[3] G. Locatelli, A. Fiordaliso, S. Boarin, and M. E. Ricotti, "Cogeneration: An option to facilitate load following in small modular reactors," *Progress in Nuclear Energy*, vol. 97, pp. 153–161, 2017.

[4] I. A. E. Agency, "Opportunities for cogeneration with nuclear energy," *NP-T-4.1*, 2017.

[5] "Nuclear–renewable hybrid energy systems for decarbonized energy production and cogeneration." `https://www-pub.iaea.org/MTCD/Publications/PDF/TE-1885web.pdf`.

[6] G. Locatelli, "Why are megaprojects, including nuclear power plants, delivered overbudget and late? reasons and remedies," *arXiv preprint arXiv:1802.07312*, 2018.

[7] M. Frogheri, A. Alemberti, and L. Mansani, "The lead fast reactor: demonstrator (alfred) and elfr design," in *International Conference on Fast Reactors and Related Fuel Cycles: Safe Technologies and Sustainable Scenarios (FR13), Paris, France*, 2013.

[8] S. Pindado and J. Cubas, "Simple mathematical approach to solar cell/panel behavior based on datasheet information," *Renewable energy*, vol. 103, pp. 729–738, 2017.

[9] M. Ragheb and A. M. Ragheb, "Wind turbines theory-the betz equation and optimal rotor tip speed ratio," *Fundamental and advanced topics in wind power*, vol. 1, no. 1, pp. 19–38, 2011.

[10] A. Al-Othman, N. N. Darwish, M. Qasim, M. Tawalbeh, N. A. Darwish, and N. Hilal, "Nuclear desalination: A state-of-the-art review," *Desalination*, vol. 457, pp. 39–61, 2019.

[11] K. Sadeghi, S. Ghazaie, E. Fedorovich, E. Sokolova, and A. Shirani, "Economic assessment of the possible desalination processes for the first unit of bushehr nuclear power plant," *Thermal Engineering*, vol. 67, pp. 271–281, 2020.

[12] P. Catrini, A. Cipollina, F. Giacalone, G. Micale, A. Piacentino, and A. Tamburini, "Thermodynamic, exergy, and thermoeconomic analysis of multiple effect distillation processes," in *Renewable Energy Powered Desalination Handbook*, pp. 445–489, Elsevier, 2018.

[13] H. T. El-Dessouky and H. M. Ettouney, *Fundamentals of salt water desalination*. Elsevier, 2002.

[14] L. Wagner, "Overview of energy storage technologies," in *Future Energy*, pp. 613–631, Elsevier, 2014.

[15] A. Oudalov, R. Cherkaoui, and A. Beguin, "Sizing and optimal operation of battery energy storage system for peak shaving application," in *2007 IEEE Lausanne Power Tech*, pp. 621–625, IEEE, 2007.

[16] T. Chen, Y. Jin, H. Lv, A. Yang, M. Liu, B. Chen, Y. Xie, and Q. Chen, "Applications of lithium-ion batteries in grid-scale energy storage systems," *Transactions of Tianjin University*, vol. 26, no. 3, pp. 208–217, 2020.

[17] A. S. Anees, "Grid integration of renewable energy sources: Challenges, issues and possible solutions," in *2012 IEEE 5th India International Conference on Power Electronics (IICPE)*, pp. 1–6, 2012.

[18] R. Ponciroli, A. Bigoni, A. Cammi, S. Lorenzi, and L. Luzzi, "Object-oriented modelling and simulation for the alfred dynamics," *Progress in Nuclear Energy*, vol. 71, pp. 15–29, 2014.

[19] M. K. Ibragimov, V. Subbotin, and P. Ushakov, "Investigation of heat transfer in the turbulent flow of liquid metals in tubes," *The Soviet Journal of Atomic Energy*, vol. 8, no. 1, pp. 48–50, 1961.

[20] R. Ponciroli, A. Cammi, S. Lorenzi, and L. Luzzi, "Control approach to the load frequency regulation of a generation iv lead-cooled fast reactor," *Energy Conversion and Management*, vol. 103, pp. 43–56, 2015.

[21] S. Sterpu, "Power system dynamic performance: Primary governing frequency response," in *2009 IEEE Bucharest PowerTech*, pp. 1–6, IEEE, 2009.

[22] "Load-frequency control and performance." `https://eepublicdownloads.blob.core.windows.net/public-cdn-container/clean-documents/pre2015/publications/ce/oh/appendix1_v19.pdf`.

[23] K. Sadeghi, S. H. Ghazaie, E. Sokolova, E. Fedorovich, and A. Shirani, "Comprehensive techno-economic analysis of integrated nuclear power plant equipped with various hybrid desalination systems," *Desalination*, vol. 493, p. 114623, 2020.

[24] J. LeSage, "Microgrid system development and analysis." `https://www.mathworks.com/videos/series/microgrid-system-development-and-analysis.html`.

[25] `https://it.weatherspark.com`.

[26] P. Morilhat, S. Feutry, C. Le Maitre, and J. M. Favennec, "Nuclear power plant flexibility at edf," 2019.

[27] "Dimensioning of current transformers for protection applications." https://store.gegridsolutions.com/faq/Documents/General/GER-3973A.pdf.

[28] "Charge/discharge control of battery energy storage system for peak shaving yahia baghzouz." https://www.sandia.gov/ess-ssl/EESAT/2009_papers/Charge%20-%20Discharge%20Control%20of%20Battery%20Energy%20Storage%20System%20for%20Peak%20Shaving.pdf.